DRAFT

SCDAP/RELAP5 BASE CASE CALCULATION FOR THE STATION BLACKOUT UNCERTAINTY STUDY

by

C. D. Fletcher
R. M. Beaton

Information Systems Laboratories, Inc.
Idaho Falls, Idaho and Rockville, Maryland

prepared for

U. S. Nuclear Regulatory Commission
Office of Nuclear Regulatory Research
Washington DC 20555

NRC Project Officer
Donald Helton
NRC Technical Advisor
Christopher F. Boyd

under

Contract No. NRC-04-05-064
Continuation of Support for System Code Analysis to Predict
Severe Accident Conditions Leading to Containment Bypass

JCN Number Y6198
RES ID: RES-C05-340

August 2006

ABSTRACT

The U. S. Nuclear Regulatory Commission has been conducting studies to evaluate the risk associated with steam generator tube failure following low probability severe accidents in pressurized water reactors. The issue relates to the sequence in which the various reactor coolant system boundary structures fail. Failures of hot leg piping, pressurizer surge line piping and the reactor vessel wall lead to discharge of fission products into the containment. Failures of steam generator tubes lead to discharge of fission products into the steam generator secondary system, from where they may be discharged to the environment through the main steam safety or secondary system power operated relief valves. Prior reports have evaluated the extent of steam generator tube structural strength degradation required to cause tube failures to precede hot leg or pressurizer tube failure for a station blackout event in a Westinghouse four-loop plant. This report documents a revised SCDAP/RELAP5 simulation for a low probability station blackout event sequence in that plant type, which updates the analysis and which is used as a base case run in a study evaluating the uncertainties in the simulation.

CONTENTS

LIST OF FIGURES

LIST OF TABLES

EXECUTIVE SUMMARY

A natural circulation of highly superheated steam can develop in the reactor coolant system (RCS) of pressurized water reactors during specific low probability station blackout (SBO) events that progress to severe accident conditions. This steam circulation can transfer significant heat from the reactor core to portions of the RCS outside of the reactor vessel. Since the pressure in the RCS can remain elevated during a SBO event sequence, the introduction of highly superheated steam into the hot leg, pressurizer surge line and steam generator (SG) tube regions of the RCS poses potential challenges for the pressure boundaries in these components. The potential for SG tubes to fail is of particular importance since their failure represents the opening of a flow path from the RCS into the SG secondary system, where the pressure relief valves could provide a direct path for the passage of core fission products to reach the environment.

The Nuclear Regulatory Commission (NRC) has been pursuing thermal-hydraulic studies to evaluate SG tube integrity. Several previous reports have documented base case and sensitivity SCDAP/RELAP5 simulations for station blackout event sequences in a Westinghouse four-loop plant. This report documents a revised base case station blackout simulation for such a plant that will be used as a base case for a subsequent study evaluating the uncertainties present in key simulation results. The calculation described here takes advantage many recent model improvements, which results in a more physical representation of the plant response.

The updated SCDAP/RELAP5 base case calculation documented in this report indicates that for stress multipliers up to 2.0 the average SG tube fails after the hot leg fails. The hottest SG tube is indicated to fail prior to the time when the hot leg fails, even for a stress multiplier of 1.0, which represents non-degraded tube strength. The stress multiplier is an indicator of the assumed SG tube material strength degradation (with, for example, a multiplier of 2.0 representing a 50% degradation).

Additional output data from the SCDAP/RELAP5 calculation are provided to enhance understanding of the plant response during the accident event sequence and to facilitate analyses performed by others involved in the project.

NOMENCLATURE

AC	alternating current
ACRS	Advisory Committee on Reactor Safeguards
AFW	auxiliary feedwater
BWR	boiling water reactor
CCFL	counter-current flow limiting
CD	compact diskette
C_D	hot leg discharge coefficient
CFD	computational fluid dynamics
C_v	flow coefficient
D	diameter
FSAR	final safety analysis report
FW	feedwater
g	acceleration due to gravity
INEEL	Idaho National Engineering and Environmental Laboratory
ISL	Information Systems Laboratories, Inc.
MFW	main feedwater
NTR	normalized temperature ratio
NRC	U. S. Nuclear Regulatory Commission
PIRT	phenomena identification and ranking table
PORV	power operated relief valve
PRA	probabilistic risk assessment
PWR	pressurized water reactor
Q	volumetric flow rate
RCP	reactor coolant pump
RCS	reactor coolant system
RV	reactor vessel
SBO	station blackout
SG	steam generator
SRV	safety relief valve
$T_{hottest\ tube}$	steam temperature at inlet of the hottest steam generator tube
$T_{cold\ tube}$	steam temperature at exit of reverse-flowing steam generator tube
$T_{hot\ leg}$	steam temperature at exit of the upper-half hot leg section
ρ	density

FOREWORD

The analyses presented in this report are performed to evaluate plant behavior during hypothetical event sequences with potential for leading to a severe accident. The occurrence of the event sequences is extremely unlikely due to multiple assumed concurrent failures of systems and components. A few of the key assumptions for the station blackout base case accident sequence are:

- Loss of off-site power for an extended period
- Failure of all diesel-electric generators to start
- Failure of the turbine-driven auxiliary feedwater system to operate
- 21 gpm (equivalent hole size) reactor coolant pump shaft seal leakage
- Steam leakage causes all steam generators to depressurize

These assumptions result in a "high-dry" condition with all four steam generators depressurized by the time any primary system ruptures are predicted to occur. No operator intervention for mitigating the accident is accounted for.

The analyses therefore do not represent best-estimate plant behavior, nor do the results indicate the most-likely outcomes of the event sequences. The results can only be put into perspective with appropriate consideration for the probability of such events occurring. The predicted results apply only for the specific analysis assumptions and may vary considerably as assumptions are changed (for example, greater reactor coolant pump shaft seal leakage rates can eliminate steam generator tube failures which are predicted at smaller leakage rates). These considerations must ultimately be accounted for in an integrated probabilistic risk assessment of severe accident induced steam generator tube failures

1.0 INTRODUCTION

The U. S. Nuclear Regulatory Commission (NRC) has for the past several years been conducting studies to evaluate the risk associated with steam generator (SG) tube failure following severe accidents in pressurized water reactors (PWRs). For PWRs with U-tube SGs, the natural circulation of superheated steam in the loop piping during severe accidents could result in sufficient heating of the SG tubes to induce creep rupture failure prior to hot leg or surge line failure. To examine the risk impacts of induced SG tube rupture and the effects of changes in the regulatory requirements for SG tube integrity, the NRC has performed severe accident thermal-hydraulic analyses to examine the pressure and temperature conditions imposed on the SG tubes. These evaluations have focused on tube integrity during station blackout (SBO) severe accident scenarios wherein the reactor coolant system (RCS) remains at high pressure, the SG water inventory is lost and no source of feedwater is assumed available. This type of event exposes the SG tubes to highly-superheated steam at the high RCS pressures associated with the opening setpoint pressures of the pressurizer power operated relief valves (PORVs) and safety relief valves (SRVs), coincident with low-pressure conditions in the SG secondary system.

Because the SBO event represents a significant risk contributor among sequences that progress to core damage and poses a threat to SG integrity, that event has been the assumed accident initiator for all of the SCDAP/RELAP5 (Reference 1) analyses performed to date. The extent of the prior analyses has been considerable. The Idaho National Engineering and Environmental Laboratory (INEEL) evaluated SBO events in the several different types of PWRs (Reference 2). Subsequently, the INEEL refined a SCDAP/RELAP5 Westinghouse four-loop plant model for simulating this accident sequence (Reference 3). Information Systems Laboratories, Inc. (ISL) evaluated the effects on the results of variations in the accident sequence and modeling assumptions (References 4 and 5). The SCDAP/RELAP5 models for SBO events represent the average tubes in the SGs. ISL developed a method (Reference 6) based on Westinghouse 1/7th-scale experimental data (Reference 7) by which the temperatures and failure criteria for the hottest SG tube can be estimated using the average SG tube output data from the SCDAP/RELAP5 calculation. ISL then extensively documented a revised base case calculation for the Westinghouse four-loop plant using the upgraded model that included the hottest tube response (Reference 8). ISL performed an extensive set of sensitivity studies evaluating various changes in SCDAP/RELAP5 modeling options, event sequence assumptions and plant configuration (Reference 9). Subsequent to the sensitivity study evaluation, additional modifications of the Westinghouse four-loop plant model were incorporated to improve the model performance, better represent the physical response of the plant and provide additional output data to facilitate analyses performed by others in the project.

This report summarizes the current SCDAP/RELAP5 Westinghouse four-loop plant model and documents the results of a revised station blackout base case calculation. This calculation will serve as the nominal case for a subsequent study that will estimate the uncertainties present in the SCDAP/RELAP5 station blackout simulations. This calculation does not necessarily represent a best-estimate simulation of the most-likely SBO accident scenario for Westinghouse four-loop plants.

Section 2 of this report provides an overview description of the SCDAP/RELAP5 plant system model and summarizes model improvements implemented since the model was fully documented in Reference 8. Section 3 documents the results of the revised SCDAP/RELAP5 station blackout base case calculation, including an evaluation of the flow of energy into, within and out of the primary reactor coolant system. A summary of the work described in this report and conclusions are given in Section 4 and references are listed in Section 5. Appendix A provides a list of the SCDAP/RELAP5 calculation channel identifiers for which additional base case calculation output data is provided on a CD which will be available to project participants.

2.0 SCDAP/RELAP5 MODEL DESCRIPTION

Section 2.1 provides an overview description of the SCDAP/RELAP5 code and the Westinghouse four-loop plant system model. Section 2.2 summarizes upgrades implemented in the plant system model since it was last fully documented.

2.1 Overview Model Description

The SCDAP/RELAP5 plant model represents the fluid volumes and structures in the core, reactor vessel and primary and secondary coolant system regions of the plant. The model also includes a simple representation of the containment. As discussed in the introduction, this plant model has been developed by INEEL and ISL over a period of many years for the specific purpose of evaluating the SBO event in a Westinghouse four-loop PWR. Reference 8 provides a detailed description of the SCDAP/RELAP5 plant model, as it existed prior to the upgrades that are summarized in Section 2.2.

The SCDAP/RELAP5 computer code (Reference 1) calculates the overall RCS thermal-hydraulic response for severe accident situations that include core damage progression and reactor vessel heat up and damage. The computer code is the result of a merging of the RELAP5 and SCDAP computer codes. Models in RELAP5 calculate the overall RCS thermal-hydraulics, control system interactions, reactor kinetics and the transport of non-condensable gases. The RELAP5 code is based on a two-fluid (steam/noncondensible mixture and water) model allowing for unequal temperatures and velocities of the fluids and the flow of fluid through porous debris and around blockages caused by reactor core damage. Models in SCDAP calculate the progression of damage in the reactor core, including the heat up, oxidation and meltdown of fuel rods and control rods, ballooning and rupture of fuel rod cladding, release of fission products from fuel rods and the disintegration of fuel rods into porous debris and molten materials. The SCDAP models also calculate the heat up and structural damage of the reactor vessel lower head which results from the slumping of reactor core material with internal heat generation.

SCDAP also includes models for calculating the creep rupture failure of structural components. Specifically important for this project is the calculation of creep failure for stainless steel and Inconel based on the creep rupture theory of Larson and Miller (Reference 10 and Reference 1, Volume 2, Section 12.0). This creep rupture failure model is employed in the plant system model to predict failure times for the hot legs, pressurizer surge line and SG tubes. The model allows one to specify a stress multiplier, wherein a multiplier of 1.0 provides a creep failure prediction for a structure with no material degradation, and multipliers greater than 1.0 may be used to represent conditions of degraded structural strength. In the plant model, creep rupture failure calculations are performed for the average SG tubes and hot legs in all four coolant loops, and for the pressurizer surge line and hottest SG tube in the pressurizer-loop SG. A stress multiplier of 1.0 is used for the hot leg and surge line structure calculations while stress multipliers from 1.0 to 7.5 are used for the SG tube calculations. The SCDAP/RELAP5-calculated predictions of structural failures are intended to provide a reasonable “first look” into that issue, not to supplant structural failure evaluations using more detailed analysis tools.

The SCDAP/RELAP5 calculations presented in this report were performed with code Version 3.3de, which contains the SCDAP source taken from SCDAP/RELAP5/MOD3.3, Version 3.3ld.

The nodalization diagrams for the revised SCDAP/RELAP5 plant model are provided in Figures 1 through 5. In these diagrams, the open areas typically represent fluid regions with arrows indicating flow paths and shaded regions representing the structures included in the model (such as fuel rods, vessel internals and piping walls). The reader is cautioned that for practical reasons the sub-structure of some components in the model cannot be accurately shown in these diagrams. As described in the following section, the upgraded model includes: (1) a core region noding that has been expended from 10 to 40 cells and (2) significantly-expanded axial noding for the primary and secondary hydrodynamic regions and the tube and tubesheet heat structures in the SGs.

The SCDAP/RELAP5 PWR SBO calculations are performed in four sequential steps, which are described as follows.

In Step 1 (steady state) a model using the reactor vessel nodalization in Figure 1 and the coolant loop nodalization in Figure 2 is used to establish full-power steady-state conditions from which the SBO transient accident sequence is initiated. Note that Figure 2 shows the nodalization for only one of the coolant loops; identical models are used for all four coolant loops (with the exception of the pressurizer and surge line, which are connected only on Loop 1).

In Step 2 (time reset), the same model is used to perform a brief restart calculation only for the purpose of resetting the problem time to zero at the start of the SBO accident sequence.

In Step 3 (event initiation), the model continues using the nodalization schemes shown in Figures 1 and 2, but model features and changes are implemented to initiate the SBO accident sequence (such as tripping the reactor, the turbine and the reactor coolant pumps and disabling feedwater). This model is run from the time of SBO event initiation until the time when the core uncovers and superheated steam begins to enter the coolant loops.

In Step 4 (post core uncovery), significant modeling changes are made so as to permit the simulation of the two different coolant loop natural circulation modes shown in Figure 5. The mode shown on the right side of Figure 5 represents a countercurrent flow situation wherein hot steam is passed through the upper halves of the hot legs to the SG inlet plenum where mixing occurs (which results in a counter flow of hot and cool steam through the SG tubes) and cool steam is returned to the reactor vessel via counter flow in the lower halves of the hot legs. The mode shown on the left side of Figure 5 represents a flow of steam from the reactor vessel upper plenum, through the hot legs and completely around the coolant loop to the reactor vessel downcomer. The model selects the coolant loop circulation mode based upon whether or not the reactor coolant pump cold leg loop seal (Component 116 in Figures 2 and 3) is filled with water, a condition which blocks steam flow around the coolant loop. This selection is made independently for each of the four coolant loops in the model. The model therefore is capable of representing both the “recirculating” and “normal” coolant loop flow behaviors shown in Figure 5. The pressurizer surge line connects on the side of the Loop 1 hot leg. Figure 4 shows

the hot leg-to-surge line connection scheme employed for joining the surge line to the upper and lower sections of Hot Leg 1.

2.2 Summary of Model Improvements

This section summarizes upgrades implemented in the plant system model since it was last fully documented in Reference 8.

SG Secondary System Valve Leakage

During 2004 a series of calculations was performed with the SCDAP/RELAP5 Westinghouse four-loop plant model to support Probabilistic Risk Assessment (PRA) analysis of station blackout events. In those calculations, the SCDAP/RELAP5 model assumed a stuck-open relief valve failure on the SG 1 secondary system, but otherwise assumed no leakage of steam from the SG secondary system. As a result of the PRA analysis it was decided that, because of the long length of the accident sequence, small steam valve leakages could by themselves effectively depressurize the SG secondary system. The SCDAP/RELAP5 plant model was modified by eliminating the assumed SG 1 stuck-open valve failure and replacing it with small, 3.23 cm^2 (0.5 in^2), assumed steam leaks affecting the secondary systems on each of the four SGs. As a result of this model change, all SGs now are significantly depressurized by the time when the RCS piping structural failures are calculated to occur. The effect of the model change is to increase the differential pressure across all SG tubes, thereby increasing the potential for their failure, while at the same time increasing the probability of occurrence for the base case event sequence (because the additional failure probability associated with the stuck-open relief valve has been removed).

The steam leak paths from the top of each SG to an assumed atmospheric pressure condition are represented in the model by VALVEs 601 through 604. These valves are modeled to open at the start of the Step 3 calculation and remain open thereafter.

Individual Modeling of the Two Pressurizer PORVs

The plant design utilizes two identical pressurizer PORVs. In prior analyses, these valves were lumped together into a single component (VALVE 157, in Figures 2 and 3) with double the steam relief capacity of one PORV. The 2004 PRA analysis requested that certain event sequences be simulated in which only one of the PORVs is opened. To meet this request, the SCDAP/RELAP5 model was modified by splitting the relief function into two components using VALVEs 157 and 159, each of which has the steam relief capacity of one pressurizer PORV.

Disabling of Equipment Following Assumed Station Battery Depletion at Four Hours

The 2004 PRA analysis also requested that event sequences be simulated in which a finite station battery depletion time is assumed (previous analyses had assumed an infinite battery life). The battery life assumption affects the assumed operability of the pressurizer PORVs, the SG secondary PORVs and the pressurizer spray system. The valve control logic in the SCDAP/RELAP5 model was modified to include disabling (and failing closed) of the pressurizer

PORVs (VALVEs 157 and 159) and SG secondary PORVs (VALVEs 185, 285, 385 and 485) at the time of battery depletion, which is assumed to occur four hours subsequent to the initiation of the station blackout event. Disabling of the pressurizer spray system is discussed below.

Pressurizer Surge Line Connection Relocated to Side of Hot Leg

For plants of Westinghouse design, the location on the circumference of the horizontal hot leg where the pressurizer surge line is connected varies from plant to plant. In the SCDAP/RELAP5 plant model, it is assumed that the surge line connects on the side of the hot leg. For the SBO event sequence, the circumferential connection location is significant from the viewpoint of the temperature of fluid which enters the surge line. If the connection is located on the top of the hot leg, then predominantly hot steam from the upper regions of the hot leg is expected to enter the surge line, thereby resulting in an early surge line structural failure. If the connection is instead located on the side of the hot leg, then a lower-temperature mixture of steam from both the upper and lower hot leg regions is expected to enter the surge line, thereby delaying surge line structural failure.

In earlier analyses (for example, in References 3, 8 and 9) the hot leg-surge line connection scheme in the SCDAP/RELAP5 plant model produced behavior more representative of a top-mounted surge line than a side-mounted surge line. Figure 4 shows the SCDAP/RELAP5 nodalization for this connection. The model used for the earlier analyses employed only VALVEs 154 and 155 (and the short PIPE 156, which is needed to accommodate the difference in elevations between the upper and lower hot leg sections). This two-valve arrangement allows for liquid residing in the surge line to drain into the lower hot leg section while at the same time allowing for steam from the upper hot leg section to enter the surge line.

For the earlier analyses, the control logic for the valves was based on the status of the pressurizer draining process (wet or dry) and on the status of the pressurizer PORVs (open or closed). After the time when the pressurizer drains, the control logic opened both valves during periods when the PORVs were open, but opened only the valve to the upper hot leg during periods when the PORVs were closed. This modeling logic therefore resulted in only hot steam from the upper hot leg section entering the surge line during the extended periods between the PORV opening cycles. With the surge line connection modeled essentially to represent a top-mounted surge line, the earlier analyses indicated that surge line failure preceded hot leg failure.

The NRC performed CFD investigations into the behavior at the hot leg-surge line connection which indicated that the flow into the surge line is drawn equally from the upper and lower hot leg regions, even during periods when the pressurizer PORVs are closed. The SCDAP/RELAP5 hot leg-surge line connection modeling was revised to better match the more physical behavior seen in the CFD calculations. The model was revised by adding a new time dependent junction component, TMDPJUN 152, in parallel with VALVE 155 as seen in Figure 4. (A caution is needed here regarding nomenclature. A SCDAP/RELAP5 “time dependent junction” component can be used to specify flow as a function of any problem variable, not just time). Control Logic was first added to select either VALVE 155 or TMDPJUN 152 for the surge line-to-lower hot leg section connection, based on the status of pressurizer draining. Prior to pressurizer draining, VALVE 155 remains active, allowing for normal draining of liquid. Subsequent to pressurizer

draining, VALVE 155 is deactivated and TMDPJUN 152 is activated. Additional logic was added to control the flow through TMDPJUN 152 to be consistent with the flow through VALVE 154. After pressurizer draining, the revised SCDAP/RELAP5 model therefore calculates flows into the surge line which are drawn equally from the upper and lower hot leg sections, regardless of the pressurizer PORV status, which is the behavior seen in the CFD analysis.

Following the change in the surge line-hot leg connection modeling described above, the steam entering the surge line in the SCDAP/RELAP5 calculation is seen to be much cooler than in the earlier analyses. This difference was found to be sufficient to cause the surge line to fail subsequent to the hot leg in the new base case analysis reported here, where in the earlier analyses the surge line failed prior to the hot leg. Since the timing of SG tube failure is measured against the earliest failure of RCS piping (whether it be surge line or hot leg), this modeling change is seen to effectively reduce the SCDAP/RELAP5-calculated SG tube failure margins from those seen in the earlier analyses.

Addition of Pressurizer Spray System Components

A Phenomena Identification and Ranking Table (PIRT) exercise was conducted in September 2005 (Reference 11) to discuss the thermal-hydraulic behavior associated with pressurized water reactor containment bypass analysis. One of the recommendations from the PIRT was to add a representation of the pressurizer spray system to the SCDAP/RELAP5 plant model. Of interest is that the spray lines, which connect from the pump-discharge cold legs to the top of the pressurizer, represent a vent path which could affect the pressurizer draining process.

The spray valve system consists of two valves, a control valve and a trickle-spray valve, in each spray line. The control valves, which are used to limit RCS pressurization, open when the RCS pressure rises moderately above the normal operating pressure and close when it falls below the normal operating pressure. The range of RCS pressures (around the nominal operating pressure) over which the spray control valves function is small, 0.345 MPa (50 psi). The function of the trickle-spray valves is to allow small but continuous flows of cold leg fluid through the spray lines during normal operation. This trickle-spray flow warms the lines, which would otherwise cool via heat loss, thus reducing the potential for shocking the pressurizer with very cold spray water. During plant operation, the spray control valves open and close in response to changes in RCS pressure (these valves require onsite or offsite AC power or battery power for operation), while the much smaller trickle-spray valves always remain open.

Features representing the pressurizer spray system were added to the SCDAP/RELAP5 plant model. Referring to Figure 2, piping and valves were connected from PIPE 122, Cell 1 to the top of the pressurizer, PIPE 150, Cell 6 to represent the spray line in Coolant Loop 1. Similar model features were added in Coolant Loop 3 to represent the second spray line of the plant. Control logic was added for the spray valves, VALVEs 165 and 168, to simulate their automatic operation in the plant. The modeled valves function to represent the combination of the spray control and trickle-spray valves in each spray line. The SBO accident sequence is a high RCS pressure event so the spray control valves open and close in response to variations in the RCS pressure response, which are driven by the opening and closing of the pressurizer relief valves.

The spray control function is assumed to be lost (causing the spray control valves to fail closed) when the station batteries are depleted, four hours after the start of the station blackout sequence.

Preliminary calculations were performed before and after the spray system had been added to the model. The addition of the spray system was seen to have a small effect on the pressurizer draining process (somewhat faster draining was observed with the spray system installed) but the model addition caused no significant change in the key outcomes of the calculation.

Expansion of Core Axial Nodalization

A second PIRT recommendation (Reference 11) regarded evaluating the sensitivity of the station blackout calculation results to variations in the core region axial nodalization. In prior analyses, the core region had been represented using five vertical channels with 10 axial nodes in each. The sensitivity of calculation results to finer core axial nodalization was evaluated using models employing 20 and 40 core axial nodes. This evaluation indicated that the thermal-hydraulic response within the core region itself was sensitive to the axial noding. Increasing the number of axial nodes was found to accelerate the progression of the core damage process.

The cause of this acceleration is believed to be related to the nature of flow patterns within the core. Even though the average total core flow rates may be the same whether using tall or short core nodes, the use of short nodes tends to create local regions (in cells with small fluid volumes) where the flow slows or stagnates, which can accelerate the fuel damage process. Once started locally, flow blockage and other effects of core damage can cause the spread of damage into adjacent regions of the core. However, the evaluation of the sensitivity to the core axial noding also showed that increasing the number of nodes did not significantly affect the response of important calculated parameters external to the core (such as hot leg and SG tube steam temperatures), nor did it affect the calculated SG tube failure margins.

In summary, expansion of the core axial nodalization was seen to accelerate the progression of core damage. But for event sequences where the RCS pressure remains high (such as the base case), core melting was never seen to precede structural failure of the hot leg and no significant effects of core nodalization variation were observed in the calculated SG tube failure margins. (For some previously-analyzed event sequences, see Reference 9, where the RCS depressurizes due to high assumed RCP shaft-seal or other leakage, core damage was seen to precede the RCS piping failure). Because the finer SCDAP/RELAP5 core axial nodalization is believed to better simulate the physical core behavior, the model employed for the base case calculation in Sections 3.1 and 3.2 employs 40 axial nodes.

Expansion of Axial Nodalization in the SG Tubesheet Region

A third PIRT recommendation (Reference 11) regarded the sensitivity of results to the axial nodalization in the SG tubesheet and tube regions. Prior analyses had been performed using an axial nodalization which included a single tube node for the region inside the tubesheet and four long tube nodes between the top of the tubesheet and the top of the tube U-bend. The PIRT recommendation was to increase the axial nodalization for the regions within the tubesheet and

active tubes, with particular attention given to expanding the nodalization for the active tube region immediately above the top of the tubesheet.

The models for all four SGs in the SCDAP/RELAP5 plant model were modified to address this PIRT recommendation and the base case calculation presented in this report was performed with the expanded SG nodalization. The axial regions within the tubesheets were expanded from one to two nodes. The axial regions for the active tubes just above the tubesheet were expanded from one to five nodes, including four small, 0.3048-m (1.0-ft), nodes immediately above the tubesheet. Nodalizations for the remaining active tube regions were expanded by doubling the number of axial nodes. It is noted that the model modifications described here reflect consistent expansions of the nodalizations employed for the primary-side fluid inside the tubes, the tube wall heat structures, and the secondary-side fluid in the SG boiler regions.

Comparisons were made of preliminary calculations performed using the original and revised SG tube region nodalizations. The results of these comparisons are as follows. The expanded nodalization inside the tubesheet region led to a small, 4-K (7-^{o}F), reduction in the temperature of steam entering the average tube region. The expanded nodalization in the lower active tube region led to a 27-K (49-^{o}F) increase in the average tube metal temperature for the first active tube region above the tubesheet. For the hottest tube, the metal temperature increase was much larger, 68 K (122 ^{o}F). These increases result because with finer axial nodalization the tube temperatures are now cited at a lower elevation, closer to the tubesheet (at the center of a short node) rather than at a higher elevation, further away from the tubesheet (at the center of a long node). The expanded SG nodalization was seen to have only a small effect (a 0.5 reduction in the tube stress multiplier) on the average SG tube failure margin. However, the expanded SG nodalization was seen to greatly reduce (in fact, completely eliminate) the tube failure margin for the hottest tube. With the original SG nodalization, a stress multiplier of 1.5 was required to cause the hottest tube to fail before the hot leg. With the revised SG nodalization, the hottest tube with a stress multiplier of 1.0 (i.e., a non-degraded tube) is predicted to fail prior to the hot leg.

Revised Estimation of Hot Leg Flows and Other Parameters Determined from CFD Analyses

The SCDAP/RELAP5 system model analyses are performed by incorporating flow resistance adjustments in the SG inlet plenum region for the purpose of matching target values for the mixing parameters. In prior analyses, the mixing parameters were the hot mixing fraction, cold mixing fraction, recirculation ratio and SG power fraction. While the hot and cold mixing fractions relate strictly to the splitting of flows from the SG tubes as they enter the SG inlet plenum, the recirculation ratio relates to the ratio of the tube region and hot leg region flows and the SG power fraction relates to the percentage of the integrated core heat which is deposited into the SGs. From a practical perspective, the rate at which heat is transported from the core to the SGs is proportional to the hot leg flow rate. Therefore, the SG power fraction represents a proxy for the hot leg circulating flow rate (i.e., toward the SG in the upper hot leg section and toward the reactor vessel in the lower hot leg section).

During a meeting to review the SCDAP/RELAP5 plant system calculation methods employed for this project (Reference 12) the Advisory Committee for Reactor Safeguards (ACRS)

commented that a modeling approach using a target value for the SG power fraction was questionable. The ACRS concern was that the portion of RCS heat deposited in the SGs should be a calculated output variable from the simulations, not a target variable to be achieved through model adjustments.

The plant model modifications described in this section were implemented both to respond to this ACRS concern and to update the model for improved understanding of the fluid mixing processes that has resulted from recent CFD analyses.

To address the SG power fraction issue, the SCDAP/RELAP5 modeling process was revised by replacing the target value for SG power fraction with a target value for hot leg discharge coefficient. Reference 13 describes experiments conducted for the purpose of evaluating buoyancy-driven flows through horizontal ducts connecting two tanks containing fluids of different densities. The experiments correlated the volumetric flow rate (Q) in the horizontal duct, the average fluid density (ρ) and the difference between the two tank fluid densities ($\Delta\rho$) by defining a hot leg discharge coefficient (C_D):

$$Q = C_D \left[g \left(\Delta\rho / \rho \right) D^5 \right]^{1/2}$$

where g is the acceleration due to gravity.

In the plant, the hot leg is analogous to the horizontal duct in the experiments and the reactor vessel and SG inlet plenum are analogous to the two tanks. The SG power fraction and the hot leg discharge coefficient both characterize the hot leg flow. Therefore, changing the SCDAP/RELAP5 model so that it employs a target hot leg discharge coefficient consistent with experiments provides an improved representation for the physical hot leg flow.

CFD analyses were performed to increase understanding of the fluid mixing processes present in the hot leg, SG inlet plenum and SG tube regions of a Westinghouse four-loop plant during a station blackout event. The CFD analyses resulted in the following recommendations for the target mixing parameters to use in the SCDAP/RELAP5 system analyses for the Westinghouse four-loop plant.

Hot Leg C_D = 0.12
Hot Mixing Fraction = 0.85
Cold Mixing Fraction = 0.85
Recirculation Ratio = 2.0
SG Tubes in Hot / Cold Regions: 41% / 59%

For the base case analysis presented in Section 3.2, flow coefficients in the four SG inlet plenum regions of the SCDAP/RELAP5 model were adjusted to achieve the above target values for hot leg C_D, hot and cold mixing fractions and recirculation ratio. The model was also modified to represent a desired 41%/59% hot/cold split of the SG tube regions. Recent analyses (References 8 and 9) had assumed a 50%/50% tube split. (It is noted that in the earlier analyses a 35%/65% split was used, based on Westinghouse 1/7th-scale transient tests. The change to a 50%/50% split was subsequently made based on Westinghouse 1/7th-scale steady state tests). The recent

analyses also assumed 10% tube plugging in each SG and this assumption was retained for the calculations presented in this report. While the SG power fraction no longer represents a target parameter for which the model is adjusted, calculated results for SG power fraction are presented for the calculations in this report for the purpose of comparison with prior analyses.

Additional Output Data to Support Detailed Structural Analysis

Model features were added to generate calculation output in a form that facilitates detailed stress analyses performed by others in the project using the ABAQUS computer code. The additional data relate to separation of the various convection and radiation wall heat transfer components for the hot leg and pressurizer surge line inside wall surfaces, and enhancement of the hot leg wall inside surface convection heat transfer coefficient based on recent CFD studies. The output data added to facilitate the detailed structural analysis are listed in Appendix A.

Additional Output Data to Support Energy Balance Analysis

Model features were added to facilitate an evaluation of the flow of energy into, within and out of the RCS during the base case calculation. The energy analysis and the added model features are described in Section 3.3.

Additional Output Data to Support Uncertainty Evaluation

The SCDAP/RELAP5 Westinghouse four-loop plant station blackout base calculation reported in Section 3.2 is to be used as the reference case for a subsequent evaluation of the uncertainties in key calculation parameters. To facilitate the uncertainty analysis, features to output results for key uncertainty study parameters were added to the model, as described in Section 3.4.

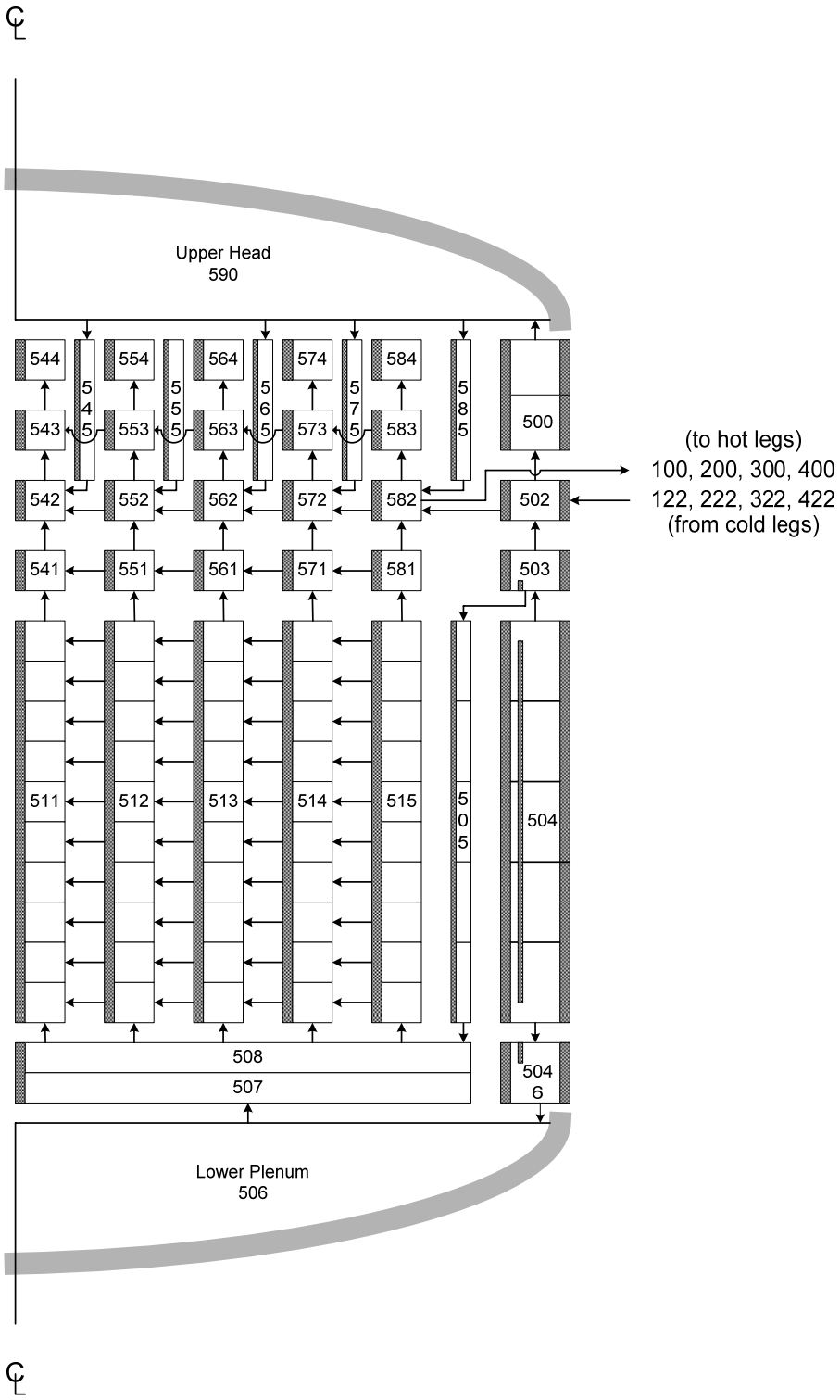

Figure 1. Reactor Vessel Nodalization.

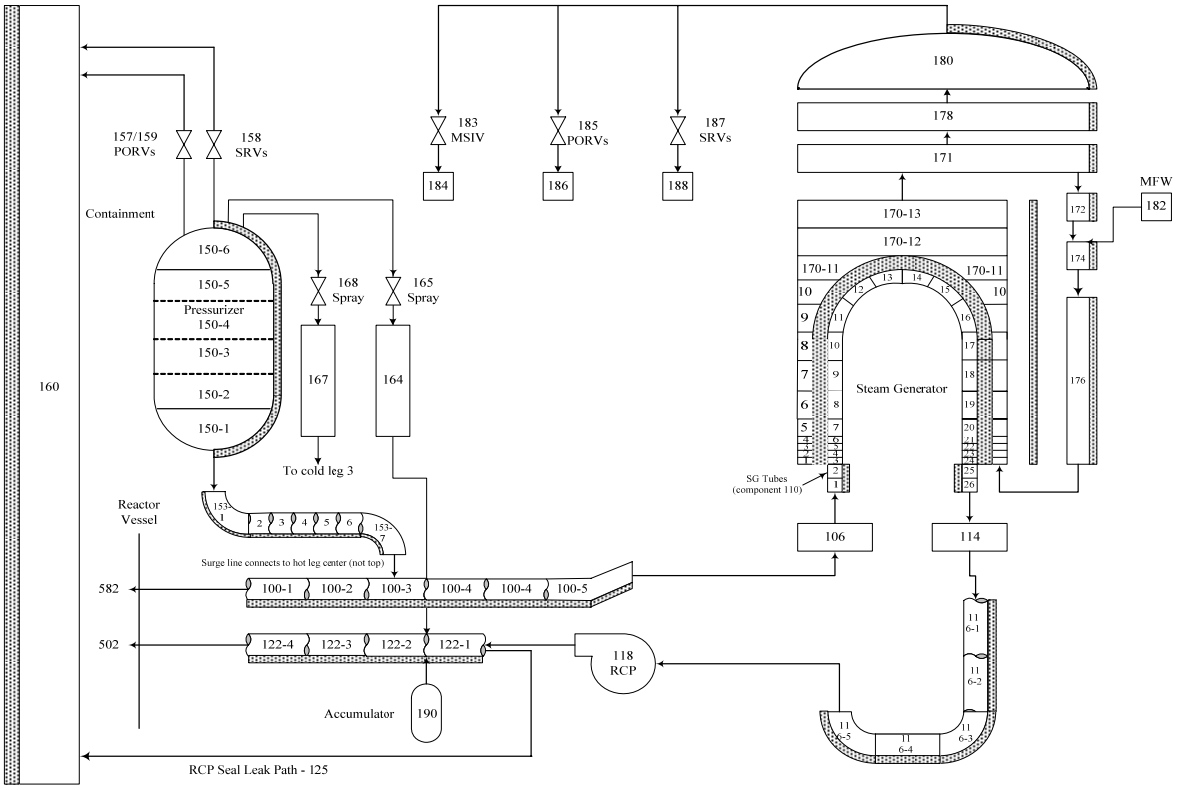

Figure 2. Loop Nodalization Excluding Provisions for Countercurrent Natural Circulation.

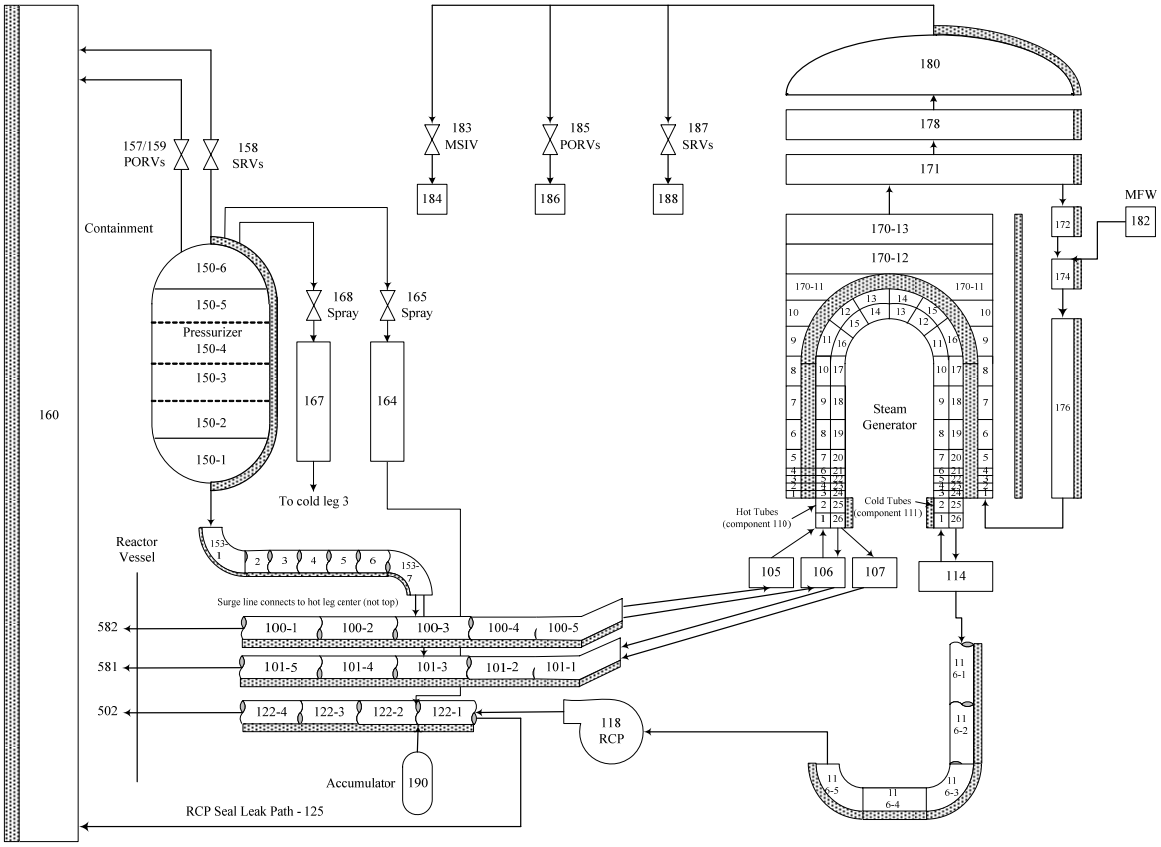

Figure 3. Loop Nodalization With Provisions for Countercurrent Natural Circulation.

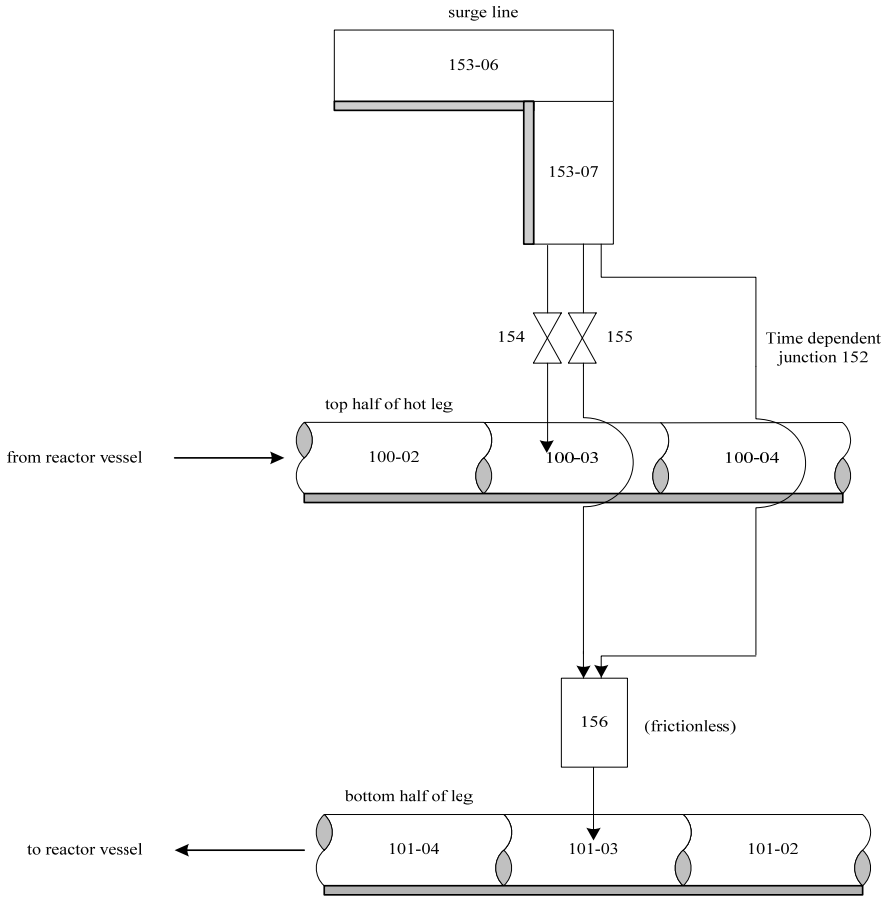

Figure 4. Surge Line Connections to the Split Hot Leg During Natural Circulation.

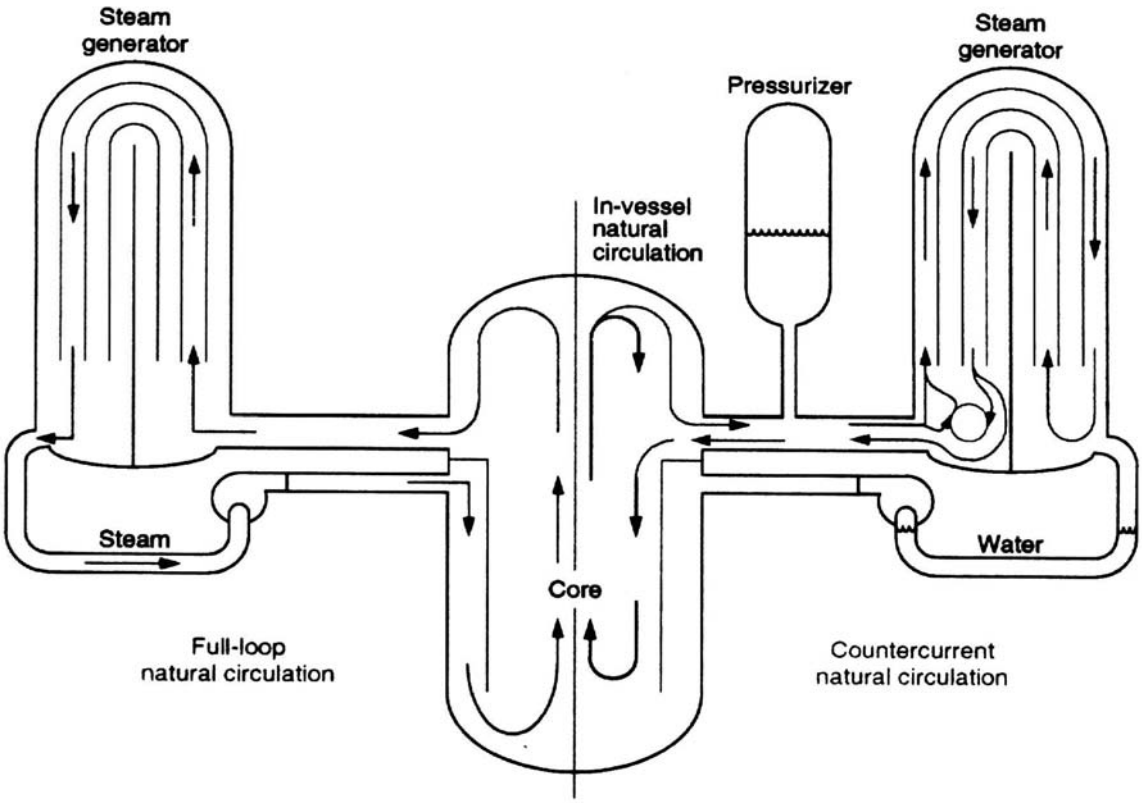

Figure 5. Natural Circulation Flow Patterns that Develop During Severe Accidents in PWRs with U-Tube Steam Generators.

3.0 BASE CASE CALCULATION RESULTS

This section documents the SCDAP/RELAP5 SBO base case calculation for a Westinghouse four-loop plant that will be used as the reference case in a subsequent study evaluating the uncertainties in this simulation. Section 3.1 documents the calculation of steady state conditions from which the transient SBO event sequence is begun. Section 3.2 documents the calculation of the transient SBO event sequence calculation. Section 3.3 evaluates the flow of energy into, out of, and within the primary RCS during the transient SBO calculation.

3.1 Steady State Calculation of Initial Conditions

The SCDAP/RELAP5 plant model was run to a steady solution over a period of 1,500 s. The file name of the input deck for the steady-state run is "uncbases1.i". The file name of a short SCDAP/RELAP5 restart calculation from the end point of the steady-state run (to reset time to zero) is "uncbases2.i". These are Steps 1 and 2 of a sequential four-step SCDAP/RELAP5 calculation process, as described in Section 2.

The calculated conditions from the end of the SCDAP/RELAP5 steady-state run are compared in Table 1 with the target values for a typical Westinghouse four-loop plant during normal full-power operation. The comparison indicates that the code-calculated parameters are in excellent agreement with the desired plant values. The calculated steady-state solution therefore represents an acceptable set of initial conditions from which to start the transient SBO accident simulation.

Table 1. SCDAP/RELAP5 Full-Power Steady State Results.

Parameter	Target Value[a]	SCDAP/RELAP5 Calculated Value
Reactor power (MW_t)	3,250	3,250
Pressurizer pressure (MPa)	15.51	15.509
Pressurizer water/steam volume (%)	60/40	61.1/38.9
Total RCS coolant loop flow rate (kg/s)	17,010	17,010
Cold leg temperature (K)	549.9	549.90
Hot leg temperature (K)	585.5	585.45
SG secondary pressure (MPa)	4.964	4.892
Feedwater temperature (K)	493.5	493.48
Steam flow rate per SG (kg/s)	440.9	439.9
Liquid volume per SG (m^3)	52.05	52.27

a. Target values are based on information for a typical Westinghouse four-loop PWR.

3.2 Transient Station Blackout Calculation

Accident Event Sequence Description

The sequence of events simulated in the SCDAP/RELAP5 SBO base case transient calculation is summarized as follows.

A loss of off-site AC power occurs when the reactor is operating at full power and with a 10% tube plugging condition in each of the four steam generators (SGs). The diesel-electric generators fail to start and as a result all AC plant power sources are lost. The loss of AC power results in reactor and turbine trips and the coast-down of the four reactor coolant pumps (RCPs). The letdown flow is isolated and the charging system functions of pressurizer level control and RCP seal injection are lost. The high and low pressure safety injection systems are not available because of the AC power loss. The accumulator systems are available for injecting coolant into the cold legs should the reactor coolant system (RCS) pressure fall below the initial accumulator pressure, 4.24 MPa (615 psia). The main feedwater flow stops and the motor-driven auxiliary feedwater (AFW) system is unavailable as a result of the AC power loss. The turbine-driven AFW system has an independent failure-to-start assumption in the event sequence being modeled, so no feedwater is available following the loss of AC power. A station battery life of four hours is assumed; after that time motor operated valves, such as the pressurizer and SG power operated relief valves (PORVs) are not considered to be operable.

The SG secondary system pressures rise because the feedwater and steam flow paths are isolated at the beginning of the event sequence. The SG power operated relief valves (PORVs) open to limit the pressure increase. Minor steam leak paths from the SGs are assumed which have the effect of slowly depressurizing all four SGs over a period of about two hours after the SG water inventory has boiled off. A steam leak flow area of 3.23 cm^2 (0.5 in^2) is assumed in each SG.

The event sequence assumes that the loss of RCP seal injection cooling flow results in partial failures of the RCP shaft seals in all four coolant pumps at the time the SBO event begins. An initial 21 gpm per pump leak rate of RCS liquid around the shaft seals into the containment is assumed. The seal leak path characteristics and flow areas are not changed over the course of the event sequence and the leak flow rates are determined by the transient fluid conditions calculated in the pumps and containment.

This low-probability event sequence results in a severe accident because none of the systems that provide normal core cooling are assumed to be operable. For a while, buoyancy-driven coolant-loop natural circulation carries hot water from the core through the SGs, transferring heat to the SG secondary water inventory. The SG water inventory is boiled and the steam is released through the SG PORVs. Since none of the feedwater systems are available, the secondary water inventory declines and is eventually fully depleted. After that time, the core decay power heats and swells the RCS water, increasing its temperature and pressure. During this process, the RCS pressure increase is limited by the opening of the pressurizer PORVs and the pressurizer safety relief valves (SRVs). However, the RCS fluid lost through those valves is not recoverable so the RCS inventory continuously declines. Eventually, the RCS inventory loss becomes extreme, the

core uncovers and the fuel starts to heat up. The fuel heat up leads to an exothermic oxidation process between the steam and the fuel rod cladding that adds heat to the fuel in addition to the decay heat from the fission process.

The basic physical processes of this event sequence during the period when the steam temperatures are rising regard the transport of hot steam from the core outward into the other regions of the reactor vessel and coolant loops. Of main concern is which structural components first reach their high-temperature failure points. A failure of SG tubes leads to discharge of radioactivity from the RCS into the SG secondary system, from which it may be released to the atmosphere via SG PORVs or SRVs. This type of release is referred to as "containment bypass." A failure of the reactor vessel or reactor coolant piping (such as the hot legs or pressurizer surge line) leads to discharge of the reactivity into the containment, from which the potential releases to the atmosphere are significantly lower. Further, a failure of the reactor vessel or reactor coolant piping depressurizes the RCS, which reduces stresses on the SG tubes and likely prevents their failure. Even in the event of SG tube failures subsequent to other RCS component failures, the reduced pressure inside the tubes will not result in a significant containment bypass release to the atmosphere.

Base Case Transient Calculation Results

The transient SBO event sequence described above was simulated using the SCDAP/RELAP5 plant model, starting from time zero at the time of the loss of off-site power. The transient calculation is performed as Steps 3 and 4 of a four-step SCDAP/RELAP5 modeling process as described in Section 2. The file name of the Step 3 input model, which is used from time zero until the time when the core uncovers, is "uncbases3.i". The file name of the Step 4 input model, which incorporates the split hot leg and SG tube modeling configuration after the time when the core uncovers, is "uncbases4.i".

The SCDAP/RELAP5 calculated sequence of events for the SBO base case is shown in Table 2. The calculated time history results of key parameter are shown in Figures 6 through 27 and are summarized as follows.

The RCS pressure response is shown in Figure 6. After a small initial increase caused by the effects of the reactor and turbine trips, the RCS pressure declines in response to the cooling provided by heat removal to the SGs and by the RCP shaft seal leaks. Figure 7 shows the SG secondary pressure responses and Figure 8 shows the RCP leak flow responses. The RCS depressurization continues until the SG secondary liquid inventories, as shown in Figure 9, have been boiled and released to the atmosphere through the SG PORVs. After the SG heat sink is lost, the cooling afforded by system heat loss to containment and pump shaft seal leak flow is insufficient to remove the RCS heat load and the RCS pressure increases to the opening setpoint pressures of the pressurizer PORVs and SRVs.

Figures 10 and 11, respectively, show the pressurizer PORV and pressurizer SRV flows. After SG dryout, the RCS pressure increase is limited by multiple cycling of the PORVs and also by two cycles of the SRVs during the period with the most challenging RCS pressure conditions. This challenge is presented when the increasing temperatures cause the RCS fluid to expand

sufficiently to completely fill the pressurizer with water. The pressurizer level response is shown in Figure 12.

The mass lost through the pressurizer PORVs and SRVs and through the RCP shaft seal leakage paths depletes the RCS inventory, the core uncovers and superheated steam flows out from the reactor vessel into the coolant loops starting at 9,222 s. Water remains trapped in the cold leg RCP-suction loop seal piping, thus blocking the path for the steam to flow all the way around the coolant loops. This blockage provides the conditions necessary for countercurrent flow through the hot legs and SG tubes. Figure 13 shows the void fractions calculated in the bottom cells of the loop seal piping. The loop seal piping in all four loops remains water filled, with only minor bubbling of steam through the loop seals, during the period of the maximum RCS pressurization. The increase in the void fraction seen at the end of the run results from relocation of a portion of the core to the reactor vessel lower head as is discussed later.

Following core uncovery, countercurrent flow of superheated steam is calculated through two circulation flow paths within each coolant loop. In one circulation path, hot steam flows upward from the SG inlet plenum through a portion (41%) of the SG tubes and cool steam returns from the SG outlet plenum through the remaining portion of the SG tubes, flowing downward as it reaches the SG inlet plenum. In the other circulation path, hot steam flows through the upper half of the hot leg to the SG inlet plenum and cooler steam is returned from the SG inlet plenum to the reactor vessel through the lower half of the hot leg. Mixing between these two circulation paths occurs in the SG inlet plenum. In Coolant Loop 1, which contains the pressurizer, steam may be diverted from the hot leg into the pressurizer surge line, and the behavior of parameters shown in the time-history plots is generally affected by the cyclic opening and closing of the pressurizer PORVs.

The flow rates in the SG 1 forward-flowing (hot) and reverse-flowing (cold) average tube sections are shown in Figure 14. The flow around this circulation path is driven by the buoyancy head created from the difference in steam densities (resulting from different temperatures) between the hot and cold tube sections. Referring to Figure 3, a positive driving head term is created in the normal upward-flowing tube region by the temperature difference between the hot steam in the tube section flowing upward from the inlet plenum (Component 110) and the cold steam in the section flowing downward to the inlet plenum (Component 111). Similarly, a negative driving head term is created in the normal downward-flowing tube region by the temperature difference between the hot steam and cold steam in the two tube sections. When these two driving head terms are added together, a net positive circulation-driving head is created because the steam temperature difference in the first term is larger than that in the second term. The declining trend in the tube circulation rate seen in Figure 14 results from two effects. First, because the initial rise in the temperature of the steam entering the SG is rapid and the SGs initially are cold, the steam temperature difference is initially large, but it declines as a result of the process which transfers heat to the SG. Second, because the entire system is experiencing a heatup, steam densities are generally declining, resulting in declining steam mass flow rates. To place the SG tube mass flow rates shown in Figure 14 into perspective, the 7.7 kg/s (17.0 lbm/s) hot tube section mass flow rate seen at 13,000 s corresponds to a steam velocity of 0.53 m/s (1.74 ft/s).

The flow rates in the Loop 1 upper and lower hot leg sections are shown in Figure 15. Unlike the SG tube circulation path where the flow rates in the hot and cold sections are the same, in the Loop 1 hot leg circulation path the flow through the upper section is greater than that in the lower section during periods when the pressurizer PORV is open (the PORV flow response is shown in Figure 10). The flow around the hot leg circulation path is driven by the buoyancy head created by the steam temperature and density differences between the two sections over the vertical portion of the hot leg and within the SG inlet plenum. The hot leg bends upward from its horizontal run to the SG inlet plenum, with an elevation rise of 0.924 m (3.03 ft) and the elevation span of the SG inlet plenum is 1.206 m (3.958 ft). The declining trend in the hot leg circulation rate results for the same reasons described above for the SG tube circulation path. To place the hot leg mass flow rates shown in Figure 15 into perspective, the 4.6 kg/s (10.1 lbm/s) upper hot leg section mass flow rate seen at 13,000 s corresponds to a steam velocity of 0.79 m/s (2.6 ft/s).

In addition to the SG tube and hot leg flow circulations, there are also flow circulations within the reactor vessel. Referring to Figures 1 and 3, flow of hot steam into the upper hot leg sections leaves the reactor vessel from Component 582 and the cooler steam flowing through the lower hot leg sections returns to the vessel at Component 581. The difference in densities between the hot and cool steam sets up circulation paths within the vessel. The cooler steam returning from the lower hot leg sections tends to flow downward through the peripheral core regions and then upward through the central core regions. Another circulation path also sets up in the reactor vessel upper plenum region, with hotter steam flowing from the core channel exits across the upper regions (Components 542, 552, 562, 572 and 582) to reach the entrances to the upper hot leg sections and with cooler steam flowing from the exits of the lower hot leg sections across the lower regions (Components 581, 571, 561, 551 and 541) toward the reactor vessel centerline. The vessel circulation is characterized in Figure 16, which shows the mass flow rates near the tops of one of the upward-flowing central core regions and one of the downward-flowing peripheral core regions (Core Channels 512 and 514, as shown in Figure 1). To place the core mass flow rates shown in Figure 16 into perspective, the 12.8 kg/s (28.2 lbm/s) central core channel mass flow rate seen at 13,000 s corresponds to a steam velocity of 0.50 m/s (1.6 ft/s).

The flow resistances of the SCDAP/RELAP5 plant model in the regions of the SG inlet plenum are preset so as to match the behavior of the hot leg discharge coefficient, recirculation ratio, hot mixing fraction and cold mixing fraction observed during Westinghouse 1/7th-scale experiments and CFD analyses simulating station blackout behavior. Figures 17 through 20 show the SCDAP/RELAP5-calculated responses for these inlet plenum mixing and flow parameters. Table 3 compares the smoothed SCDAP/RELAP5-calculated values for these parameters (averaged over the four coolant loops) with their nominal target values at 13,000 s. The calculated parameter values vary with the cyclic opening and closing of the pressurizer PORVs. The rate of variation increases significantly as the system heatup rate becomes large. 13,000 s was chosen as the time for the comparison in Table 3 because parameter values at that time remain relatively stable and yet are relatively close to the values experienced at the time when the critical structural failures occur. Smoothed data for these parameters are calculated only for the period after the circulation processes have been well established and before the occurrence of the creep rupture structural failures. Further, only data from times within that period when the pressurizer PORVs are closed is used in calculating the smoothed parameters. Table 3 shows

excellent agreement of the smoothed SCDAP/RELAP5-calculated and target values for hot leg discharge coefficient, hot and cold mixing fractions and recirculation ratio.

The responses of the hot leg discharge coefficients for the four coolant loops are shown in Figure 17. As described in Section 2, this parameter characterizes the countercurrent flow in a horizontal pipe between two tanks containing fluids of different densities. As shown in Table 3, the average SCDAP/RELAP5 calculated value for the hot leg discharge coefficient in the four coolant loops is within 0.6% of the 0.12 target value.

The recirculation ratio, hot mixing fraction and cold mixing fraction responses are shown in Figures 18, 19 and 20, respectively. The recirculation ratio is defined as the ratio of the SG tube mass flow rate to the hot leg mass flow rate. The mixing fractions are defined as the portions of the flow entering the SG inlet plenum which are directed to the "mixing" plenum (Cell 106 as seen in Figure 3). The hot mixing fraction is thus the portion of the upper hot leg flow which is directed to the mixing plenum while the cold mixing fraction is the portion of the "cold" tube return flow which is directed to the mixing plenum. As shown in Table 3, the target value for the recirculation ratio is 2.0 and the target value for the hot and cold mixing fractions is 0.85. The average SCDAP/RELAP5 calculated values for the hot and cold mixing fractions in the four coolant loops are within 0.4% of the target value. The average SCDAP/RELAP5 calculated value for the recirculation ratio in the four coolant loops is within 0.9% of the target value.

The responses of the SG power fractions are shown in Figure 21. This parameter is defined as the ratio of the heat removed to each SG (to the tubes, tubesheet, inlet plenum wall and outlet plenum wall) to the total core heat (fission product decay and fuel rod oxidation heat). The SG power fractions are calculated on an integrated basis, starting at the time of core uncovery. The power fractions increase after the core uncovers as the hot steam flows outward through the hot legs and into the SGs. A first peak in the SG power fractions occurs during the period when the fuel rod oxidation process is peaking. The oxidation heat is immediately absorbed by the fuel rods, thereby reducing for a time the fraction of the core heat that is absorbed by the SGs. After the oxidation process subsides, the excess heat that was absorbed in the fuel rods is dissipated into the steam and transported outward into the coolant loops and SGs, causing the SG power fractions to again rise. Note that no target value for SG power fraction is listed in Table 3, as was done in prior analyses. For this analysis, the previously-used target SG power fraction for the modeling process has been replaced with a target hot leg discharge coefficient. The calculated SG power fraction responses, which are shown in Figure 21 and listed in Table 3, are provided only for purposes of comparison with prior analyses.

The hydrogen generation rate response is shown in Figure 22. The oxidation process begins gradually as a result of metal water reaction on the exterior of the fuel rod cladding in the highest-power core regions. The oxidation rate increases rapidly as fuel temperatures climb and the process spreads into lower power regions of the core. The fuel rod oxidation process starts at 10,733 s and the peak oxidation rate is reached at 13,417 s. The major peak in the oxidation rate seen in Figure 22 occurs because the process accelerates as a result of fuel rod cladding rupture and the involvement of the cladding inner surfaces (in addition to the outer surfaces). The peak core oxidation power is 334.1 MW and during the period of its peak the oxidation power is the dominant contributor to the system heatup. To place the significance of the oxidation power into

perspective, at the time of its peak the oxidation power is 11.2 times the fission product decay power and 10.3% of the plant normal-operation full rated thermal power.

Figure 23 compares the thermal responses for the key structures in Loop 1. The data shown represent the average temperatures across the structure thickness at the hottest axial locations. The pressurizer surge line temperature presented is at the end of the line adjacent to the hot leg. The hot leg temperature presented is for the upper half of the hot leg adjacent to the reactor vessel. The average and hottest SG tube temperatures presented are for the upward-flowing tube sections just above the top of the tubesheet.

As the hot leg steam temperatures rise, the rates at which the structure temperatures increase vary, depending on the structure thickness. The temperatures of the thin-wall SG tubes respond quickly to an increasing steam temperature, while the temperature of the thicker pressurizer surge line responds more slowly and the still-thicker hot leg structure temperature responds even more slowly. As expected, because the hottest steam is modeled at its inlet, the temperature of the hottest SG tube structure increases more rapidly than the temperature of the average SG tube structure.

The start of the pressurizer surge line heatup is delayed until the pressurizer empties at 10,637 s. Before that time, liquid intermittently drains out of the pressurizer into the surge line during periods when the pressurizer PORVs are closed. This draining cools the steam inside the surge line and the surge line wall. This behavior affects the response of the surge line heat structure and not the hot leg or SG tube heat structures. After the pressurizer empties, the pressurizer PORVs continue to cycle and hot steam is drawn upward through the surge line without the cooling benefit afforded by liquid draining downward. The surge line wall is much thinner than the hot leg wall; the surge line thickness is 3.572 cm [1.406 inches] while the hot leg thickness is 6.350 cm (2.500 inches). Once pressurizer draining is complete, this difference in wall thickness causes the pressurizer surge line wall to heat up more rapidly than the hot leg wall.

Pressurizer PORV cycling ceases at 14,400 s (four hours after event initiation) when the station batteries are assumed to be depleted. Afterward, the RCS pressure increases, but not sufficiently to open the pressurizer SRVs (see Figures 6 and 11) until the very end of the transient calculation. The turnover in the surge line structure temperature in Figure 23 reflects the cessation of surge line steam flow. With neither the pressurizer PORVs nor SRVs opening, the flow of increasingly-hotter steam through the surge line stops and the heat loss from the outside of the surge line to the containment cools the surge line wall. Figure 24 shows a detailed view of the structure temperature responses from Figure 23 overlaid with the SCDAP/RELAP5-calculated failure times for the structures.

Figures 25 through 27 compare the Larson-Miller creep rupture damage indexes for the surge line, hot leg and SG tube structures. The damage index indicates the accumulation of creep damage as a fraction of the creep that will produce structural failure (i.e., failure occurs at the time the index value reaches 1.0). The creep rupture model allows use of a stress multiplier that represents the effect on the creep calculation corresponding to a specific degree of degradation in the strength of a structure due to other factors, such as cracks that were present before the accident event sequence started. For the surge line and hot leg structures only a stress multiplier

of 1.0 is used. A set of stress multipliers from 1.0 to 7.5, in increments of 0.5, is used for the SG tube structures as a means to introduce tube material strength degradation as an analysis variable..

Figure 25 compares the damage indexes for the pressurizer surge line and the four hot legs. The failure of Hot Leg 1 occurs first, followed by failures of Hot Legs 2, 3 and 4 and then by the failure of the surge line (the calculated creep rupture failure times for all structures in the model are listed in Table 4).

Figure 26 compares the damage indexes for Hot Leg 1 and the average tubes in SG 1. The figure shows that an average tube with a stress multiplier of 2.0 or lower is predicted to fail after the time when Hot Leg 1 fails. In other words, tubes that are subjected to the average steam conditions on the inside are not expected to fail before Hot Leg 1 as long as degradation of the tube strength has not progressed past the point where a tube will fail when subjected to a stress of only (1.0 / 2.0 =) 50% of the stress that would fail a non-degraded tube.

Figure 27 compares the damage indexes for Hot Leg 1 and the hottest tube in SG 1. This figure and the event times in Table 4 indicate that the hottest tube with a stress multiplier of 1.0 is predicted to fail 155 s prior to the time when Hot Leg 1 fails. In other words, even non-degraded tubes that are subjected to the hottest steam conditions on the inside are expected to fail before Hot Leg 1.

The evaluation of the hottest tube behavior is based on an assumption regarding the temperature of the steam which enters it. The hottest tube steam inlet temperature is determined from the Normalized Temperature Ratio (NTR), which is defined:

$$NTR = (T_{hottest\ tube} - T_{cold\ tube}) / (T_{upper\ hot\ leg} - T_{cold\ tube})$$

The denominator represents the total range of steam temperatures in the SG inlet plenum region, with the hottest steam entering the plenum from the upper hot leg section and the coolest steam entering the plenum from return flow through the cold average tubes. The NTR therefore indicates an inlet plenum temperature range from 0.0 to 1.0, with 1.0 representing the hot incoming flow from the hot leg and 0.0 representing the cold return flow from the tube bundle. Further information on the NTR and its selection can be found in Section 2.10 of Reference 8.

The base case run assumes a NTR of 0.625. Since the hottest tube is predicted to fail prior to the hot leg in the base case run, a side study was performed to evaluate the sensitivity of that finding to variation in the assumed NTR. A sensitivity run performed with the NTR reduced to 0.525 indicated that the time difference between hottest tube failure and hot leg failure is reduced from 155 s to 20 s, but the hottest tube (with 1.0 stress multiplier) still fails prior to the hot leg. By extrapolating the results from the base and sensitivity runs, it is estimated a NTR of 0.510 would result in coincident failures for the hottest tube and the hot leg. The file name of the sensitivity run input model is “ntr525.i”.

Note that the structural damage predictions provided with SCDAP/RELAP5 are intended to represent only rough indications of damage occurrence. These indications are useful when, for

example, comparing the damage potential for one accident sequence with the damage potential of another sequence. Damage predictions from which major project conclusions will be drawn will be made by other project participants, using the SCDAP/RELAP5-calculated pressures, steam temperatures and heat transfer coefficients as boundary conditions in detailed stress analysis models.

The SCDAP/RELAP5 calculation continued beyond the times of the hot leg and pressurizer surge line structural failures. A relocation of molten control rod absorber to the reactor vessel lower head is calculated (starting at 15,548 s), followed by a relocation of molten core fuel (starting at 17,038 s and representing approximately 15% of the core fuel) to the reactor vessel lower head region. The run failed at 17,189 s as a result of steam explosion effects caused by the molten core fuel slumping into the liquid-filled reactor vessel lower head region.

To facilitate analyses performed by others in the project, data for selected output channels from the revised SCDAP/RELAP5 station blackout base case calculation are provided on the CD which is available to others in the project. The selected additional data channels are identified in Appendix A.

Table 2. Sequence of Events from the SCDAP/RELAP5 SBO Base Case Calculation.

Event Description	Event Time (s)
TMLB' SBO event initiation (loss of AC power, reactor trip, turbine trip, feedwater flow stops, reactor coolant pump trip, reactor coolant pump shaft seal leaks begin, steam generator steam leaks begin).	0
Reactor coolant pump rotors coast to a stop, coolant loop natural circulation begins	106
SG dry-out (99% void in bottom secondary cell), SG1 / SG2 / SG3 / SG4.	5,905 / 5,983 / 5,983 / 6,018
Pressurizer PORV cycling begins.	7,148
First pressurizer SRV cycle, open/close.	8,605 / 8,714
Loop natural circulation flow interrupted by steam collecting in SG tube U-bends, SG1 /SG2 /SG3 / SG4.	8,673 / 8,579 / 8,595 / 8,618
Second pressurizer SRV cycle, open / close.	9,033 / 9,087
Collapsed liquid level falls below the top of the fuel heated length (6.323 m above bottom of lower head).	9,150
Steam at the core exit begins to superheat, hot leg countercurrent circulation begins.	9,222
Collapsed liquid level falls below the bottom of the fuel heated length (2.666 m above bottom of lower head).	10,079
Pressurizer empties	10,637
Onset of fuel rod oxidation.	10,733
First control rod cladding failure.	12,150
First fuel rod cladding rupture.	13,003
Peak fuel rod oxidation rate reached.	13,417
Hottest SG tube creep rupture failure (SG 1, non-degraded, 1.0 stress multiplier).	13,475
Hot Leg 1 fails by creep rupture.	13,630
Hot Legs 2, 3 and 4 fail by creep rupture.	13,700
Pressurizer surge line fails by creep rupture.	13,960
Station batteries assumed to be depleted, motor operated valves are no longer operable.	14,400
Average SG tube creep rupture failure (SG 1, non-degraded, 1.0 stress multiplier).	14,590
First relocation of control rod absorber material to reactor vessel lower head.	15,548
Approximately 15% of core fuel relocates to the reactor vessel lower head.	17,038
End of calculation. Run fails due to steam explosion resulting from molten core slumping into the water-filled reactor vessel lower head.	17,189

Table 3. Comparison of Target and SCDAP/RELAP5-Calculated SG Inlet Plenum Mixing and Flow Parameters.

Parameter	Target Value	SCDAP/RELAP5 Calculated Value
Assumed Split of SG Tubes into Hot/Cold Regions	41%/59%	41%/59%
Average Hot Leg Discharge Coefficient	0.12	0.1207
Average Hot Mixing Fraction	0.85	0.853
Average Cold Mixing Fraction	0.85	0.847
Average Recirculation Ratio	2.0	1.982
Portion of the Integrated Total Core Heat Addition which is Absorbed in the Four SGs	Not Applicable	28.4%

Table 4. Summary of Calculated Creep Rupture Failure Times from the Base Case Calculation.

Structure		Calculated Failure Time (s)
Pressurizer surge line		13,960
Hot Leg 1 / Hot Leg 2 / Hot Leg 3 / Hot Leg 4		13,630 / 13,700 / 13,700 / 13,700
SG 1 / SG 2/ SG 3 / SG 4		
Average SG Tube, Stress Multiplier:	1.0	14,590 / 14,650 / 14,630 / 14,650
	1.5	13,930 / 13,970 / 13,960 / 13,970
	2.0	13,660 / 13,675 / 13,670 / 13,675
	2.5	13,510 / 13,525 / 13,520 / 13,525
	3.0	13,410 / 13,420 / 13,420 / 13,425
	3.5	13,355 / 13,365 / 13,360 / 13,365
	4.0	13,225 / 13,240 / 13,235 / 13,240
	4.5	13,150 / 13,170 / 13,160 / 13,170
	5.0	13,115 / 13,135 / 13,125 / 13,135
	5.5	13,095 / 13,115 / 13,105 / 13,115
	6.0	13,085 / 13,105 / 13,095 / 13,105
	6.5	13,080 / 13,100 / 13,090 / 13,100
	7.0	13,075 / 13,095 / 13,085 / 13,095
	7.5	13,075 / 13,095 / 13,085 / 13,095
SG 1		
Hottest SG Tube, Stress Multiplier:	1.0	13,475
	1.5	13,395
	2.0	13,320
	2.5	12,950
	3.0	12,590
	3.5	12,325
	4.0	12,170
	4.5	12,080
	5.0	12,045
	5.5	12,025
	6.0	12,015
	6.5	12,010
	7.0	12,005
	7.5	12,005

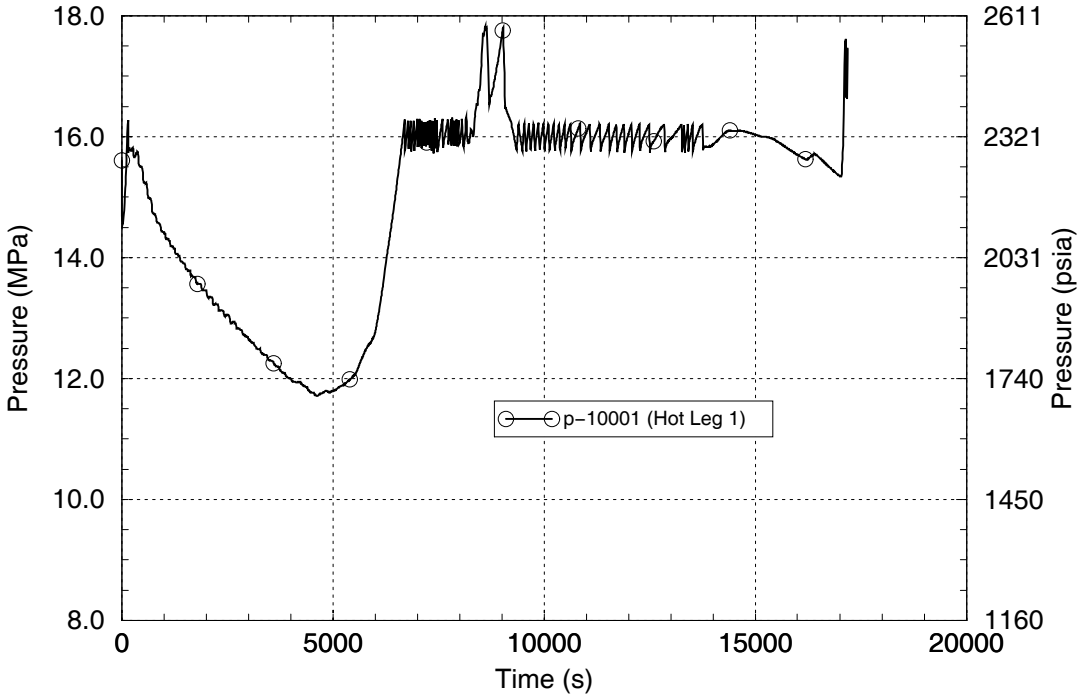

Figure 6. Reactor Coolant System Pressure.

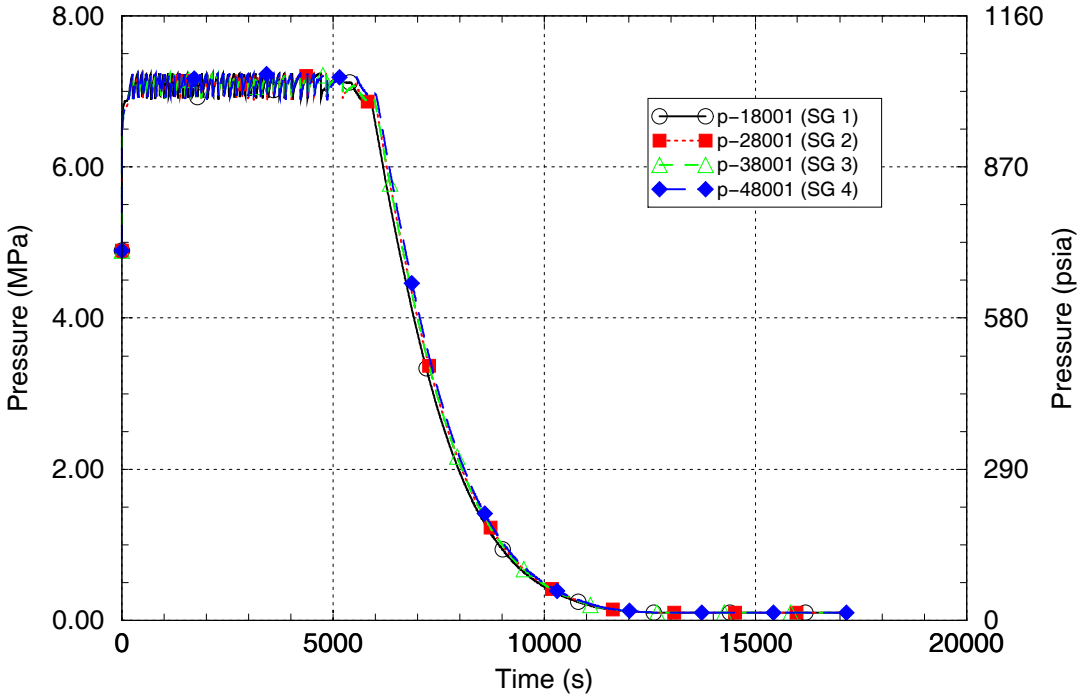

Figure 7. Steam Generator Secondary Pressures.

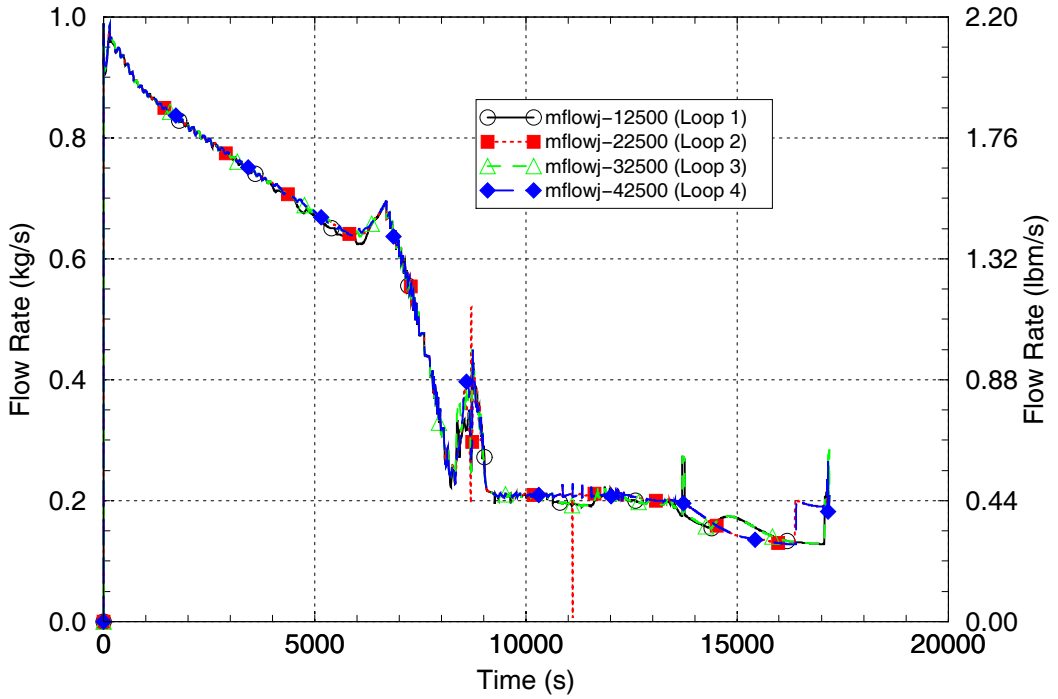

Figure 8. Reactor Coolant Pump Shaft Seal Leakage Flows.

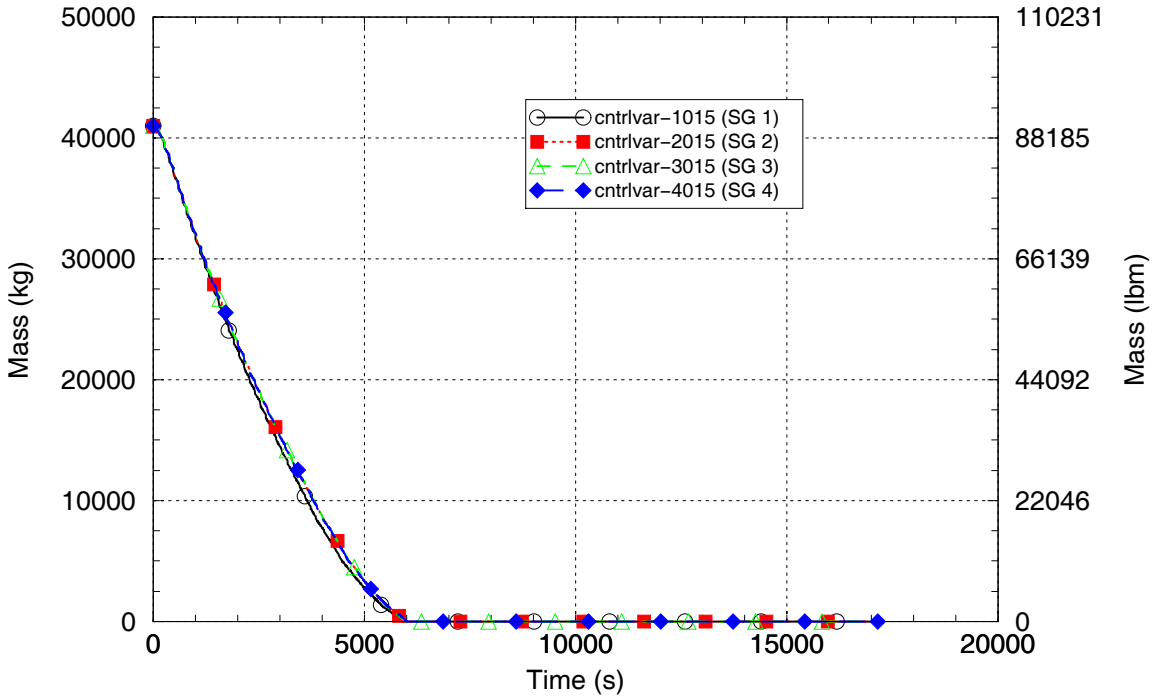

Figure 9. Steam Generator Secondary Liquid Masses.

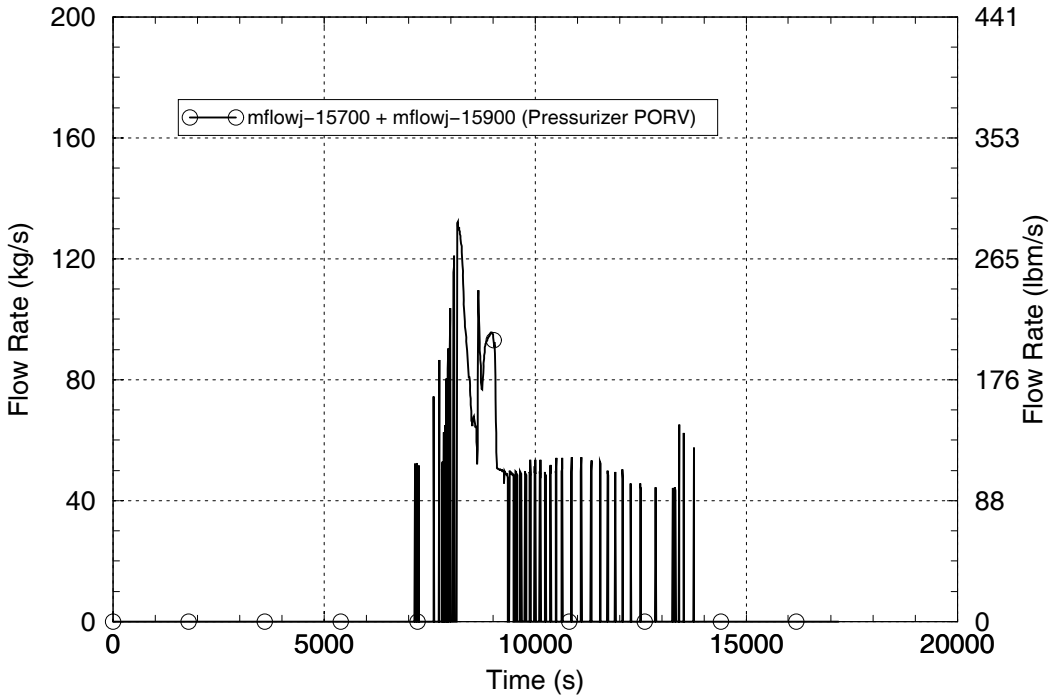

Figure 10. Total Pressurizer PORV Flow.

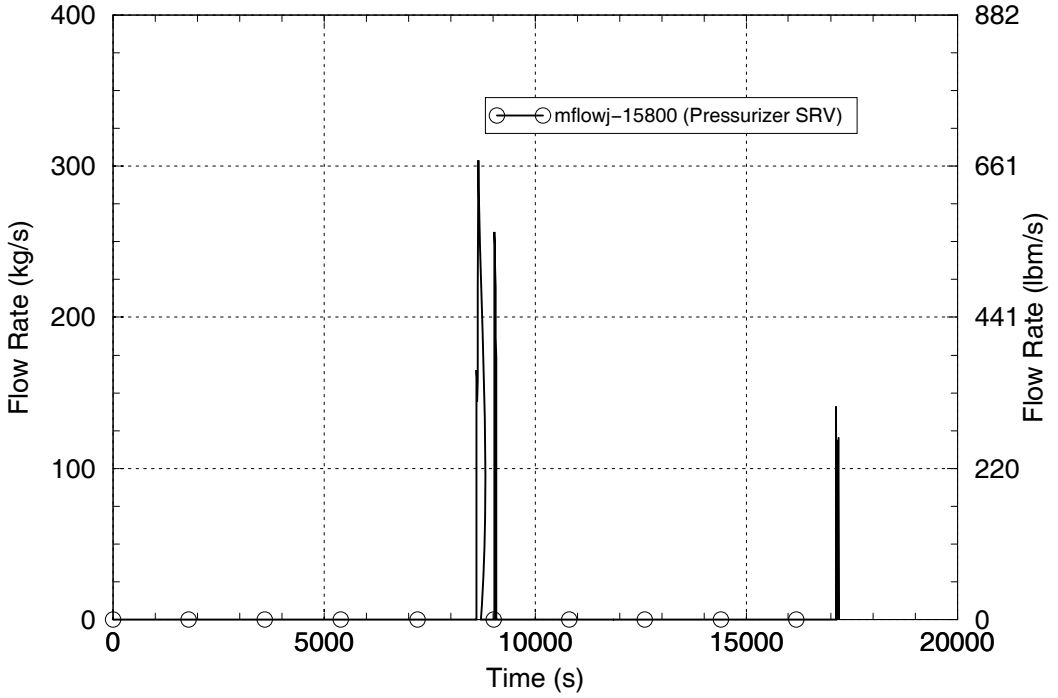

Figure 11. Pressurizer SRV Flow.

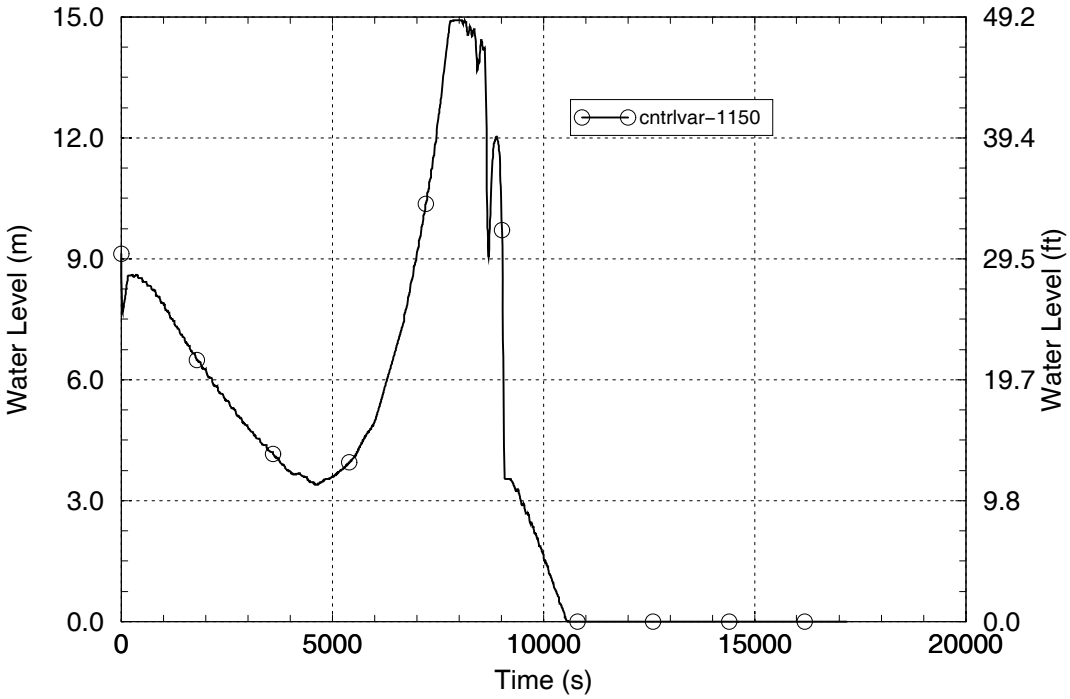

Figure 12. Pressurizer Level.

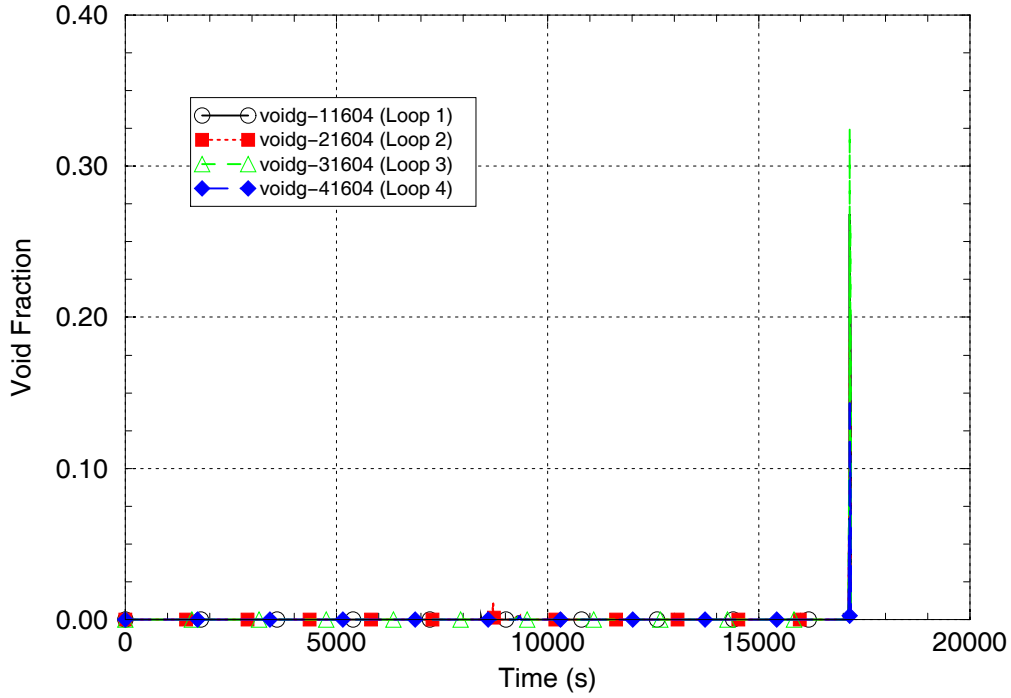

Figure 13. Reactor Coolant Pump Loop Seal Void Fractions.

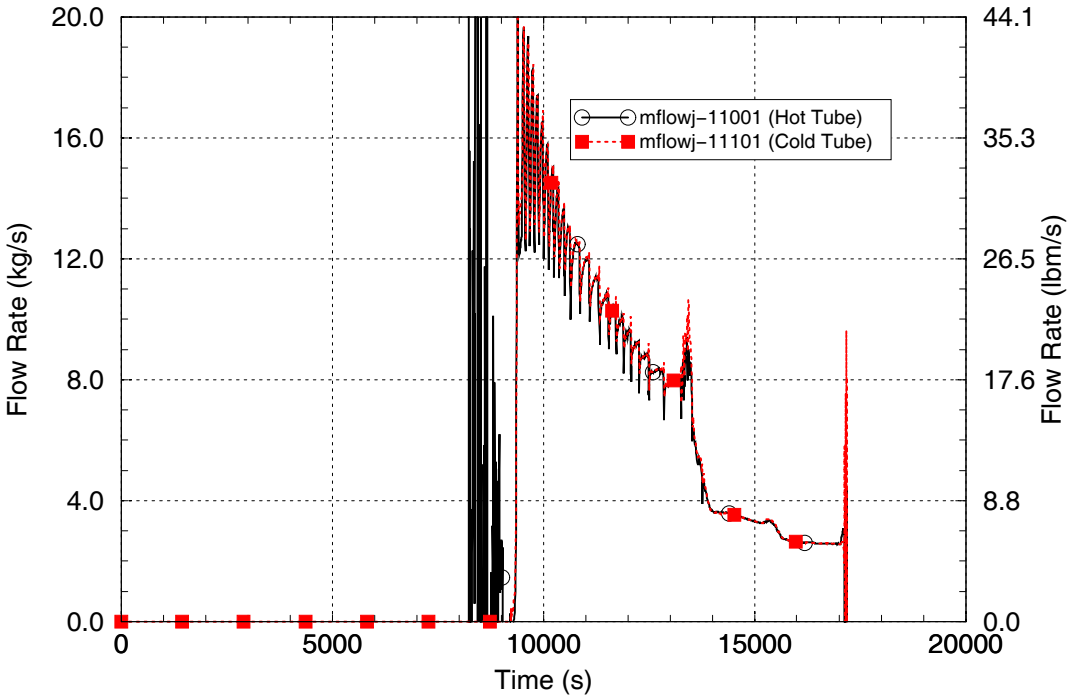

Figure 14. SG 1 Hot and Cold Average Tube Flows.

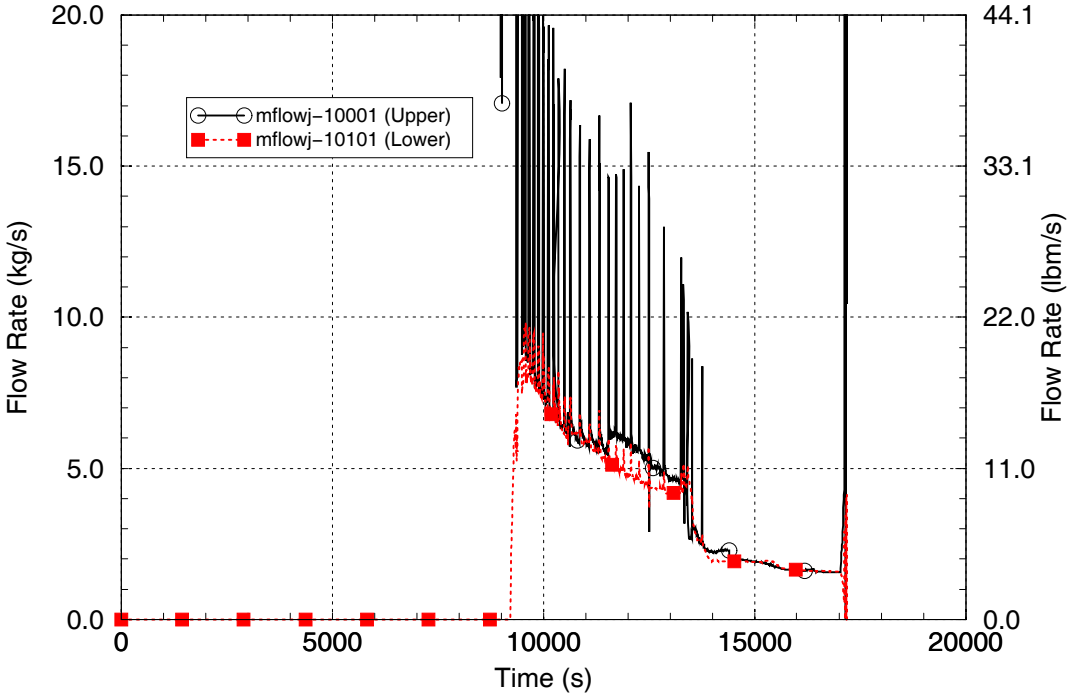

Figure 15. Hot Leg 1 Upper and Lower Section Flows.

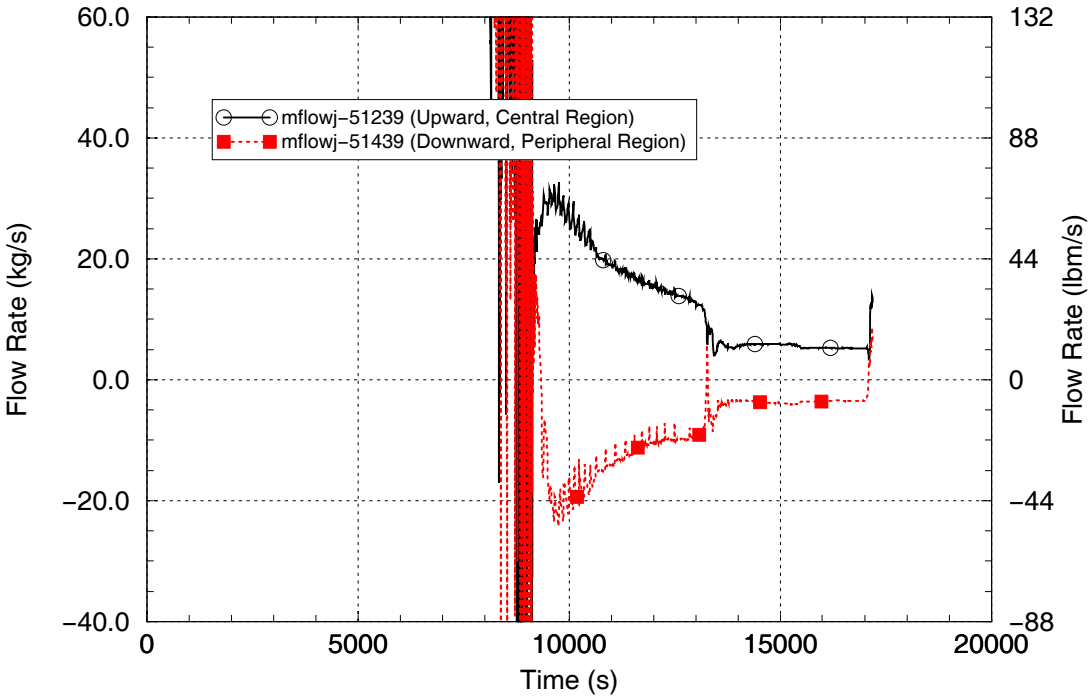

Figure 16. Vessel Circulation Flows.

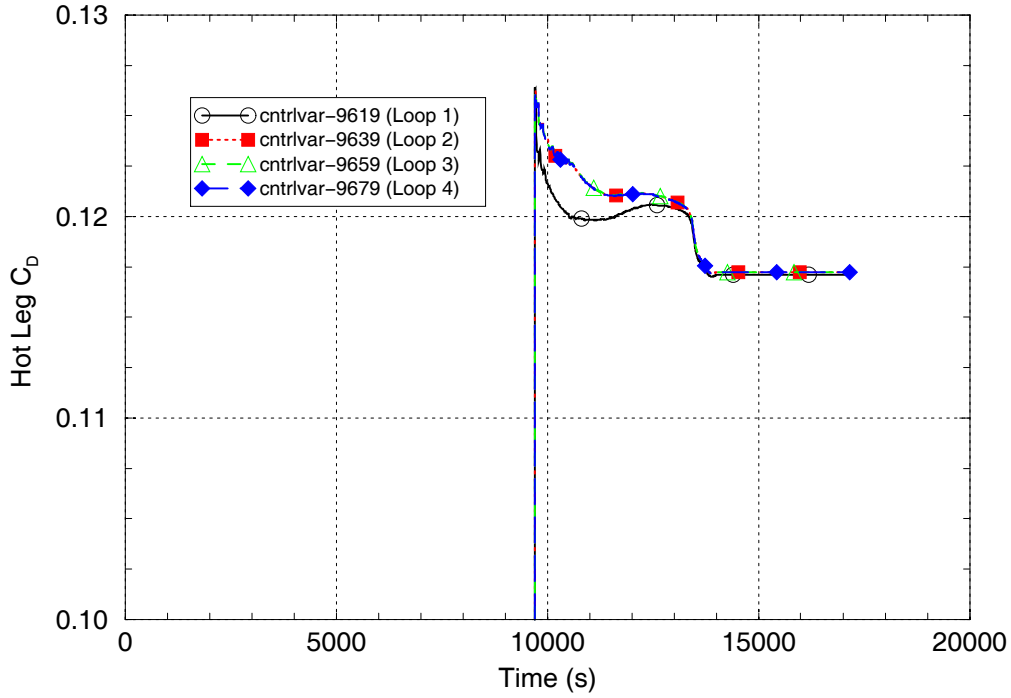

Figure 17. Hot Leg Discharge Coefficients.

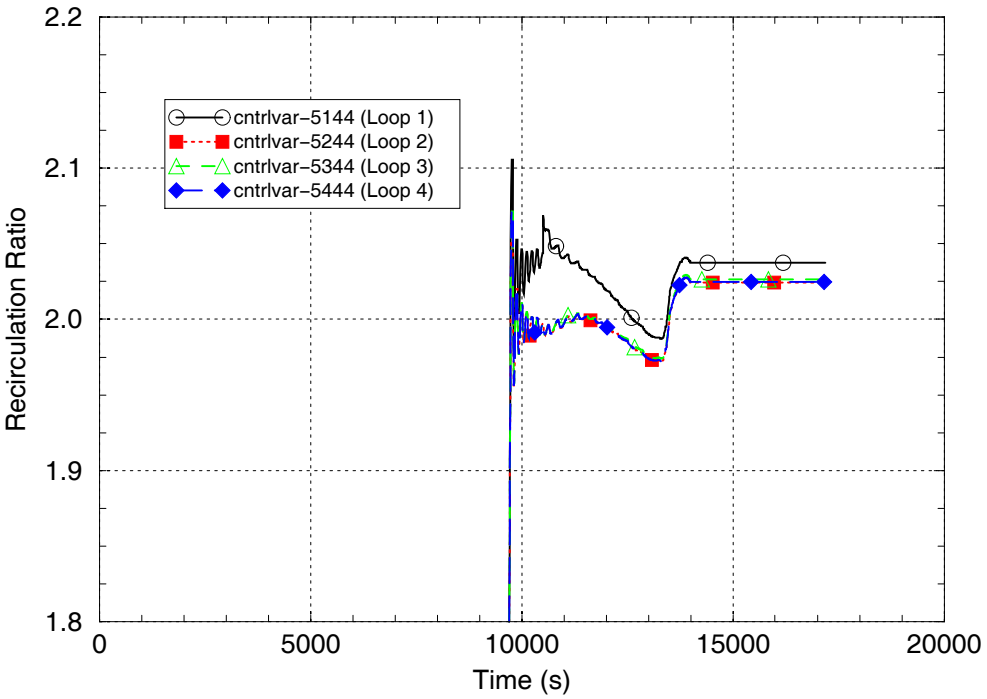

Figure 18. Recirculation Ratios.

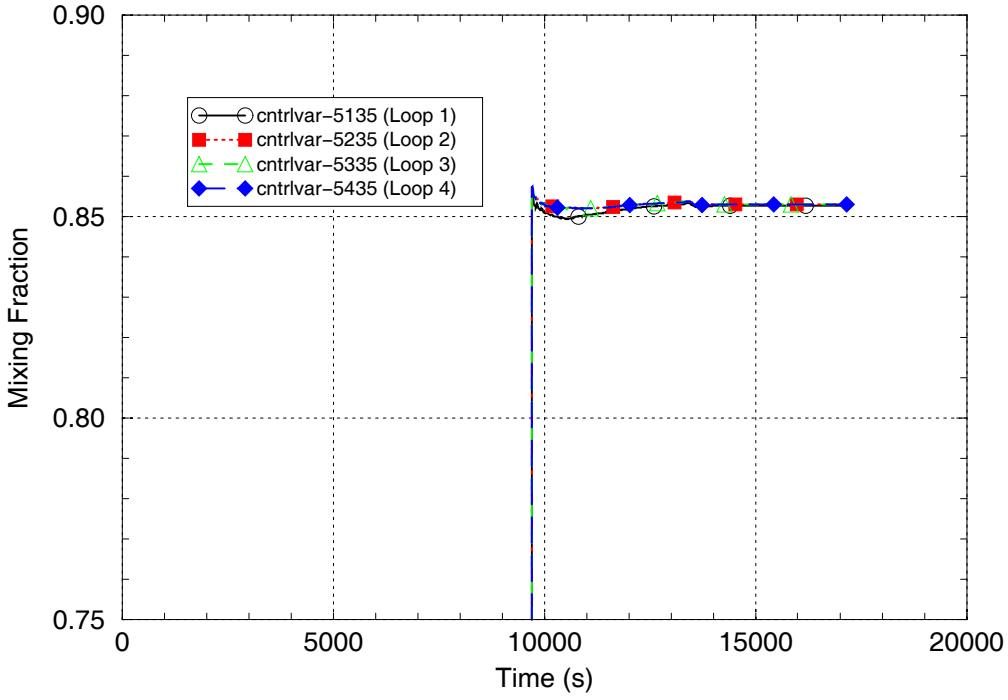

Figure 19. Hot Mixing Fractions.

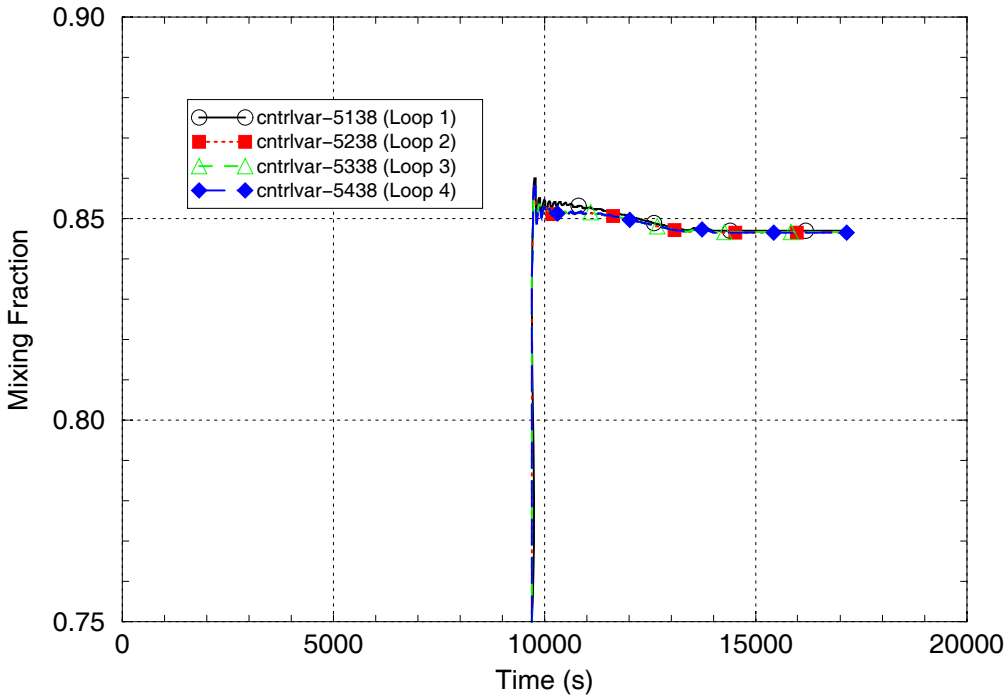

Figure 20. Cold Mixing Fractions.

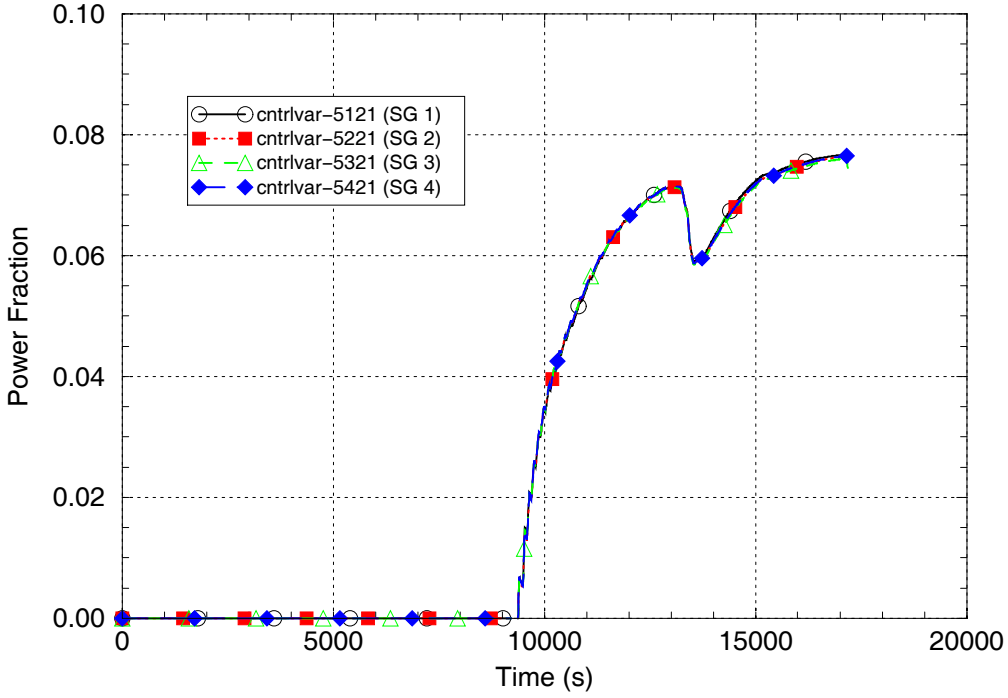

Figure 21. SG Power Fractions.

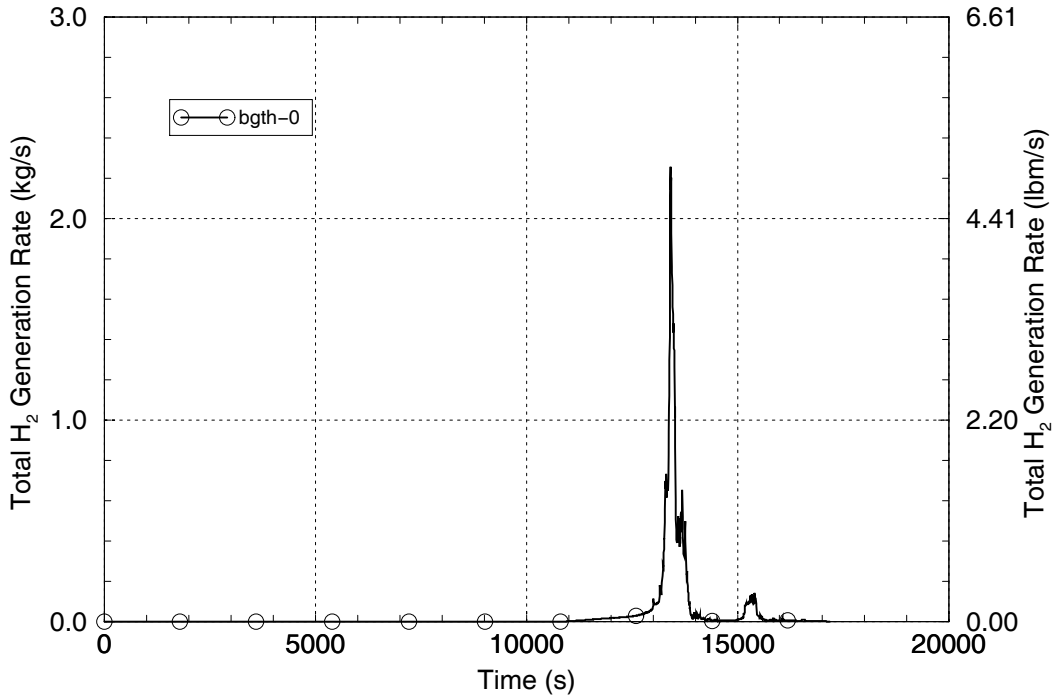

Figure 22. Hydrogen Generation Rate.

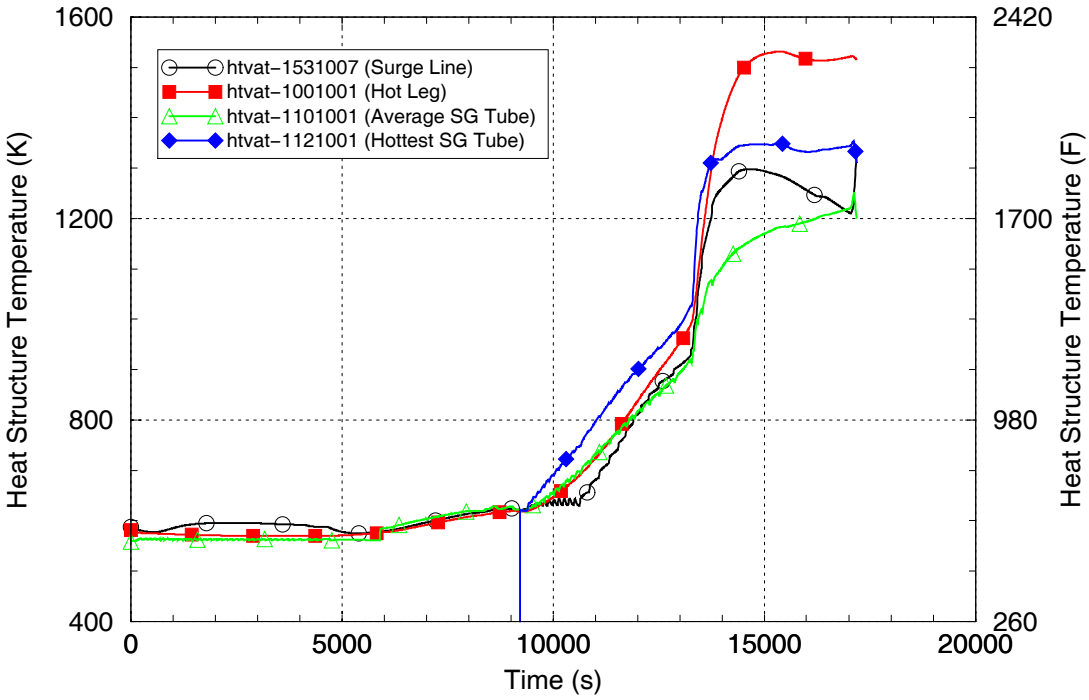

Figure 23. Loop 1 Structure Temperatures.

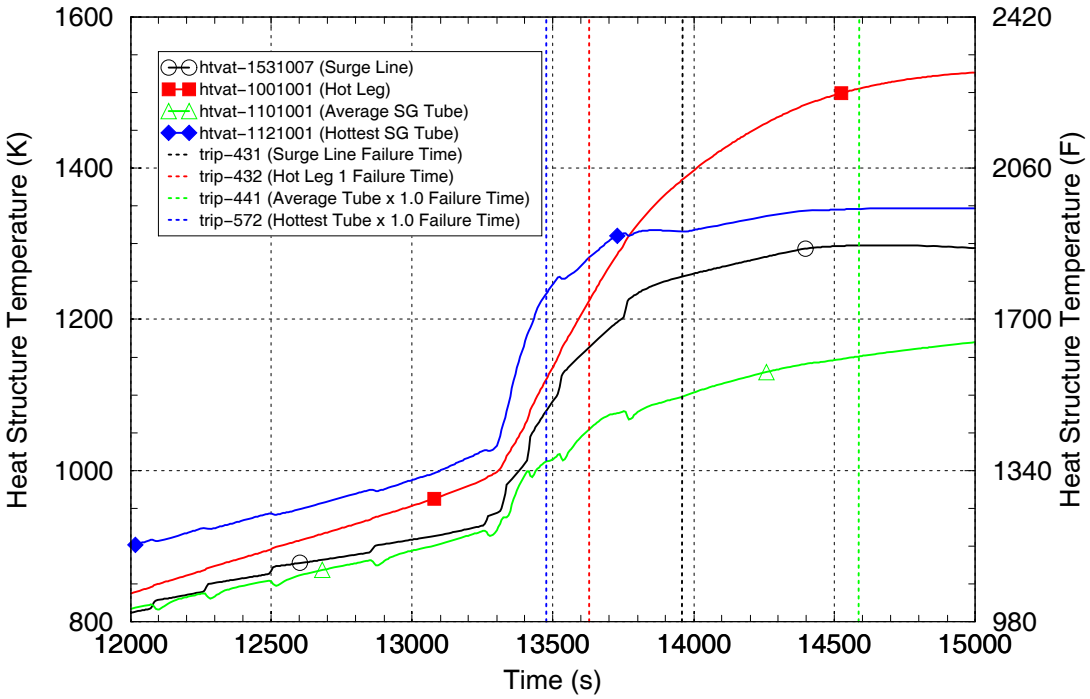

Figure 24. Correspondence Between Loop 1 Structure Temperatures and Failure Times.

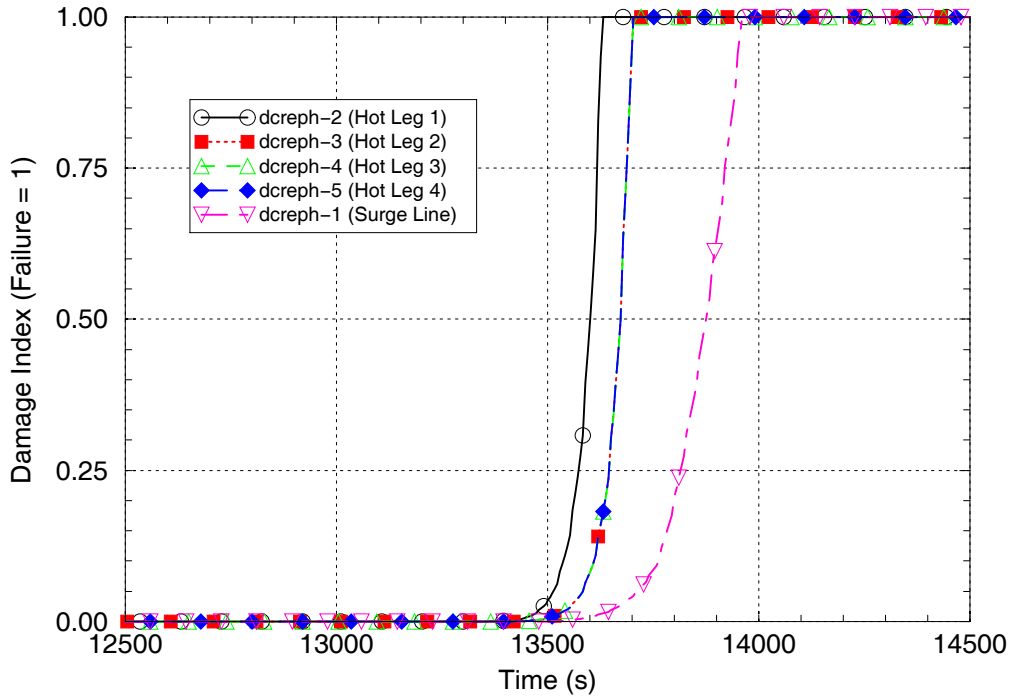

Figure 25. Hot Leg and Pressurizer Surge Line Creep Rupture Damage Indexes.

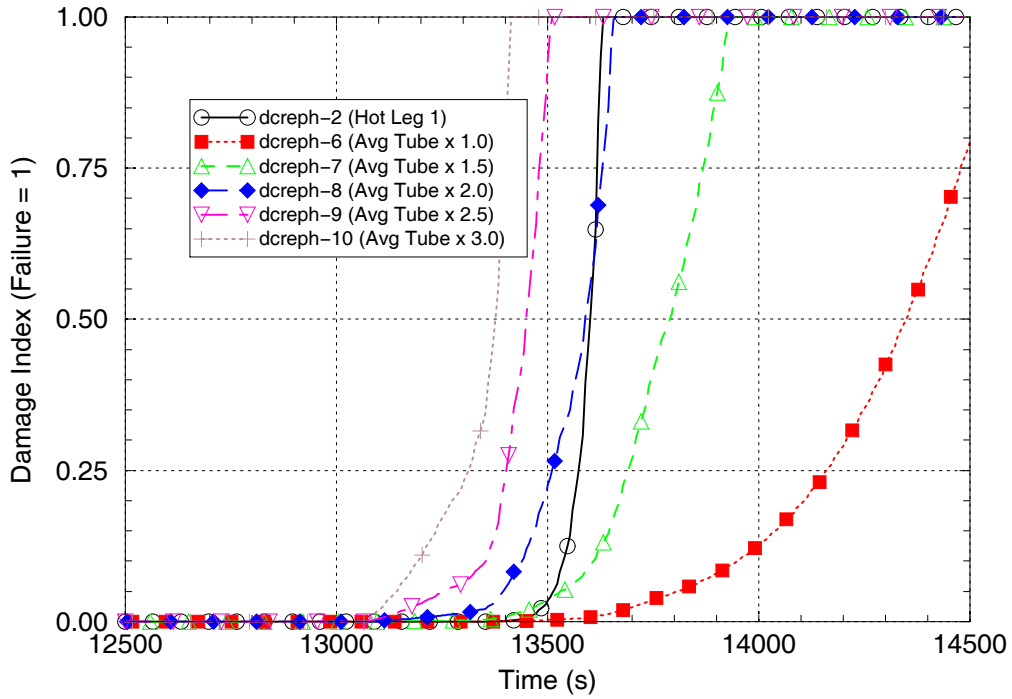

Figure 26. SG 1 Average Tube and Hot Leg 1 Creep Rupture Damage Indexes.

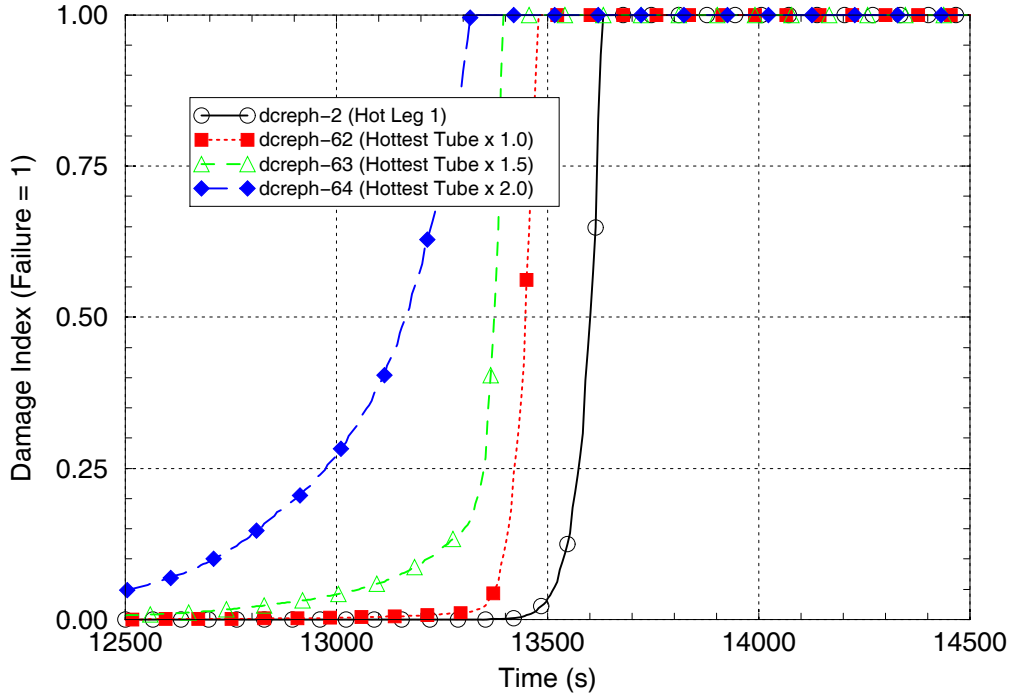

Figure 27. SG 1 Hottest Tube and Hot Leg 1 Creep Rupture Damage Indexes.

3.3 Analysis of Primary RCS Energy Flow

An analysis of simplified energy balance data was performed for the purpose of understanding the distribution and flow of energy in the primary RCS during the heatup phase of the station blackout base case SCDAP/RELAP5 calculation in Section 3.2. This energy balance analysis considered the flow of energy into, within, and out of the primary RCS fluid over the event sequence after the time when the core uncovers. In this analysis, the primary RCS includes the fluid in the regions of the reactor vessel, hot legs, SG plenums, the interior of the SG tubes, reactor coolant pumps, cold legs, pressurizer and surge line.

Energy Balance Model and Analysis Approach

The RCS fluid was subdivided into the control volume scheme shown in Figure 28. It is noted that this figure has not been updated to reflect the recently-added pressurizer spray system model connections between the two control volumes representing the pumps/cold legs and the control volume representing the pressurizer/surge line. Table 5 summarizes the specific RCS fluid regions contained within each control volume. The calculated behavior among the three coolant loops that are not connected to the pressurizer is virtually identical during the calculated event sequence; the RCS fluid in those three loops was lumped together for the purposes of the energy balance analysis.

Because the SCDAP/RELAP5 model nodalization scheme is more detailed than the energy balance control volume scheme, the energy balance information for each control volume represents a summation of data over the SCDAP/RELAP5 hydrodynamic fluid cells that, when combined, make up the control volume regions. Control variables were added to the SCDAP/RELAP5 plant model to calculate the rate of energy flow into and out of each of the control volume and the rate of change of the energy stored within each control volume. Inflows of energy result when fluid flows into a control volume and as heat is transferred from structures to the fluid. Outflows of energy result when fluid flows out of a control volume and as heat is transferred from the fluid to structures.

Since the opening and closing of the pressurizer relief valves cause the system fluid flows and wall heat transfer rates to oscillate considerably during the SCDAP/RELAP5 calculation, it was desirable to smooth the energy balance data through integration. Additional control variables were added to the SCDAP/RELAP5 model to calculate integrated data for the fluid inflow, fluid outflow, wall heat addition and net energy storage for each of the control volumes.

Table 6 lists the control variables that contain the key integrated energy balance data for the control volumes. Note that data calculated with the control variables is in units of Joules. For control volume fluid energy storage, positive and negative values respectively represent increases and decreases in the control volume fluid energy. For fluid-structure heat transfer, positive values represent a transfer of heat from the structures to the fluid and negative values represent a transfer of heat from the fluid to the structures (consistent with the SCDAP/RELAP5 convention). For energy flow out of the RCS through valves and leaks, positive values represent flows leaving the RCS.

As would be expected, the energy flow patterns vary over the course of the transient sequence as fluid distributions, fluid conditions and the phenomena that dominate the RCS system thermal-hydraulic response change. For clarity, the transient event sequence after the time when core uncovers is subdivided into five phases for which the RCS energy flows are separately evaluated. Table 7 lists the calculation time periods covering the five phases of the event sequence. The criteria for selecting the time periods for the five phases and the RCS behavior during each phase are summarized as follows:

Phase 1, Pressurizer Draining (9,222 s - 10,637 s) This phase extends from the time when the core uncovers to the time when the pressurizer tank has emptied. During this phase the water remaining in the pressurizer at the time of core uncovering drains out of the pressurizer and downward through the surge line toward the hot leg. Superheated steam coming up the surge line from the hot leg tends to vaporize this liquid, which enhances steam production and steam flow. The pressurizer PORVs cycle open and closed to limit the RCS pressurization and much steam and fluid energy is lost from the RCS through the flow out the pressurizer PORVs. This loss of RCS inventory causes the pressurizer level to decline until the tank is empty. Fuel and steam temperatures are generally still low and the core power is generated only as a result of the fission product decay process. The summary energy balance data for this phase are provided in Table 8.

Phase 2, Empty System Heatup (10,637 s - 13,200 s) This phase extends from the time when the pressurizer tank has emptied until the time when the system heatup causes the fuel rod oxidation rate to increase to the point where the core power is produced roughly equally by fission product decay and fuel rod oxidation. During this phase the pressurizer has completely drained and the RCS (except for the loop seals and the reactor vessel lower plenum and head) is filled with vapor. The pressurizer PORVs continue to cycle open and closed. Fuel temperatures, steam temperatures and the fuel rod oxidation power are all rising. The summary energy balance data for this phase are provided in Table 9.

Phase 3, Peak Fuel Rod Oxidation (13,200 s - 13,475 s) This phase extends from the time when the core power is produced roughly equally by fission product decay and fuel rod oxidation, through the peak in the oxidation rate and up to the time when the first significant structural failure is encountered. The failure time for the hottest SG tube structure with a stress multiplier of 1.0 was selected as the end time for this phase. Except for the loop seals and the reactor vessel lower plenum and head, the RCS is filled with a mixture of steam and hydrogen, which is released by the oxidation process. The pressurizer PORVs continue to cycle open and closed. Fuel and steam temperatures are now rising more rapidly. During this phase the core power is dominated by the fuel rod oxidation process, not by the fission product decay. The oxidation power peaks at about 11.2 times the fission decay power and then begins to fall as the cladding is consumed. A key feature of this phase is that the heat produced by the oxidation process tends, at first, to be retained locally in the fuel rods and core regions of the RCS. The summary energy balance data for this phase are provided in Table 10.

Phase 4, Structure Failure (13,475 s – 14,590 s) The time period for this phase includes the failure times for all remaining significant structures: hot legs, pressurizer surge line and average

SG tubes with stress multipliers lower than 3.0. The failure time for the average SG tube with a stress multiplier of 1.0 was used as the end time for this phase. Except for the loop seals and the reactor vessel lower plenum and head, the RCS is filled with a mixture of steam and hydrogen. Before 14,400 s (4 hours, the assumed station battery depletion time), the pressurizer PORVs continue to cycle open and closed, but less frequently during this phase than during the earlier phases. The fuel rod oxidation power continues to decline and during this phase the core power is produced roughly equally by the fission product decay and fuel rod oxidation processes. A key feature of this period is that the heat that had built up in excess in the fuel and core regions during the rapid peak of the oxidation process is carried by the flow of the RCS fluid outward into the coolant loops. It is the arrival of this excess heat in the loop components which quickly drives the structure temperatures upward, leading to their failure. The summary energy balance data for this phase are provided in Table 11.

Phase 5, Post-Structure Failure (14,590 s – 15,500 s) This phase extends from the time when the average SG tube with a 1.0 stress multiplier fails up until the time when molten control rod absorber is relocated to the reactor vessel lower head. The pressurizer PORVs are no longer functional because the station batteries are assumed to be depleted. The fuel rod oxidation power remains low and is only a very small portion of the total core power. The system fluid and structure temperatures (which had risen in order to remove the excess core power produced during the peak oxidation phase) are roughly at the levels which are needed to remove the now-lower core power. This effect causes the fluid and structure temperatures to generally stop rising and level off during this phase of the accident sequence. The summary energy balance data for this phase are provided in Table 12. The energy analysis is truncated at 15,500 s because afterward the RCS energy balance is controlled by the relocation of large quantities of molten materials (control rod absorber and fuel rods) which cause significant changes in the RCS configuration.

The SCDAP/RELAP5-calculated control variables related to the energy balance were extracted from the calculation output and manipulated with a post-processor. The energy balance data available on a CD available to others in the project are summarized in Appendix A.

Analysis of RCS Energy Flows During the Event Sequence Calculation

The behavior of the energy flows into, within and out of the RCS are summarized as follows. Figures 29 through 37 show the transient behavior of the various energy flow terms. Because the energy flow rates oscillate significantly with the open/close cycling of the pressurizer relief valves, it was necessary to smooth the energy flow rates through integration. The data points shown with the triangle symbols in these figures are located in the middle of the periods for the five phases and represent the average integrated energy flow during each phase. The data points are joined with solid lines in the figures only for clarity.

Figure 29 shows the average total core power resulting from fission product decay heat and fuel rod oxidation heat. The data for the first two phases represents the fission product decay power, prior to the onset of significant fuel rod oxidation. The increase seen in the third phase results from the acceleration and peaking of the fuel rod oxidation process. During the fourth and fifth

phases the oxidation process is mostly complete and the core power is once again dominated by the fission product decay heat, which declines as a function of time after reactor trip.

Figures 30 and 31 respectively portray the percentages of the integrated total core power that are retained in the fuel and transferred to the core fluid. The figures show that, except during the peak in the oxidation process in Phase 3, about 20% of the core heat is retained in the fuel and about 80% of the core heat is transferred to the fluid in the core. The spike in total core power during the peak oxidation period causes these percentages to significantly change, with about 60% of the core heat retained locally in the fuel (where the oxidation process deposits it) and only about 40% of the core heat transferred to the core fluid. Subsequent to the oxidation peak during Phase 3, the passage of time allows the "excess" oxidation heat which had built up in the fuel to flow into the core fluid and from there to be distributed throughout the RCS.

Figure 32 shows the integrated changes in the reactor vessel fluid energy over the five phases, expressed as a percentage of the integrated total core power (negative values indicate a loss of fluid energy). During Phases 1 and 2, the negative vessel energy inventory change is caused by the loss of liquid mass from the reactor vessel as the core fluid is boiled off and the downcomer level declines. The small positive changes seen in Phases 3 through 5 reflect an increase in vessel fluid energy resulting from heating the vessel fluid to very high temperatures and releasing high-energy hydrogen from the fuel rod oxidation process directly into it.

Figure 33 shows the integrated changes in the pressurizer fluid energy for the five phases, expressed as a percentage of the integrated total core power (negative values indicate a loss of fluid energy). The figure reflects the rapid loss of liquid from the pressurizer as it empties due to draining during Phase 1 and the passing of liquid and steam through the PORVs when those valves open to limit the RCS pressurization during Phases 1 through 4. The PORVs fail closed after the station batteries are assumed to be depleted at 4 hours (14,400 s). During Phase 5 the figure therefore reflects a situation where the PORVs can no longer cycle open and closed and the pressurizer region is stagnant and vapor-filled.

Figure 34 shows the integrated changes in the fluid energy for RCS regions other than the reactor vessel and pressurizer for the five phases, expressed as a percentage of the integrated total core power (negative values indicate a loss of fluid energy). For Phase 1, the figure reflects the loss of liquid mass from the hot and cold legs as the liquid remaining at the time of core uncovering drains into the reactor vessel or is swept out of the RCS through the pressurizer PORVs. During Phases 2 through 4, the hot leg, SG primary and cold leg regions of the plant are vapor-filled and the small negative energy changes seen in the figure reflect a loss of vapor mass as the fluid temperatures increase. The fluid becomes hotter and its specific energy becomes higher, but its density becomes lower and the net result is a lower absolute fluid energy.

Figure 35 shows the integrated flow of energy out of the RCS by way of the pressurizer PORVs and reactor coolant pump shaft seal leaks for the five phases expressed as a percentage of the integrated total core power. In this figure, negative values indicate a flow of energy out of the RCS. The figure indicates a high rate of energy flow out of the RCS during Phase 1, followed by successively smaller energy flows during Phases 2 through 5. The high rate of RCS energy loss during Phase 1 reflects a continued high rate of steam production prior to the time when the core

completely empties of liquid. Opening of the pressurizer PORVs causes liquid in the core to flash and the steam produced requires the PORVs to both cycle frequently and remain open for extended periods in order to control the RCS pressure. After the core dries out near the end of Phase 1, the core steam production rate falls, the PORVs cycle open less frequently and remain open for shorter periods. The reduced rates of RCS energy loss for Phases 2, 3 and 4 reflect this lowered demand on the pressurizer PORVs. The station batteries are depleted prior to the start of Phase 5 and the small negative RCS energy loss seen in the figure results solely from the RCP shaft seal leakage.

Figure 36 shows the integrated flow of heat from the tubes of the four SGs to the fluid inside the tubes for the five phases, expressed as a percentage of the integrated total core power. In this figure, negative values represent transfer of heat from the fluid inside the SG tubes to the tube inner wall surface. Note that the figure shows only data for the heat transferred between the tube wall and the fluid; heat transferred between the fluid and other SG structures (the walls of the spherical inlet and outlet plenum walls, the plenum divider plate and the tubesheet) is not included here. The figure shows that, except for the peak oxidation period when much heat initially stays in the fuel, the portion of the total core heat which flows to the SG tubes is relatively stable at between about 13% and 23%.

Figure 37 shows the integrated flow of heat from all RCS structures other than SG tubes to the fluid inside the RCS for the five phases, expressed as a percentage of the integrated total core power. In this figure, negative values represent transfer of heat from the fluid to the structures. The structures represented by this data include the reactor vessel cylindrical wall and spherical upper and lower head walls, reactor vessel internals (core barrel, support plates, columns, etc.), hot leg, cold leg and pressurizer surge line pipe walls, the pressurizer tank wall, steam generator spherical inlet and outlet plenum walls and the SG tubesheets. When compared with the very thin SG tube structures which have a large heat transfer area, these structures are in general very thick, but with much smaller heat transfer areas. The figure shows that prior to the peak fuel rod oxidation period the portion of the total core heat which flows to these structures is between about 20% and 40%. After the peak fuel rod oxidation period, this percentage increases to about 55%. The increase reflects: (1) the close proximity of the thick reactor vessel heat structures to the hot vapor in the core and (2) the massive heat sinks provided by these thick-wall heat structures in general.

Regarding the effectiveness of heat sinks provided by the thick-wall structures, a key feature of the station blackout transient event sequence is that vapor temperatures are for the most part continuously increasing. Consider first a situation where structures might be subjected to a large step-change increase in fluid temperature, but where the fluid temperature is held constant afterward. In that situation, heat flows from the fluid into the colder wall, but the temperature increase that is induced in the wall near the surface tends to restrict the subsequent flow of heat into the wall; the fluid-wall heat transfer process becomes limited by conduction heat transfer within the wall. Now consider the situation we have here, where the vapor temperatures continuously increase. The heat transfer process still induces a temperature increase in the wall near the surface. But, because the vapor temperatures continue increasing, the fluid-to-wall differential temperature remains high and wall heat sink remains very effective.

Table 5. Description of Control Volumes for the Energy Balance Analysis.

Control Volume Number	RCS Fluid Region Included in the Control Volume	Notes
1	Reactor core	Includes heat structures for fuel rods. Heat generation considered due to core fission product decay and fuel rod metal-water oxidation.
2	Reactor vessel region above the core and inside the core barrel	Includes heat structures for vessel wall and internals in the upper head and plenum region.
3	Coolant Loop 1 hot leg	Includes heat structures for hot leg wall.
4	SG 1 inlet plenum	Includes heat structures for tube sheet and plenum wall.
5	SG 1 tubes	The portions of the tubes located inside the tubesheet are considered to be part of the inlet and outlet plena. The SG 1 tube control volume was separated into three sub-control volumes: 5A (Hot average tubes, upward-flowing section), 5B (Hot average tubes, downward-flowing section) and 5C (Cold average tubes, upward and downward-flowing section).
6	SG 1 outlet plenum	Includes heat structures for tube sheet and plenum wall
7	Coolant Loop 1 cold leg, reactor coolant pump and pressurizer spray line	Includes heat structures for the cold leg wall. Fluid exits the system via reactor coolant pump shaft seal leak.
8	Coolant Loop 2/3/4 hot leg	Includes heat structures for hot leg wall.
9	SG 2/3/4 inlet plenum	Includes heat structures for tube sheet and plenum wall
10	SG 2/3/4 tubes	The portions of the tubes located inside the tubesheet are considered to be part of the inlet and outlet plena.
11	SG 2/3/4 outlet plenum	Includes heat structures for tube sheet and plenum wall.
12	Coolant Loop 2/3/4 cold legs, reactor coolant pumps and pressurizer spray line.	Includes heat structures for the cold leg walls. Fluid exits the system via reactor coolant pump shaft seal leaks.
13	Reactor vessel downcomer, lower head and lower plenum regions	Includes heat structures for the vessel wall and internals.
14	Pressurizer tank and surge line	Includes heat structures for the tank and surge line walls. Fluid exits the system via flow through the pressurizer PORVs and SRVs.

Table 6. List of Control Variables with Integrated Energy Balance Data.

Control Volume Number and Region	Data Type	CNTRLVAR Number
1 Reactor core	Fission product decay heat Fuel rod oxidation heat Total of decay and oxidation heats Heat retained in the fuel Heat transferred to the fluid from fuel Energy stored in the control volume fluid	8142 8147 8152 8157 8132 8122
2 Reactor vessel region above the core and inside the core barrel	Heat transferred from structures to fluid Energy stored in the control volume fluid	8242 8230
3 Coolant Loop 1 hot leg	Heat transferred from structures to fluid Energy stored in the control volume fluid	8332 8324
4 SG 1 inlet plenum	Heat transferred from structures to fluid Energy stored in the control volume fluid	8422 8414
5 SG 1 tubes	5A hot average tube upflow section Heat transferred from structures to fluid Energy stored in the control volume fluid 5B hot average tube downflow section Heat transferred from structures to fluid Energy stored in the control volume fluid 5C cold average tube up and downflow sections Heat transferred from structures to fluid Energy stored in the control volume fluid	 8531 8522 8532 8523 8533 8524

Control Volume Number and Region	Data Type	CNTRLVAR Number
6 SG 1 outlet plenum	Heat transferred from structures to fluid Energy stored in the control volume fluid	8622 8614
7 Coolant Loop 1 cold leg and reactor coolant pump	Heat transferred from structures to fluid Energy stored in the control volume fluid Energy lost out pump shaft seal leak	8722 8714 8723
8 Coolant Loop 2/3/4 hot leg	Heat transferred from structures to fluid Energy stored in the control volume fluid	8872 8869
9 SG 2/3/4 inlet plenum	Heat transferred from structures to fluid Energy stored in the control volume fluid	8932 8929
10 SG 2/3/4 tubes	Heat transferred from structures to fluid Energy stored in the control volume fluid	9072 9065
11 SG 2/3/4 outlet plenum	Heat transferred from structures to fluid Energy stored in the control volume fluid	9132 9129
12 Coolant Loop 2/3/4 cold leg and reactor coolant pump	Heat transferred from structures to fluid Energy stored in the control volume fluid Energy lost out pump shaft seal leaks	9232 9229 9241
13 Reactor vessel downcomer, lower head and lower plenum regions	Heat transferred from structures to fluid Energy stored in the control volume fluid	9322 9316
14 Pressurizer tank and surge line	Heat transferred from structures to fluid Energy stored in the control volume fluid Energy lost out pressurizer relief valves	9432 9424 9436

Table 7. Subdivision of the Station Blackout Calculation into Phases

Phase Number	Time Period of the Phase (s)	Phase Title	Results Presented in Table
1	9,222 to 10,637	Pressurizer Draining	8
2	10,637 to 13,200	Empty System Heatup	9
3	13,200 to 13,475	Peak Fuel Rod Oxidation	10
4	13,475 to 14,590	Structure Failure	11
5	14,590 to 15,500	Post Structure Failure	12

Table 8. Summary of Integrated Energy Flows during Phase 1, Pressurizer Draining.

RCS Region and Type of Energy Flow	Integrated Energy Flow from 9,222 s to 10,637 s (as % of Total Integrated Core Power over Same Period)
Reactor Vessel	
Total Core Heat	100.0
Heat Retained in Fuel	13.8
Heat Transferred from Fuel to Fluid	86.2
Heat Transferred from Other Structures to Fluid	-8.6
Energy Stored in Fluid	-50.7
Coolant Loop 1 Hot Leg, SG, Pump and Cold Leg	
Heat from Hot Tube Upflow Section to Fluid	-1.0
Heat from Hot Tube Downflow Section to Fluid	-0.9
Heat from Cold Tube Section to Fluid	-1.3
Total Heat from SG Tubes to Fluid	-3.2
Heat Transferred from Other Structures to Fluid	-2.4
Energy Stored in Fluid	-6.4
Energy Lost through Pump Shaft Seal Leak Flow	-1.7
Coolant Loop 2/3/4 Hot Legs, SGs, Pumps and Cold Legs	
Total Heat from SG Tubes to Fluid	-9.9
Heat Transferred from Other Structures to Fluid	-7.2
Energy Stored in Fluid	-18.4
Energy Lost through Pump Shaft Seal Leak Flows	-5.1
Pressurizer and Surge Line	
Heat Transferred from Structures to Fluid	-1.2
Energy Stored in Fluid	-19.5
Energy Lost through PORV Flows	-141.8
Summary for Entire Reactor Coolant System	
Heat Added to Fluid from Core Fuel Rods	86.2
Heat Transferred from Structures to Fluid	-32.5
Heat Lost through PORVs and Pump Leak Flows	-148.6
Energy Stored in Fluid	-95.0

Table 9. Summary of Integrated Energy Flows during Phase 2, Empty System Heatup.

RCS Region and Type of Energy Flow	Integrated Energy Flow from 10,637 s to 13,200 s (as % of Total Integrated Core Power over Same Period)
Reactor Vessel	
Total Core Heat	100.0
Heat Retained in Fuel	25.4
Heat Transferred from Fuel to Fluid	74.6
Heat Transferred from Other Structures to Fluid	-15.0
Energy Stored in Fluid	-9.6
Coolant Loop 1 Hot Leg, SG, Pump and Cold Leg	
Heat from Hot Tube Upflow Section to Fluid	-2.1
Heat from Hot Tube Downflow Section to Fluid	-1.5
Heat from Cold Tube Section to Fluid	-1.3
Total Heat from SG Tubes to Fluid	-4.9
Heat Transferred from Other Structures to Fluid	-5.2
Energy Stored in Fluid	-1.7
Energy Lost through Pump Shaft Seal Leak Flow	-1.7
Coolant Loop 2/3/4 Hot Legs, SGs, Pumps and Cold Legs	
Total Heat from SG Tubes to Fluid	-14.7
Heat Transferred from Other Structures to Fluid	-15.4
Energy Stored in Fluid	-5.8
Energy Lost through Pump Shaft Seal Leak Flows	-5.0
Pressurizer and Surge Line	
Heat Transferred from Structures to Fluid	-5.5
Energy Stored in Fluid	-5.1
Energy Lost through PORV Flows	-29.3
Summary for Entire Reactor Coolant System	
Heat Added to Fluid from Core Fuel Rods	74.6
Heat Transferred from Structures to Fluid	-60.7
Heat Lost through PORVs and Pump Leak Flows	-36.0
Energy Stored in Fluid	-22.2

Table 10. Summary of Integrated Energy Flows during Phase 3, Peak Fuel Rod Oxidation.

RCS Region and Type of Energy Flow	Integrated Energy Flow from 13,200 s to 13,475 s (as % of Total Integrated Core Power over Same Period)
Reactor Vessel	
Total Core Heat	100.0
Heat Retained in Fuel	60.7
Heat Transferred from Fuel to Fluid	39.3
Heat Transferred from Other Structures to Fluid	-7.2
Energy Stored in Fluid	11.8
Coolant Loop 1 Hot Leg, SG, Pump and Cold Leg	
Heat from Hot Tube Upflow Section to Fluid	-1.1
Heat from Hot Tube Downflow Section to Fluid	-0.5
Heat from Cold Tube Section to Fluid	-0.2
Total Heat from SG Tubes to Fluid	-1.8
Heat Transferred from Other Structures to Fluid	-2.3
Energy Stored in Fluid	-2.1
Energy Lost through Pump Shaft Seal Leak Flow	-0.3
Coolant Loop 2/3/4 Hot Legs, SGs, Pumps and Cold Legs	
Total Heat from SG Tubes to Fluid	-5.1
Heat Transferred from Other Structures to Fluid	-6.6
Energy Stored in Fluid	-6.4
Energy Lost through Pump Shaft Seal Leak Flows	-1.0
Pressurizer and Surge Line	
Heat Transferred from Structures to Fluid	-3.0
Energy Stored in Fluid	-4.5
Energy Lost through PORV Flows	-13.0
Summary for Entire Reactor Coolant System	
Heat Added to Fluid from Core Fuel Rods	39.3
Heat Transferred from Structures to Fluid	-26.0
Heat Lost through PORVs and Pump Leak Flows	-14.3
Energy Stored in Fluid	-1.2

Table 11. Summary of Integrated Energy Flows during Phase 4, Structure Failure.

RCS Region and Type of Energy Flow	Integrated Energy Flow from 13,475 s to 14,590 s (as % of Total Integrated Core Power over Same Period)
Reactor Vessel	
Total Core Heat	100.0
Heat Retained in Fuel	15.2
Heat Transferred from Fuel to Fluid	84.8
Heat Transferred from Other Structures to Fluid	-21.4
Energy Stored in Fluid	8.7
Coolant Loop 1 Hot Leg, SG, Pump and Cold Leg	
Heat from Hot Tube Upflow Section to Fluid	-3.4
Heat from Hot Tube Downflow Section to Fluid	-1.7
Heat from Cold Tube Section to Fluid	0.1
Total Heat from SG Tubes to Fluid	-5.0
Heat Transferred from Other Structures to Fluid	-7.3
Energy Stored in Fluid	-1.5
Energy Lost through Pump Shaft Seal Leak Flow	-1.0
Coolant Loop 2/3/4 Hot Legs, SGs, Pumps and Cold Legs	
Total Heat from SG Tubes to Fluid	-14.8
Heat Transferred from Other Structures to Fluid	-21.9
Energy Stored in Fluid	-4.5
Energy Lost through Pump Shaft Seal Leak Flows	-3.0
Pressurizer and Surge Line	
Heat Transferred from Structures to Fluid	-5.0
Energy Stored in Fluid	-1.9
Energy Lost through PORV Flows	-4.6
Summary for Entire Reactor Coolant System	
Heat Added to Fluid from Core Fuel Rods	84.8
Heat Transferred from Structures to Fluid	-75.4
Heat Lost through PORVs and Pump Leak Flows	-8.6
Energy Stored in Fluid	0.8

Table 12. Summary of Integrated Energy Flows during Phase 5, Post-Structure Failure.

RCS Region and Type of Energy Flow	Integrated Energy Flow from 14,590 s to 15,500 s (as % of Total Integrated Core Power over Same Period)
Reactor Vessel	
Total Core Heat	100.0
Heat Retained in Fuel	17.8
Heat Transferred from Fuel to Fluid	82.2
Heat Transferred from Other Structures to Fluid	-22.7
Energy Stored in Fluid	0.4
Coolant Loop 1 Hot Leg, SG, Pump and Cold Leg	
Heat from Hot Tube Upflow Section to Fluid	-4.7
Heat from Hot Tube Downflow Section to Fluid	-1.9
Heat from Cold Tube Section to Fluid	0.8
Total Heat from SG Tubes to Fluid	-5.8
Heat Transferred from Other Structures to Fluid	-7.7
Energy Stored in Fluid	-0.8
Energy Lost through Pump Shaft Seal Leak Flow	-1.6
Coolant Loop 2/3/4 Hot Legs, SGs, Pumps and Cold Legs	
Total Heat from SG Tubes to Fluid	-17.5
Heat Transferred from Other Structures to Fluid	-23.7
Energy Stored in Fluid	-2.0
Energy Lost through Pump Shaft Seal Leak Flows	-4.5
Pressurizer and Surge Line	
Heat Transferred from Structures to Fluid	-0.8
Energy Stored in Fluid	0.2
Energy Lost through PORV Flows	0.0
Summary for Entire Reactor Coolant System	
Heat Added to Fluid from Core Fuel Rods	82.2
Heat Transferred from Structures to Fluid	-78.2
Heat Lost through PORVs and Pump Leak Flows	-6.1
Energy Stored in Fluid	-2.2

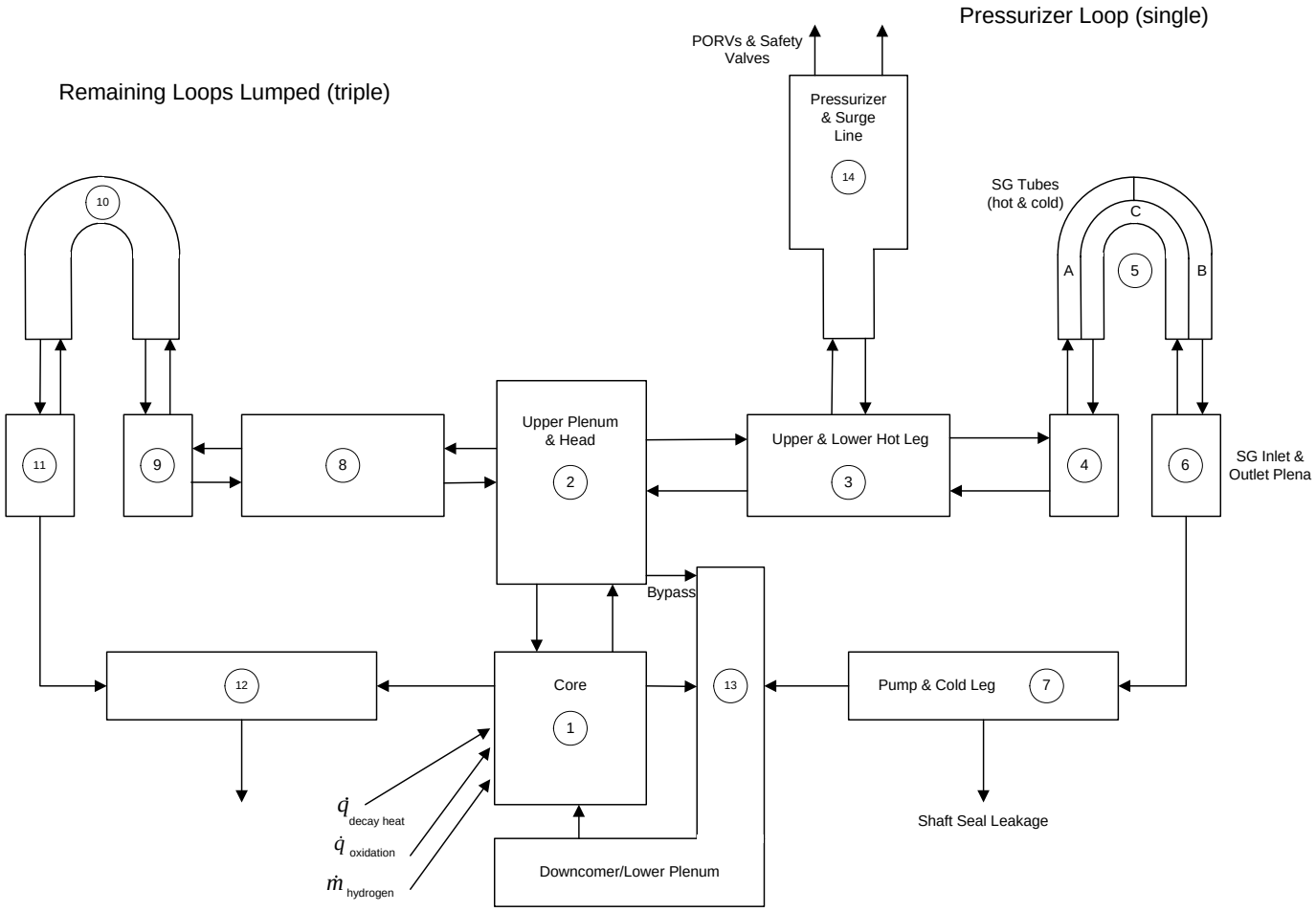

Figure 28. Control Volume Arrangement for the Energy Balance Analysis.

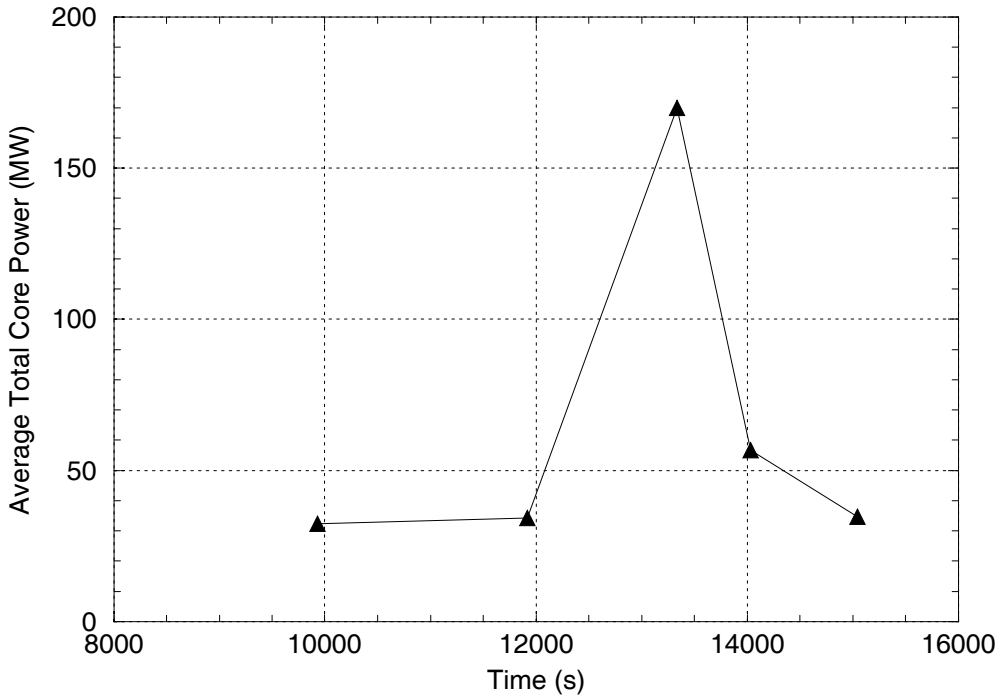

Figure 29. Average Total Core Power Generated During the Five Phases of the Station Blackout Base Case Calculation.

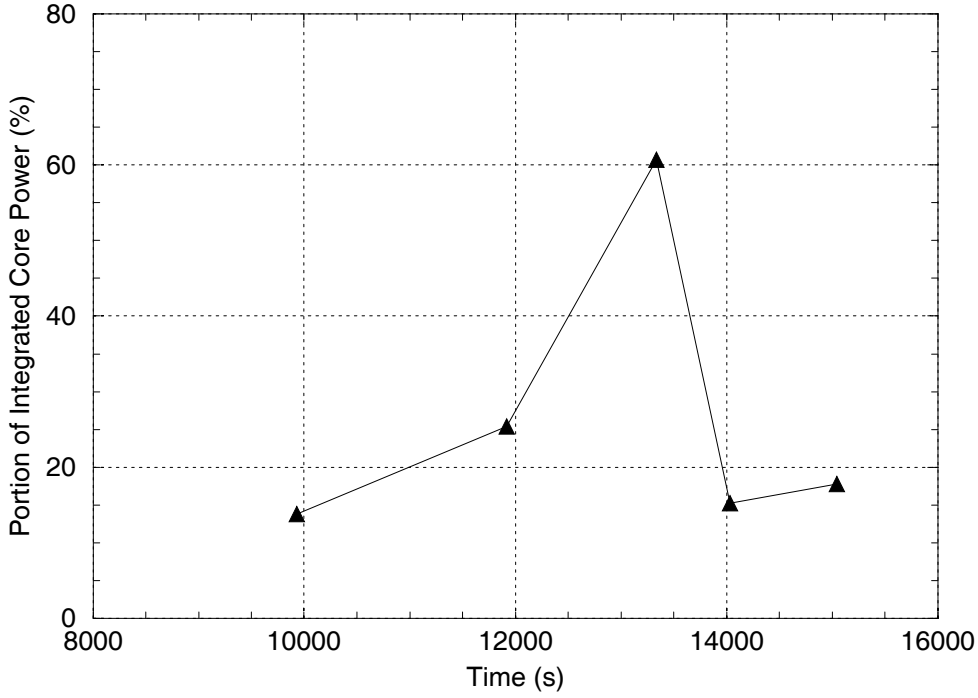

Figure 30. Portion of the Integrated Core Power Retained in the Fuel During the Five Phases of the Station Blackout Base Case Calculation.

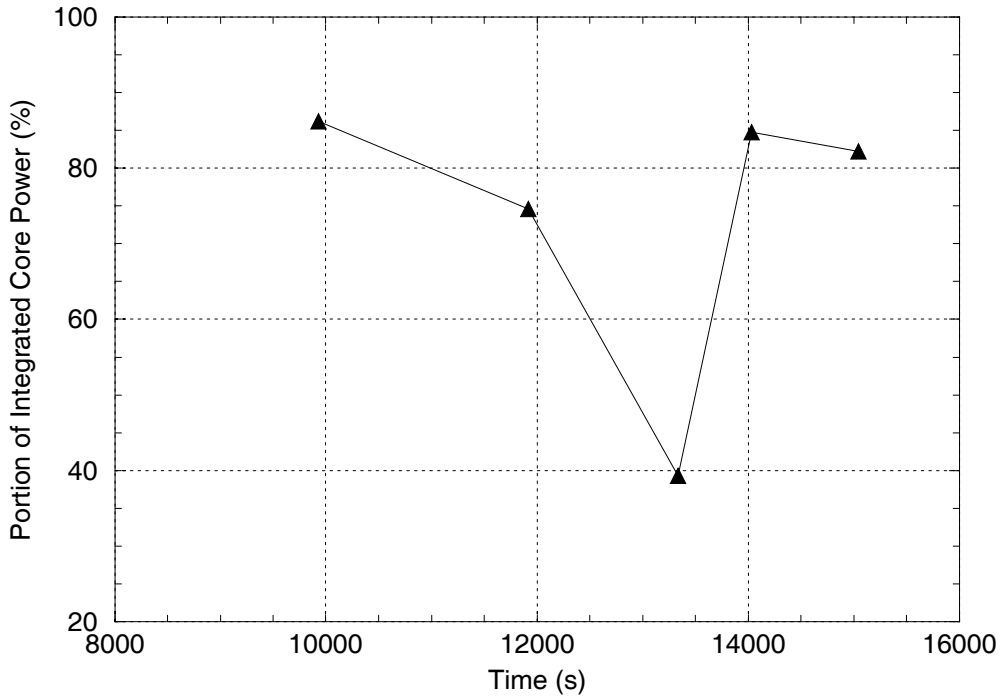

Figure 31. Portion of the Integrated Core Power Transferred to the Core Fluid During the Five Phases of the Station Blackout Base Case Calculation.

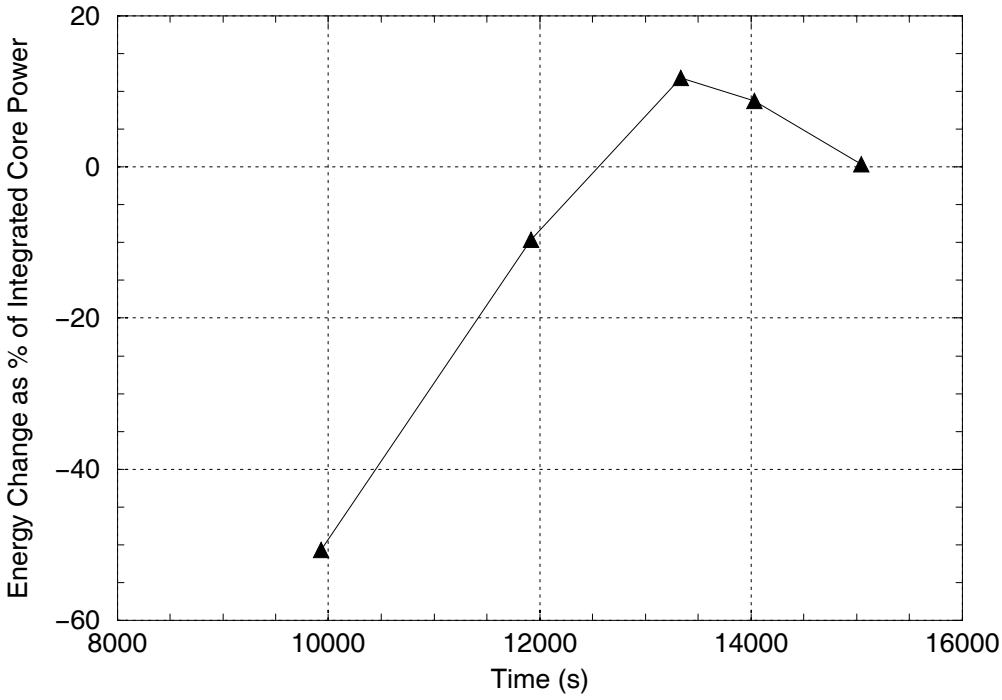

Figure 32. Change in Reactor Vessel Fluid Energy During the Five Phases of the Station Blackout Base Case Calculation.

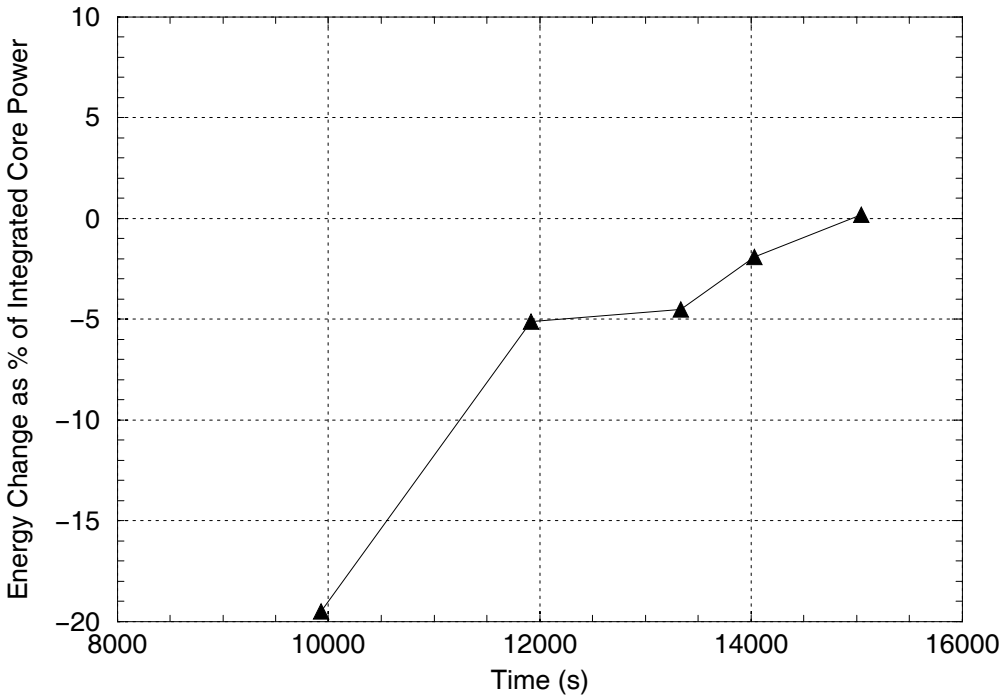

Figure 33. Change in Pressurizer Fluid Energy During the Five Phases of the Station Blackout Base Case Calculation.

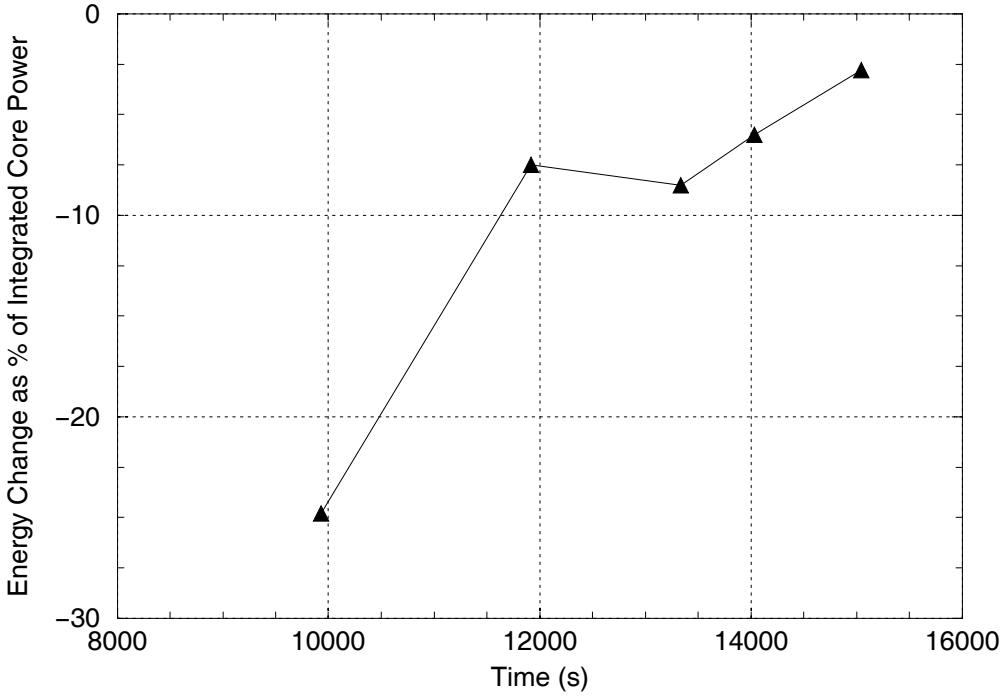

Figure 34. Change in Fluid Energy in RCS Regions Other Than the Reactor Vessel and Pressurizer During the Five Phases of the Station Blackout Base Case Calculation.

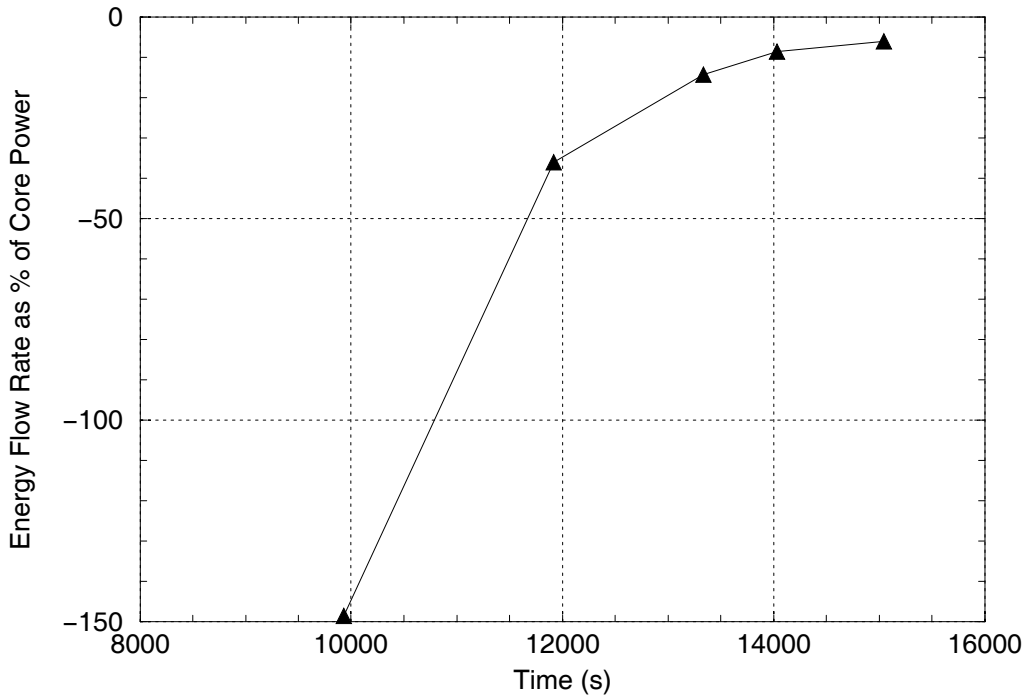

Figure 35. Integrated Flow of Energy Through the Pressurizer PORVs and Reactor Coolant Pump Shaft Seal Leaks During the Five Phases of the Station Blackout Base Case Calculation.

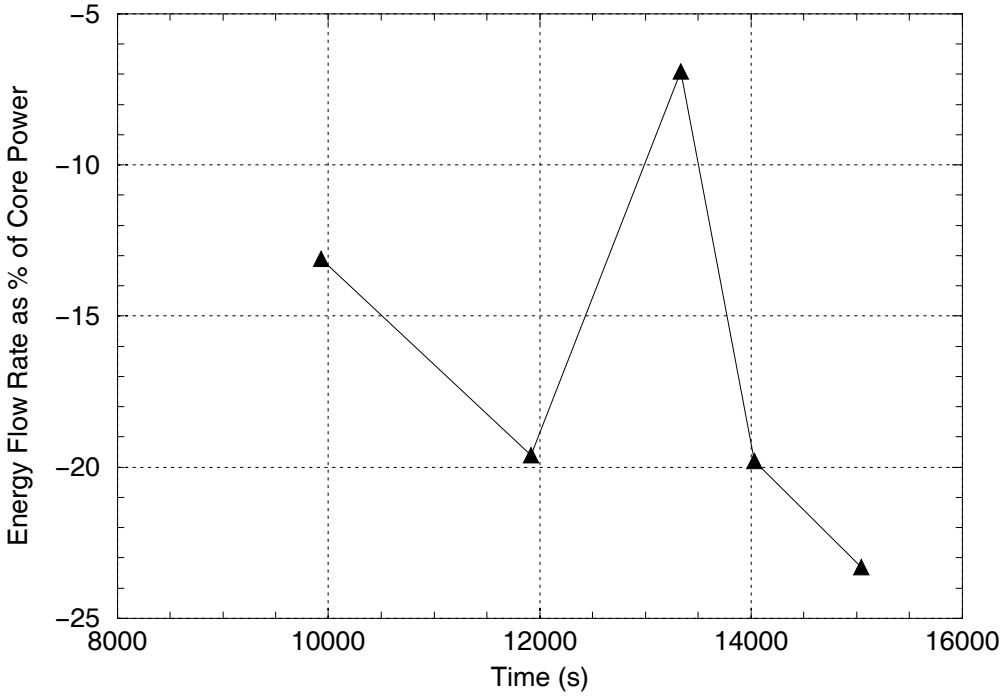

Figure 36. Integrated Heat Transfer Rate from SG Tubes to Fluid During the Five Phases of the Station Blackout Base Case Calculation.

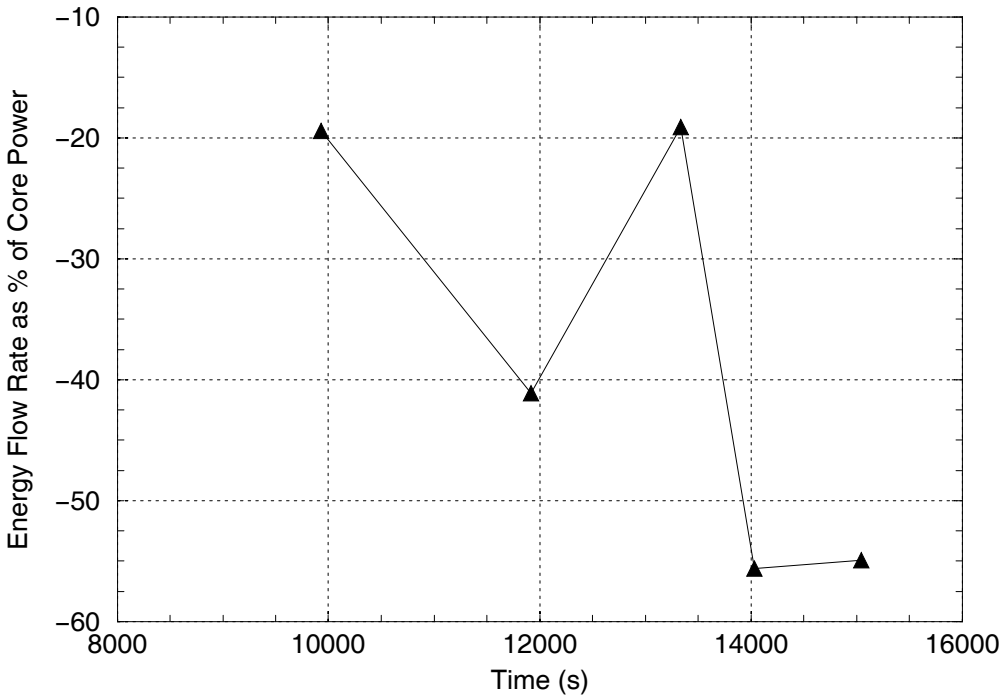

Figure 37. Integrated Heat Transfer Rate from All Structures (Except SG Tubes) to Fluid During the Five Phases of the Station Blackout Base Case Calculation.

3.4 Base Case Parameter Values for Uncertainty Study

The base case calculation documented in Section 3.2 is to be used as the reference case for a subsequent study estimating the uncertainties in key parameters for SCDAP/RELAP5 calculations of PWR station blackout events. Table 13 lists the key parameters and the SCDAP/RELAP5-calculated reference/base case values for those parameters. These key parameters represent the dependent variables for the uncertainty study. The key parameter list was developed through a Phenomena Identification and Ranking Table (PIRT) exercise in September 2005 (Reference 11). For the purpose of comparing results for key parameter among many similar runs in the uncertainty study, it is necessary to both smooth the parameter output and select times for their evaluation which can adjust for the effects of event sequence timing differences among the runs. The following information describes the smoothing approaches taken for the key parameters and the selections for the evaluation times.

The average and hottest SG tube failure margins represent the SG tube stress multipliers that result in tube failure coincident with the earliest RCS piping failure. The failure margins are expressed to two digits after the decimal point (rather than in multiples of 0.5, as has been done in the past) in order to generate data with sufficient detail for use in the uncertainty evaluation. The failure margin values are generally calculated by interpolating the failure time data for structures from Table 4. For cases where SG tube failure precedes the earliest RCS piping failure even when using a tube stress multiplier of 1.0, the failure margin is indicated as < 1.00 and the time interval by which tube failure precedes the earliest RCS piping failure is provided.

The average and hottest SG tube metal temperatures represent the smoothed (100-s lag) values for the average temperatures (across the tube wall thickness) at the time of the earliest RCS piping failure. The data are taken for the first axial SG tube wall heat structure above the top of the tubesheet in SG 1, where the tube temperatures are the highest. The time of earliest RCS piping failure (Hot Leg 1 at 13,630 s in the base case calculation) was selected because the SG tube failure margins are most affected by the relative relationships between the SG tube and RCS piping wall temperatures as the failure conditions for both structures are approached.

The hot leg steam temperature and wall inside surface heat transfer coefficient represent smoothed (100-s lag) values for those parameters 100 s after the time of the peak in the fuel rod oxidation rate. The data are taken for the first axial cell (adjacent to the reactor vessel) in the upper section of Hot Leg 1, where the hot leg temperature is the highest. The evaluation time (13,417 s + 100 s = 13,517 s in the base case calculation) was selected because it is the time, as the hot leg failure is approaching, when the rate of increase in the smoothed steam temperature is the highest. For the hot leg upper section, the wall heat transfer in the model represents a combination of convection from steam to the wall, radiation from steam to the wall and radiation to the opposing surfaces of the lower hot leg section wall (see Section 2.9 of Reference 8). The differential temperature for the wall-to-wall radiation heat transfer process is different from the two steam-to-wall heat transfer processes, and this complicates the calculation of a single, effective hot leg inside wall heat transfer coefficient. For the purposes here, the total heat transfer coefficient is calculated by dividing the total wall heat flux (from all three of the heat transfer processes) by the differential temperature between the steam and wall inside surface.

The pressurizer surge line steam temperature and wall inside surface heat transfer coefficient represent smoothed (100-s lag) values for those parameters 100 s after the time of the peak in the fuel rod oxidation rate. The data are taken for the axial cell of the surge line adjacent to Hot Leg 1, where the surge line temperature is the highest. The evaluation time (13,417 s + 100 s = 13,517 s in the base case calculation) was selected because it is the time, as the surge line failure is approaching, when the rate of increase in the smoothed steam temperature is the highest.

Table 13. Base Case Values of Key Parameters for Subsequent Uncertainty Evaluation.

Key Parameter (see text for details)	SCDAP/RELAP5 Model Parameter(s)	Base Case Value
Average SG Tube Failure Margin	DCREPH 2, DCREPH 6-19	2.10
Hottest SG Tube Failure Margin	DCREPH 2, DCREPH 62-75	< 1.00 Failure of non-degraded hottest tube precedes hot leg failure by 155 s
Average SG Tube Metal Temperature	CNTRLVAR 701	1021.7 K
Hottest SG Tube Metal Temperature	CNTRLVAR 706	1239.6 K
Hot Leg Steam Temperature	CNTRLVAR 714	1776.0 K
Hot Leg Wall Inside Surface Heat Transfer Coefficient	CNTRLVAR 720	423.1 W/m^2-K
Pressurizer Surge Line Steam Temperature	CNTRLVAR 727	1373.0 K
Pressurizer Surge Line Wall Inside Surface Heat Transfer Coefficient	CNTRLVAR 732	490.9 W/m^2-K

4.0 SUMMARY AND CONCLUSIONS

The NRC has been pursuing thermal-hydraulic studies to evaluate SG tube integrity during severe accidents. This report documents an updated SCDAP/RELAP5 system simulation of a base case station blackout event sequence in a typical Westinghouse four-loop pressurized water reactor. The model used for the base case calculation has been extensively improved as a result of addressing ACRS and PIRT review comments on the analysis methods, and from a better understanding of the pertinent fluid mixing processes, which has recently been gained through complementary CFD analyses.

The SCDAP/RELAP5 base case calculation reported here indicates that for a Westinghouse four-loop plant a stress multiplier of greater than 2.0 is required for the average SG tube to fail before the hot leg fails. The calculation also indicates that the hottest SG tube fails prior to the hot leg, even when a stress multiplier of 1.0, representing non-degraded tube strength condition, is used. These SG tube failure margins are smaller than have generally been seen in prior SCDAP/RELAP5 analyses for this event in a Westinghouse four-loop plant.

The reduced SG tube failure margins reported here resulted from the combined effects of multiple modeling changes. In this respect the most important modeling changes implemented are judged to be (in decreasing order of importance):

(1) Expanding the axial nodalization in the SG region (especially the significant shortening of the first active tube axial node above the top of the tubesheet), which leads to hotter SG tube metal temperatures and earlier SG tube failure,
(2) Switching from a SG power fraction target to a more physically-based hot leg discharge coefficient target in the model-adjustment procedure, which increases the hot leg flow rate and the SG heating rate, leading to earlier SG tube failure, and
(3) Moving the pressurizer surge line connection from the top to the side of the hot leg pipe, which lowers the temperature of steam entering the surge line and delays the surge line failure, such that the hot leg now fails prior to the surge line.

The base case calculation reported here will be used as the reference case in a subsequent study that will evaluate the uncertainties in the simulation of key calculated parameters.

5.0 REFERENCES

1. L. J. Siefken et al., *SCDAP/RELAP5/MOD3.3 Code Manual,* NUREG/CR-6150, INEL-96/0422, Revision 2, Idaho National Engineering and Environmental Laboratory, January 2001.
2. D. L. Knudson, L. S. Ghan, and C. A. Dobbe, *SCDAP/RELAP5 Evaluation of the Potential for Steam Generator Tube Ruptures as a Result of Severe Accidents in Operating Pressurized Water Reactor*s, Idaho National Engineering and Environmental Laboratory, EXT-98-00286, Revision 1, September 1998.
3. Typical Westinghouse Four-Loop Plant Design Differences Letter Report (title pending review).
4. L. W. Ward and V. V. Palazov, *Sequence Variations, Task 3.2: Accident Sequence Variations*, Information Systems Laboratories, Inc., ISL-NSAD-NRC-01-004, September 2001.
5. L. W. Ward and V. V. Palazov, *Sequence Variations, Task 3.3: Potential Conservatisms*, Information Systems Laboratories, Inc., ISL-NSAD-NRC-01-004 (Draft) , March 2002.
6. L. W. Ward, *Tube-to-Tube Temperature Variations During the Station Blackout Event, Task 3.5: Tube-to-Tube Temperature Variations*, Information Systems Laboratories, Inc., ISL-NSAD-TR-02-03, (Draft) August 2002.
7. W. A. Stewart, et al., "Natural Circulation Experiments for PWR High Pressure Accidents," EPRI Project No. RP2177-5, Westinghouse Electric Corp., December 1992.
8. Typical Westinghouse Four-Loop Plant Revised Base Case Calculation Letter Report (title pending review).
9. Typical Westinghouse Four-Loop Plant Sensitivity Evaluation Letter Report (title pending review).
10. F. R. Larson and J. Miller, "A Time Temperature Relationship for Rupture and Creep Stress," *Transactions of the ASME*, July 1952, pp. 765-775.
11. "Minutes of PIRT Meeting on Containment Bypass Issue," C. D. Fletcher, Information Systems Laboratories, Inc., email to PIRT meeting participants, October 13, 2005.
12. Minutes, Advisory Committee on Reactor Safeguards, Joint Materials and Metallurgy and Thermal-Hydraulic Subcommittees Meeting, "Steam Generator Action Plan," February 3-4, 2004, Rockville MD.
13. S. J. Leach and H. Thompson, "An Investigation of Some Aspects of Flow into Gas Cooled Reactors Following an Accidental Depressurization," Journal of British Nuclear Energy Society, Vol. 14, No. 3, 1975, pp. 243-250.

APPENDIX A - SUMMARY OF ADDITIONAL DATA PROVIDED ON CD

The data provided electronically on the CD accompanying this letter is summarized as follows:

Cover Letter and Attachment

PDF electronic files of the cover letter and attachment of this transmittal.

Standard Files for the Revised SCDAP/RELAP5 Westinghouse Four-Loop Plant Station Blackout Base Case Calculation Described in Sections 3.1 and 3.2

Input, output and demux plot files are provided for each of the four calculation steps. Input files are named uncbasesX.i and printed output files are named uncbasesX.o (where "X" is the calculation step number, 1 through 4). The demux file, containing all plotted data covering the full period of Steps 1 through 4, is named uncbases4.dmx.

Supplemental Data for the Revised SCDAP/RELAP5 Westinghouse Four-Loop Plant Station Blackout Base Case Calculation Described in Sections 3.1 and 3.2

To facilitate analyses performed by others in the project, additional output data channels have been stripped from the demux output file and stored separately. The additional data channels stored are listed in Tables A-1 through A-11. The list includes all known data requests from other analysts in the project; please advise should you need additional data from the base case calculation.

Output Data from the Energy Balance Analysis Described in Section 3.3

The SCDAP/RELAP5-calculated control variables related to the energy balance analysis were extracted from the base case calculation output and manipulated with a post-processor. The resulting energy balance data are available in two forms on the CD. First, files beginning with "out" contain the values of the integrated energy data at the end times of the periods for each of the five phases. The integrated energy data for these files are referenced to zero at the time of core uncovering. For example file "out13475.txt" contains the integrated energy data from the SCDAP/RELAP5 calculation at 13,475 s (which is the end time for Phase 3, Peak Fuel Rod Oxidation and the start time for Phase 4, Structure Failure). Second, files beginning with "diff" contain the changes in the integrated energy data that occurred during each of the five phases. For example file "diff_13475_14590.txt" contains the change in the integrated energy data between 13,475 s and 14,590 s, the span of the Phase 4, Structure Failure.

Note that, for working purposes, the CD contains data files for all energy balance related control variables, many of which are not pertinent for an understanding of the overall energy balance. For simplicity and clarity, it is recommended that the reader refer only to the control variables listed in Table 6, which represent the top-level terms of the RCS energy balance.

The data is provided in units of Joules. For energy balance control volume fluid energy storage, positive and negative values respectively represent increases and decreases in the control volume fluid energy. For fluid-structure heat transfer, positive values represent a transfer of heat from the structures to the fluid and negative values represent a transfer of heat from the fluid to the structures. For energy flow out of the RCS through valves and leaks, positive values represent flows leaving the RCS.

Table A-1. Supplemental Pressure Data

Channel Identifiers PCCCNN P = Pressure CCC = Component Number NN = Axial Cell Number Units: Pa	Location
p10001	Hot Leg 1 upper section, cell adjacent to the reactor vessel
p11001	SG 1 average tube, inside lowermost active cell
p12204	Cold Leg 1, adjacent to the reactor vessel
p15307	Pressurizer surge line, cell adjacent to hot leg
p16001	Containment
p18001	SG 1 steam dome pressure
p20001	Hot leg 2 upper section, cell adjacent to the reactor vessel
p21001	SG 2 average tube, inside lowermost active cell
p22204	Cold Leg 2, cell adjacent to the reactor vessel
p28001	SG 2 steam dome pressure
p38001	SG 3 steam dome pressure
p48001	SG 4 steam dome pressure

Table A-2. Supplemental Steam Temperature Data

Channel Identifiers TempgCCCNN Tempg = Steam Temperature CCC = Component Number NN = Axial Cell Number **Cntrlvar76X3**[1] X = 1 through 9 Units: K	Location
tempg10001 through tempg10005	Hot Leg 1 upper section, axial cells 1 (at reactor vessel end) through 5 (at SG end)
tempg10101 through tempg10105	Hot Leg 1 lower section, axial cells 1 (at SG end) through 5 (at reactor vessel end)
tempg 10501	SG 1 hot inlet plenum
tempg10601	SG 1 mixing inlet plenum
tempg 10701	SG 1 cold inlet plenum
tempg11003 through tempg11013	SG 1 hot average tube, axial cells 3 (just above tubesheet) through 13 (at top of the U-bend)
tempg112003through tempg112013	SG 1 hottest tube, axial cells 3 (just above tubesheet) through 13 (at top of the U-bend). Component 112, not shown on diagrams, see Reference 8, Section 2.10.
tempg 12201 through tempg12204	Cold Leg 1 from the pump discharge to the reactor vessel
tempg15301 through tempg15307	Pressurizer surge line, axial cells 1 (at pressurizer end) through 7 (at hot leg end)
tempg16001	Containment – this is the sink temperature used for the primary and secondary system heat losses
tempg20001 through tempg20005	Hot Leg 2 upper section, axial cells 1 (at reactor vessel end) through 5 (at SG end)
tempg20101 through tempg20105	Hot Leg 2 lower section, axial cells 1 (at SG end) through 5 (at reactor vessel end)
tempg21003 through tempg21013	SG 2 hot average tube, axial cells 3 (just above tubesheet) through 13 (at top of the U-bend)
tempg22201 through tempg22204	Cold Leg 2 from the pump discharge to the reactor vessel
tempg56101	Exit of average core channel
Cntrlvar7603, Cntrlvar7613, Cntrlvar7623, Cntrlvar7633, Cntrlvar7643, Cntrlvar7653, Cntrlvar7663, Cntrlvar7673, Cntrlvar7683, Cntrlvar7693,	Hot Leg 1 upper and lower section steam temperatures. X = 0, 2, 4, 6, 8 for upper section from reactor vessel toward the SG and X = 1, 3, 5, 7, 9 for lower section also from reactor vessel toward the SG. See Footnote 1.

1 – Control variables 76X3 represent the Hot Leg 1 steam temperatures to be used in conjunction with the control variable 8X0Y convection-only heat transfer coefficients described in Note 5 of Table A-4.

Table A-3. Supplemental Wall Temperature Data

Channel Identifiers HttempCCCGNNNXX Httemp = Wall Temperature CCCG = Component/Geometry Number NNN = Axial Heat Structure Number XX = Mesh Point Number Units: K	Location
httemp1001001XX through httemp1001005XX	Hot Leg 1 upper section wall, connected to hot leg Component 100, Cell 1 (NNN = 001, reactor vessel end) through Cell 5 (NNN = 005, SG end). Mesh points range from 1 (XX = 01) on inside surface to 9 (XX = 09) on outside surface.
httemp1011001XX through httemp1011005XX	Hot Leg 1 lower section wall, connected to hot leg Component 101, Cell 1 (NNN = 001, SG end) through Cell 5 (NNN = 005, reactor vessel end). Mesh points range from 1 (XX = 01) on inside surface to 9 (XX = 09) on outside surface.
httemp1051001XX	SG 1 hot inlet plenum wall, XX=1 for inside surface and XX=6 for outside surface.
httemp1061001XX	SG 1 mixing inlet plenum wall, XX=1 for inside surface and XX=6 for outside surface.
httemp1071001XX	SG 1 cold inlet plenum wall, XX=1 for inside surface and XX=6 for outside surface.
httemp1101001XX through httemp1101011XX	SG 1 average tube wall, connected to tube Component 110, Cell 3 (NNN = 001, just above tubesheet) through Cell 13 (NNN = 011, at U-bend). Only channels for surface mesh points are included, XX = 01 for inside surface and XX = 09 for outside surface.
httemp1121001XX through httemp1121011XX	SG 1 hottest tube wall, connected to hottest tube Component 112, Cell 3 (NNN = 001, just above tubesheet) through Cell 13 (NNN = 011, at U-bend). Only channels for surface mesh points are included, XX = 01 for inside surface and XX = 09 for outside surface. Component 112, not shown on diagrams, see Reference 8, Section 2.10.
httemp1531001XX through httemp1531007XX	Pressurizer surge line wall, connected to surge line Component 153, Cell 1 (NNN = 001, pressurizer end) through Cell 7 (NNN = 007, hot leg end). Mesh points range from 1 (XX = 01) on inside surface to 9 (XX = 09) on outside surface.

httemp2001001XX through httemp2001005XX	Hot Leg 2 upper section wall, connected to hot leg Component 200, Cell 1 (NNN = 001, reactor vessel end) through Cell 5 (NNN = 005, SG end). Mesh points range from 1 (XX = 01) on inside surface to 9 (XX = 09) on outside surface.
httemp2011001XX through httemp2011005XX	Hot Leg 2 lower section wall, connected to hot leg Component 201, Cell 1 (NNN = 001, SG end) through Cell 5 (NNN = 005, reactor vessel end). Only channels for surface mesh points are included, XX = 01 for inside surface and XX = 09 for outside surface.
httemp2071001XX	SG 2 cold inlet plenum wall, XX=1 for inside surface and XX=6 for outside surface.
httemp2101001XX through httemp2101011XX	SG 2 average tube wall, connected to tube Component 210, Cell 3 (NNN = 001, just above tubesheet) through Cell 13 (NNN = 011, at U-bend). Only channels for surface mesh points are included, XX = 01 for inside surface and XX=09 for outside surface.
httemp222100101	Cold Leg 2 inside surface temperature at reactor coolant pump discharge.

Table A-4. Supplemental Heat Transfer Coefficient Data

Channel Identifiers IMPORTANT: SEE FOOTNOTES FOR USE OF THIS DATA **Cntrlvar7XX2** Heat Transfer Coefficient[1] XX = 01 through 17 **Cntrlvar73XX** Heat Transfer Coefficient[2] XX = 01 through 17 **TestdaXX** Heat Transfer Coefficient[3] XX = 01 through 17 **HthtcCCCGNNNSS** Heat Transfer Coefficient[4] CCCG = Component/Geometry Number NNN = Axial Heat Structure Number SS = Surface Identifier **Cntrlvar8X0Y** Heat Transfer Coefficient[5] X = 1 through 5 Y = 3 or 6 Units: W/m^2-K	Location
Convection-Only Heat Transfer Coefficient cntrlvar7012, cntrlvar7022, cntrlvar7032, cntrlvar7042, cntrlvar7052	Inside surface of Hot Leg 1 upper section wall, connected to hot leg Component 100, Cell 1 (XX = 01, reactor vessel end) through Cell 5 (XX = 05, SG end).
Convection-Only Heat Transfer Coefficient Cntrlvar7062, cntrlvar7072, cntrlvar7082, cntrlvar7092, cntrlvar7102	Inside surface of Hot Leg 1 lower section wall, connected to hot leg Component 101, Cell 1 (XX = 06, SG end) through Cell 5 (XX = 10, reactor vessel end).
Convection-Only Heat Transfer Coefficient cntrlvar7112, cntrlvar7122, cntrlvar7132, cntrlvar7142, cntrlvar7152, cntrlvar7162, cntrlvar7172	Inside surface of pressurizer surge line wall, connected to surge line Component 1531, Cell 1 (XX = 11, pressurizer end) through Cell 7 (XX = 17, hot leg end).

Steam-Wall Radiation Only Heat Transfer Coefficient cntrlvar7301, cntrlvar7302, cntrlvar7303, cntrlvar7304, cntrlvar7305	Inside surface of Hot Leg 1 upper section wall, connected to hot leg Component 100, Cell 1 (XX = 01, reactor vessel end) through Cell 5 (XX = 05, SG end).
Steam-Wall Radiation Only Heat Transfer Coefficient cntrlvar7306, cntrlvar7307, cntrlvar7308, cntrlvar7309, cntrlvar7310	Inside surface of Hot Leg 1 lower section wall, connected to hot leg Component 101, Cell 1 (XX = 06, SG end) through Cell 5 (XX = 10, reactor vessel end).
Steam-Wall Radiation Only Heat Transfer Coefficient cntrlvar7311, cntrlvar7312, cntrlvar7313, cntrlvar7314, cntrlvar7315, cntrlvar7316, cntrlvar7317	Inside surface of pressurizer surge line wall, connected to surge line Component 1531, Cell 1 (XX = 11, pressurizer end) through Cell 7 (XX = 17, hot leg end).
testda1, testda2, testda3, testda4, testda5	Inside surface of Hot Leg 1 upper section wall, connected to hot leg Component 100, Cell 1 (XX = 01, reactor vessel end) through Cell 5 (XX = 05, SG end).
testda6 testda7, testda8, testda9, testda10	Inside surface of Hot Leg 1 lower section wall, connected to hot leg Component 101, Cell 1 (XX = 06, SG end) through Cell 5 (XX = 10, reactor vessel end).
testda11, testda12, testda13, testda14, testda15, testda16, testda17	Inside surface of pressurizer surge line wall, connected to surge line Component 1531, Cell 1 (XX = 11, pressurizer end) through Cell 7 (XX = 17, hot leg end).
hthtc1001001SS through hthtc1001005SS	Hot Leg 1 upper section wall, connected to hot leg Component 100, Cell 1 (NNN = 001, reactor vessel end) through Cell 5 (NNN = 005, SG end). Surface identifier is SS = 00 on inside surface and SS = 01 on outside surface.
hthtc1011001SS through hthtc1011005SS	Hot Leg 1 lower section wall, connected to hot leg Component 101, Cell 1 (NNN = 001, SG end) through Cell 5 (NNN = 005, reactor vessel end). Surface identifier is SS = 00 on inside surface and SS = 01 on outside surface.
hthtc105100100	SG 1 hot inlet plenum wall, inside surface.
hthtc106100100	SG 1 mixing inlet plenum wall, inside surface.
hthtc107100100	SG 1 cold inlet plenum wall, inside surface.

hthtc1101001SS through hthtc1101011SS	SG 1 average tube wall, connected to tube Component 110, Cell 3 (NNN = 001, just above tubesheet) through Cell 13 (NNN = 011, at U-bend). Surface identifier is SS = 00 on inside surface and SS = 01 on outside surface.
hthtc1121001SS through hthtc1121011SS	SG 1 hottest tube wall, connected to hottest tube Component 112, Cell 3 (NNN = 001, just above tubesheet) through Cell 13 (NNN = 011, at U-bend). Surface identifier is SS = 00 on inside surface and SS = 01 on outside surface. Component 112, not shown on diagrams, see Reference 8, Section 2.10.
hthtc1531001SS through hthtc1531007SS	Pressurizer surge line wall, connected to surge line Component 153, Cell 1 (NNN = 001, pressurizer end) through Cell 7 (NNN = 007, hot leg end). Surface identifier is SS = 00 on inside surface and SS = 01 on outside surface.
hthtc2001001SS through hthtc2001005SS	Hot Leg 2 upper section wall, connected to hot leg Component 200, Cell 1 (NNN = 001, reactor vessel end) through Cell 5 (NNN = 005, SG end). Surface identifier is SS = 00 on inside surface and SS = 01 on outside surface.
hthtc2011001SS through hthtc2011005SS	Hot Leg 2 lower section wall, connected to hot leg Component 201, Cell 1 (NNN = 001, SG end) through Cell 5 (NNN = 005, reactor vessel end). Surface identifier is SS = 00 on inside surface and SS = 01 on outside surface.
hthtc2101001SS through Hthtc2101011SS	SG 2 average tube wall, connected to tube Component 210, Cell 3 (NNN = 001, just above tubesheet) through Cell 13 (NNN = 011, at U-bend). Surface identifier is SS = 00 on inside surface and SS = 01 on outside surface.
Convection-Only Heat Transfer Coefficient Cntrlvar8103, cntrlvar8203, cntrlvar8303, cntrlvar8403, cntrlvar8503	Inside surface of Hot Leg 1 upper section wall (Y = 3), connected to hot leg Component 100, Cell 1 (X = 1, reactor vessel end) through Cell 5 (X = 5, SG end).
Convection-Only Heat Transfer Coefficient Cntrlvar8106, cntrlvar8206, cntrlvar8306, cntrlvar8406, cntrlvar8506	Inside surface of Hot Leg 1 lower section wall (Y = 6), connected to hot leg Component 101, Cell 5 (X = 1, reactor vessel end) through Cell 1 (X = 5, reactor SG end). Note that the axial numbering convention for this set of control variables is in the reverse direction of the lower hot leg section cell numbering.

1 – The control variable (cntrlvar) parameters 70X2 and 71X2 listed in this table represent the convection-only heat transfer coefficient for use in ABAQUS analyses of the Hot Leg 1 and pressurizer surge line regions. These heat transfer coefficients contain no contribution from steam-to-wall or wall-to-wall radiation heat transfer. Based on CFD analysis, these heat transfer coefficients include a 50% enhancement in the normal SCDAP/RELAP5 convection heat transfer in the upper and lower hot leg sections.

2 – The control variable (cntrlvar) parameters 73XX listed in this table represent the heat transfer coefficient due only to steam-to-wall radiation heat transfer for use in ABAQUS analyses of the Hot Leg 1 and pressurizer surge line regions. These heat transfer coefficients contain no contribution from convection or wall-to-wall radiation heat transfer.

3 – The developmental assessment test (testda) parameters listed in this table represent the convection-only portion of the SCDAP/RELAP5 calculated heat transfer coefficient (parameter hthtc, see Note 4) for the Hot Leg 1 and pressurizer surge line regions. These heat transfer coefficients do not include the 50% enhancement for the hot leg described in Note 1. The testda parameters are provided only for reference should the data needs for the ABAQUS input later change.

4 – Parameter hthtc represents the combination of the convective and (where applied) steam-to-wall thermal radiation processes, but does not include effects of wall-to-wall thermal radiation process (where applied). For ABAQUS analysis of the Hot Leg 1 and pressurizer surge line region, the cntrlvar parameters described in Note 1 are to be used (the hthtc parameters are provided only for reference). For analyses in regions other than the hot leg and pressurizer surge line (for example, steam generator tube analyses), the hthtc parameters should be used.

5 – Additional control variables were developed in order to represent different expected heat transfer coefficient behavior in Hot Leg 1 during periods when pressurizer relief valves are open than when they are closed. Control variables 8X0Y represent the Hot Leg 1 convection-only steam-to-wall heat transfer coefficient response. During periods when all pressurizer relief valves are closed these control variables have the same values as the original convection-only heat transfer coefficients given by control variables 7XX2 and described in Note 1 above. During periods when any pressurizer relief valve (PORV or SRV) is open, these control variables represent convection-only heat transfer coefficients based on the net, co-current flows toward the surge line connection in the upper and lower Hot Leg 1 sections using the Dittus-Boelter correlation without the enhancement described in Note 1. The heat transfer coefficient responses provided by control variables 8X0Y include the effects of switching back and forth between the two processes, depending on the current status of the pressurizer relief valves. Note that when applying control variables 8X0Y as the heat transfer coefficients, the steam temperatures given by control variables 76X3 should be used (rather than the SCDAP/RELAP5 calculated cell steam temperatures), see Table A-2. The steam temperatures represented by control variables 76X3 also include the effects of switching between separated or combined hot leg flows based on the pressurizer valve status.

Table A-5. Supplemental Heat Flux Data

Channel Identifiers HtrnrCCCGNNNSS or HftotCCCGNNNSS Htrnr or Hftot = Heat Flux[1] CCCG = Component/Geometry Number NNN = Axial Heat Structure Number SS = Surface Identifier Units: W/m^2	Location
hftot1001001SS through hftot1001005SS or htrnr1001001SS through htrnr1001005SS	Hot Leg 1 upper section wall, connected to hot leg Component 100, Cell 1 (NNN = 001, reactor vessel end) through Cell 5 (NNN = 005, SG end). Surface identifier is SS = 00 on inside surface and SS = 01 on outside surface. Use parameter Hftot for inner surface and parameter Htrnr for outer surface
hftot1011001SS through hftot1011005SS or htrnr1011001SS through hthtc1011005SS	Hot Leg 1 lower section wall, connected to hot leg Component 101, Cell 1 (NNN = 001, SG end) through Cell 5 (NNN = 005, reactor vessel end). Surface identifier is SS = 00 on inside surface and SS = 01 on outside surface. Use parameter Hftot for inner surface and parameter Htrnr for outer surface
htrnr105100100	SG 1 hot inlet plenum wall, inside surface.
htrnr106100100	SG 1 mixing inlet plenum wall, inside surface.
htrnr107100100	SG 1 cold inlet plenum wall, inside surface.
htrnr1101001SS through htrnr1101011SS	SG 1 average tube wall, connected to tube Component 110, Cell 3 (NNN = 001, just above tubesheet) through Cell 13 (NNN = 011, at U-bend). Surface identifier is SS = 00 on inside surface and SS = 01 on outside surface.
htrnr1121001SS through htrnr1121011SS	SG 1 hottest tube wall, connected to hottest tube Component 112, Cell 3 (NNN = 001, just above tubesheet) through Cell 13 (NNN = 011, at U-bend). Surface identifier is SS = 00 on inside surface and SS = 01 on outside surface. Component 112, not shown on diagrams, see Reference 8, Section 2.10.
htrnr1531001SS through htrnr1531007SS	Pressurizer surge line wall, connected to surge line Component 153, Cell 1 (NNN = 001, pressurizer end) through Cell 7 (NNN = 007, hot leg end). Surface identifier is SS = 00 on inside surface and SS = 01 on outside surface.

hftot2001001SS through hftot2001005SS or htrnr2001001SS through htrnr2001005SS	Hot Leg 2 upper section wall, connected to hot leg Component 200, Cell 1 (NNN = 001, reactor vessel end) through Cell 5 (NNN = 005, SG end). Surface identifier is SS = 00 on inside surface and SS = 01 on outside surface. Use parameter Hftot for inner surface and parameter Htrnr for outer surface.
hftot2011001SS through hftot2011005SS or htrnr2011001SS through hthtc2011005SS	Hot Leg 2 lower section wall, connected to hot leg Component 201, Cell 1 (NNN = 001, SG end) through Cell 5 (NNN = 005, reactor vessel end). Surface identifier is SS = 00 on inside surface and SS = 01 on outside surface. Use parameter Hftot for inner surface and parameter Htrnr for outer surface.
htrnr2101001SS through htrnr2101011SS	SG 2 average tube wall, connected to tube Component 210, Cell 3 (NNN = 001, just above tubesheet) through Cell 13 (NNN = 011, at U-bend). Surface identifier is SS = 00 on inside surface and SS = 01 on outside surface.

1 – Parameter htrnr represents the combined heat flux from convection and steam-to-wall thermal radiation (where applied) processes. Parameter hftot represents the combined heat flux from convection, steam-to-the wall thermal radiation (where applied) and wall-to-wall thermal radiation (where applied) processes. Both parameter htrnr and hftot include the effect of the multiplier placed on the combination of hot leg convection and steam-to-wall heat transfer intended to represent the enhancement of the convection portion of the heat transfer.

Table A-6. Supplemental Average Wall Temperature Data

Channel Identifiers HtvatCCCGNNN Htvat = Ave. Temperature CCCG = Component/Geometry Number NNN = Axial Heat Structure Number Units: K	Location
htvat1001001 through htvat1001005	Hot Leg 1 upper section wall, connected to hot leg Component 100, Cell 1 (NNN = 001, reactor vessel end) through Cell 5 (NNN = 005, SG end).
htvat1011001 through htvat1011005	Hot Leg 1 lower section wall, connected to hot leg Component 101, Cell 1 (NNN = 001, SG end) through Cell 5 (NNN = 005, reactor vessel end).
htvat1101001 through htvat1101011	SG 1 average tube wall, NNN = 001 at tube sheet, NNN = 011 at U bend.
htvat1121001 through htvat1121011	SG 1 hottest tube wall, NNN = 001 at tube sheet, NNN = 011 at U bend.
htvat1221001	Cold Leg 1 wall adjacent to the reactor coolant pump discharge.
htvat1531007	Pressurizer surge line at hot leg end.
htvat2001001 through htvat2001005	Hot Leg 2 upper section wall, connected to hot leg Component 200, Cell 1 (NNN = 001, reactor vessel end) through Cell 5 (NNN = 005, SG end).
htvat2011001 through htvat2011005	Hot Leg 2 lower section wall, connected to hot leg Component 101, Cell 1 (NNN = 001, SG end) through Cell 5 (NNN = 005, reactor vessel end).
htvat2101001 through htvat2101011	SG 2 average tube wall, NNN = 001 at tube sheet, NNN = 011 at U bend.

Table A-7. Supplemental Mass Flow Rate Data

Channel Identifiers MflowjCCCXX Mflowj = Mass Flow Rate CCC = Component Number XX = Junction Number Units: kg/s	Location
mflowj12203	Cold Leg 1, near the reactor vessel.
mflowj12500	Reactor Coolant Pump 1 shaft seal leak.
mflowj22203	Cold Leg 2, near the reactor vessel.
mflowj22500	Reactor Coolant Pump 2 shaft seal leak.

Table A-8. Supplemental Liquid Temperature Data

Channel Identifiers TempfCCCXX Tempf = Liquid Temperature CCC = Component XX = Volume Number Units: K	Location
tempf12204	Cold Leg 1, cell adjacent to the reactor vessel.
tempf22204	Cold Leg 2, cell adjacent to the reactor vessel.

Table A-9. Supplemental Velocity Data

Channel Identifiers VelfCCCXX VelgCCCXX Velf = liquid velocity Velg = vapor velocity CCC = Component Number XX = volume number Units: m/s	Location
velf12204	Cold Leg 1 liquid velocity in cell adjacent to reactor vessel.
velg12204	Cold Leg 1 vapor velocity in cell adjacent to reactor vessel.
velf22204	Cold Leg 2 liquid velocity in cell adjacent to reactor vessel.
velg22204	Cold Leg 2 vapor velocity in cell adjacent to reactor vessel.

Table A-10. Supplemental Void Fraction

Channel Identifier VoidgCCCXX VoidgjCCCXX Voidg = Volume Void Voidgj = Junction Void CCC = Component XX = Volume or Junction Number Units: dimensionless	Location
voidg12204	Cold Leg 1, cell adjacent to reactor vessel.
voidgj12500	Reactor Coolant Pump 1 at the shaft seal leak location.
voidg22204	Cold Leg 2, cell adjacent to reactor vessel.
voidgj22500	Reactor Coolant Pump 2 at the shaft seal leak location.

Table A-11. Supplemental Pressurizer Relief Valve Status Indicator

Channel Identifier Units: dimensionless	Data Format
cntrlvar7400	This control variable describes the status of the pressurizer PORVs and SRVs. The control variable has a value of 1.0 if any pressurizer PORV or SRV is open. The control variable has a value of 0.0 if all pressurizer PORVs and SRVs are closed. See Footnote 5 of Table A-4.